

CELEBRATING 25 YEARS
CREWES



CONSORTIUM FOR RESEARCH IN ELASTIC WAVE EXPLORATION SEISMOLOGY



— *2013 Sponsors Meeting* —

Banff Park Lodge Resort Hotel and Conference Centre

December 4th - December 6th —



Providing Advanced Seismic Imaging to the Geophysics Community for 25 years



UNIVERSITY OF
CALGARY



Research Report 2013
Volume 25

In this volume...

Report Summaries

On the memory stick...

Complete Reports
Student Theses



UNIVERSITY OF
CALGARY



CREWES Project faculty, staff and students, October 2013

Left to Right:

Front Row: Kevin Bertram, Oliver Lahr, Shahin Moradi, Rolf Maier, Laura Baird, Joe Wong, John Bancroft

Second Row: Patricia Gavotti, Jessica Dongas, Bona Wu, Tianci Cui, Penny Pan, Gary Margrave (director), Roy Lindseth, Eric Gallant, Dave Henley, Chris Harrison, Davood Nowroozi

Third Row: Shahin Jabbari, Saul Guevara, Sina Esmaili, Jian Sun, Wenyong Pan, Kevin Hall

Fourth Row: Helen Isaac, Steve Kim, Jesse Kolb, Marcelo Guarido, Rafael Asuaje, Kris Innanen, Babatunde Arenrin, Raul Cova, Shahpoor Moradi, Hassan Khaniani

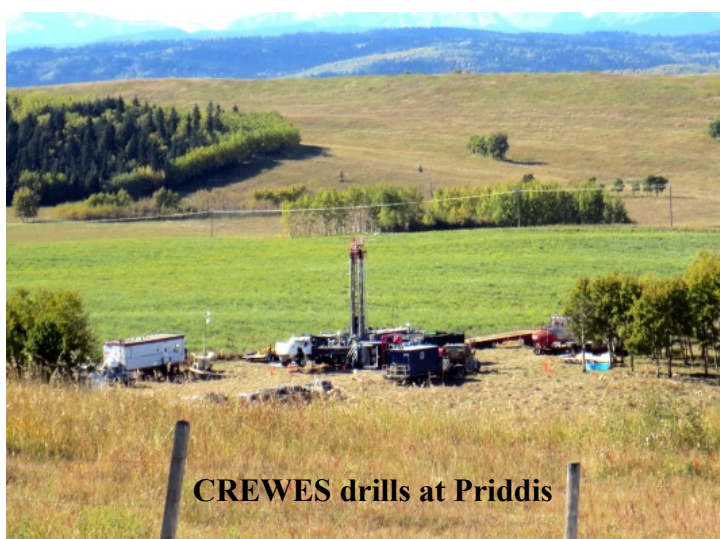
Back Row: Chris Petten, Jean Cui, Larry Lines, Don Lawton, Khaled Al Dulaijan, Mohammed Alarfaj, Michael Lamoureux, Adrian Smith, Vladimir Zubov

CREWES 2013

Welcome to our 25th annual Sponsors meeting. CREWES traces its origin to the year 1988 when Professors Rob Stewart, Don Lawton, and Jim Brown decided that the University-Industry consortium model could work in Canada to fund research and training in exploration seismology. We now have 25 years of history to document the clarity of their vision. Over this period, CREWES has seen 102 students complete Masters degrees and 36 complete PhD's. There have been 1521 CREWES research reports which resulted in 556 expanded (4-page) abstracts at the major geophysical conventions. We have had 97 different Sponsor Companies at various times with the average year seeing us with a sponsorship somewhere between 20 and 30. At this time, we have a total of 24 sponsors which is down a bit from last year.

In 2013, we have had 5 PhD's defenses (a record for a single year) and 3 MSc's. We anticipate a few more defences before the New Year. Presently there are 30 graduate students in the project, split equally between PhD's and MSc's. Almost half (13) are new to the project this year.

This year, our field effort centered around drilling and instrumenting a geophysical observation well at our Priddis test site 70km west of campus. After a full year of extensive effort to get the required consent from government, the University, and the local residents, we finally began drilling on September 30 as shown at right. After a week's effort, we had two 150m boreholes, both cased and



cemented, with a 40 level 3C geophone tool permanently installed in one, the other being vacant for temporary tools. In the month of October we acquired initial seismic data around the site and are now in the process of analyzing this. This was a significant effort, unique in our project's history, and we regard it as infrastructure that will enrich our research in the next 5 years.

On a related note, we are in the final months of our current 5-year NSERC grant (NSERC is the Canadian federal funding agency for science and engineering) and we are planning a re-application. CREWES has had such grants essentially continuously since the early 1990's and they amount to strong leveraging of Sponsor dollars. In addition, the application process forces us to develop a long-term research plan that is subsequently subjected to peer review. Our new proposal is focused on advancing inversion methods and is described in

a research report in this year's collection. We invite you to review this proposal and provide us with your opinions and feedback.

Our productivity this year and the technical relevance and difficulty of our research stand very strongly next to our past efforts. While we are proud of our project and our work, we are also cognizant that we are completely reliant on the continued support of our Sponsors and NSERC. This research volume represents the collective effort of our project to return value to our Sponsors and contribute meaningfully to the knowledge and experience base.

We hope you enjoy our meeting and give us your feedback on the quality and effectiveness of our research. Please feel free to make suggestions or offer guidance as you see fit. If the opportunity arises, we always welcome the possibility of your direct involvement in our ongoing research.

Thank you all for your continued and generous support, and thank you for attending our annual meeting.

Calgary, Alberta
December, 2013

Gary Margrave
CREWES Director

Table of Contents

CREWES 2013	i
Table of Contents	iii
2013 CREWES Sponsors	x
CREWES Personnel	xi
Student Theses	xviii

A physical model investigation of P and S wave azimuthal anisotropy on transmission

Khaled Al Dulaijan, Gary Margrave, and Joe Wong 1

Kinematic structural forward modeling for fault trajectory prediction in seismic interpretation

Mohammed Alarfaj* and Don C. Lawton..... 2

Preliminary results using Acceleware's AxRTM API

Babatunde Arenrin, Gary Margrave, and Rolf Maier..... 3

Turning-ray tomography and tomostatics

Babatunde Arenrin*, Gary Margrave, and John Bancroft 4

Seismic interpretation of the Canterbury Plains, New Zealand

Jessie M. Arthur and Don C. Lawton 5

Estimation of Converted Waves Static Corrections Using CMP Cross-Correlation of Surface Waves

Roohollah Askari, Robert J. Ferguson, J. Helen Isaac CREWES, Department of Geoscience, University of Calgary..... 6

Analysis of multicomponent seismic data recorded with a new hydraulic thumper source

Rafael Asuaje..... 7

Comments on wavefield propagation using Reverse-time and Downward continuation

John C. Bancroft 8

Modelling migration, and inversion using Linear Algebra

John C. Bancroft* and Rod Blais 9

Resolution enhancement with deconvolution after migration

John C. Bancroft, Thais Guirigay, Naser Yousefzadeh, and Helen Isaac 10

* Presenter

CREWES in the Field, acquisition and preliminary results	
Kevin L. Bertram*, Malcolm B. Bertram, Kevin W. Hall, Eric V. Gallant, Don C. Lawton, Gary F. Margrave and Kristopher A.H. Innanen.....	11
Recent data from the Priddis Geophysical Observatory	
Malcolm B Bertram, Don C Lawton, Kevin W Hall, Kevin L Bertram, Eric V Gallant.....	12
A hybrid tomography method for crosswell seismic inversion	
Danping Cao and Wenyuan Liao	13
Comparison of Q-estimation methods: an update	
Peng Cheng and Gary F. Margrave.....	14
Cross-correlation based time warping of one-dimensional seismic signals	
David Cho	15
Approximate- vs. full-Hessian in FWI: 1D analytical and numerical experiments	
Raul Cova and Kris Innanen	16
An interferometric solution for raypath-consistent shear wave statics	
Raul Cova*, David Henley and Kris Innanen	17
Non-stationary S-wave statics	
Raul Cova, David Henley and Kris Innanen.....	18
Seismic modeling and inversion for reflections from fractures	
Xiaoqin (Jean) Cui*, Laurence R. Lines and Edward S. Krebs.....	19
Anelastic (poroviscoelastic) medium – the S_H – wave problem	
P.F. Daley	20
Higher order analytic approximations to the $\hat{P}\hat{P}$ and $\hat{P}\hat{S}$ reflection coefficients – numerical methods and results	
P.F Daley	21
More numerical experiments in high frequency edge diffraction	
P. F. Daley	22
Recovering low frequency for impedance inversion by frequency domain deconvolution	
Sina Esmaeili and Gary F. Margrave	23
Inversion of seismic data for assessing fluid replacement in the Nisku Formation	
Patricia E. Gavotti* and Don C. Lawton	24
Seismic processing workflow for supressing coherent noise while retaining low-frequency signal	
Patricia E. Gavotti and Don C. Lawton	25

Analysis of S-waves generated by explosive sources in boreholes: modeling and the Priddis experiment	
Saul E. Guevara*, and Gary F. Margrave	26
Converted-wave processing in a complex area: near surface and depth imaging challenges	
Saul E. Guevara, Gary F. Margrave, Babatunde Arenrin, John C. Bancroft, and William M. Agudelo.	27
The role of source modeling in prestack depth migration for AVO estimation	
Saul E. Guevara and Gary F. Margrave	28
Wave mode separation for a surface with slope using the free-surface response	
Saul E. Guevara, Gary F. Margrave and Don C. Lawton.....	29
Installation of new observation wells at the Priddis Geophysical Observatory	
Kevin W. Hall*, Kevin L. Bertram, Malcolm B. Bertram, Eric V. Gallant, Gary F. Margrave, Don C. Lawton	30
Updates to readlas	
Kevin W. Hall and Gary F. Margrave	31
Harnessing harmonics for imaging thin shallow reflectors	
Christopher B. Harrison, Gary Margrave, Michael Lamoureux*, Arthur Siewert, Andrew Barrett and Helen Isaac	32
Through the looking glass: using X-T plane distortions for wavefield separation	
David C. Henley and Joe Wong.....	33
Undoing wavefield interference for AVAZ measurements	
David C. Henley and Faranak Mahmoudian	34
Which way is up?—experiences with processing physical modeling data	
David C. Henley* and Joe Wong	35
Identifying internal multiples using 1D prediction: physical modelling and land data examples	
Melissa Hernandez and Kris Innanen	36
A collision theory of seismic waves applied to elastic VSP data	
Kris Innanen and Kevin Hall.....	37
A framework for multiparameter full waveform inversion of precritical reflection seismic data	
Kris Innanen.....	38

How AVO information can be practically incorporated in full waveform inversion	
Kris Innanen.....	39
Internal multiple prediction in the continuous wavelet transform maxima domain	
Kris Innanen*	40
Seismic processing with continuous wavelet transform maxima	
Kris Innanen.....	41
Geophysical characterization of the near-surface at Priddis, Alberta	
J. Helen Isaac, Lei Zhi, Malcolm Bertram, Don C. Lawton, and L. R. Bentley.....	42
Squeezing more out of 2D seismic data: Processing and interpretation of a pseudo-3D seismic survey from New Zealand	
J. Helen Isaac and Don C. Lawton	43
An analysis of time-lapse phase shifts using perturbation theory	
Shahin Jabbari and Kristopher A. Innanen	44
A framework for linear and nonlinear S-wave and C-wave time-lapse difference AVO	
Shahin Jabbari and Kristopher A. Innanen	45
Iterative multiparameter elastic waveform inversion using prestack Kirchhoff approximation	
Hassan Khaniani*, John C. Bancroft and Eric von Lunen.....	46
Linear and nonlinear poroelastic AVO	
Steven Kim and Kris Innanen	47
Detection and characterization of anelastic AVF with the Gabor transform	
Jesse M. Kolb, Kristopher A. H. Innanen	48
Can we see a velocity ramp in reflection seismic data	
Michael P. Lamoureux, Peter C. Gibson, Gary F. Margrave	49
A new S-wave seismic source	
Don C. Lawton*, Eric V. Gallant, Malcolm B. Bertram, Kevin W. Hall, Kevin L. Bertram	50
Viscosity estimation using seismic inversion	
Laurence R. Lines*, Fereidoon Vasheghani and R. Phillip Bording.....	51
The art of well tying with new MATLAB tools	
Heather J.E. Lloyd* and Gary F. Margrave.....	52
Phase and group velocity measurements from physically modeled transmission gathers	
Faranak Mahmoudian, Gary Margrave, and Joe Wong.....	53

Finite-difference models with an internal water-bottom boundary condition Peter M. Manning and Joe Wong	54
CREWES 5-year research plan: Towards broadband multicomponent seismology and practical iterated inversion Gary Margrave, Kris Innanen, Don Lawton, John Bancroft, Michael Lamoureux, and Larry Lines	55
New features in SYNGRAM Gary F. Margrave.....	56
Q tools: Summary of CREWES software for Q modelling and analysis Gary F. Margrave.....	57
Why seismic to well ties are difficult Gary F. Margrave*	58
Parallel VSP Experiment Paul E. McGee and Robert J. Ferguson.....	59
Velocity-stress finite-difference modeling of poroelastic wave propagation Shahin Moradi* and Don C. Lawton.....	60
Viscoelastic scattering potentials and inversion sensitivities Shahpoor Moradi* and Kris Innanen.....	61
Fracture analysis using multicomponent seismic attributes: example from Saskatchewan Andrew Nicol and Don Lawton.....	62
Reservoir simulation for a CO₂ sequestration project Davood Nowroozi and Donald C. Lawton.....	63
1D internal multiple prediction in a multidimensional world: errors and recommendations Pan Pan* and Kris Innanen.....	64
Numerical analysis of 1.5D internal multiple prediction Pan Pan and Kris Innanen.....	65
A review of internal multiple prediction Pan Pan and Kris Innanen	66
1D scalar full waveform inversion inferring convergence properties with analytic and numerical examples Wenyong Pan, Kris Innanen	67
A comparison of different scaling methods for least-squares inversion/migration Wenyong Pan, Kris Innanen, Gary Margrave	68
Efficient full waveform inversion with phase encoded pseudo-Hessian Wenyong Pan, Kris Innanen, Gary Margrave	69

Efficient pseudo Gauss-Newton full waveform inversion in the time-ray parameter domain	
Wenyong Pan*, Kris Innanen, Gary Margrave.....	70
Multisource reverse time migration in anisotropic media	
Wenyong Pan, Kris Innanen, Gary Margrave	71
On the role of the deconvolution imaging condition in full waveform inversion	
Wenyong Pan*, Gary Margrave, Kris Innanen.....	72
Poroeastic scattering potentials and inversion sensitivities	
Wenyong Pan, Kris Innanen	73
Thin-bed AVO and AVF continued	
Wenyong Pan, Kris Innanen	74
Exploring potential applications of Gaussian Ball Filters in Sharpe’s Hollow Cavity Model	
Christopher C. Petten, Gary F. Margrave	75
The S function and its applications	
Brian Russell*	76
Madagascar - a powerful software package for multidimensional data analysis and reproducible computational experiments	
Adrian D. Smith, Sergey Fomel, Robert J. Ferguson.....	77
Processing of tissue sensing adaptive radar data - an analogue for georadar	
Adrian D. Smith, Jérémie Bourqui, Yuhong (Kay) Liu, Elise C. Fear, Robert J. Ferguson.....	78
Imaging lateral discontinuities with reflected surface waves	
Robert R. Stewart, Craig Hyslop, and Minyu Zhang	79
Searching for the 2010 Haiti earthquake fault	
Robert R. Stewart, Eray Kocel, Paul Mann, and Li Chang	80
Controlling a land vibrator with m-sequences: a field test	
Joe Wong, Malcolm Bertram, Kevin Bertram, Eric Gallant, and Kevin Hall	81
Exact formulas for qP, qS_V, and SH group velocities in VTI media	
Joe Wong.....	82
Operating instructions for mFD2D, MATLAB code for generating seismograms in 2D elastic media	
Joe Wong.....	83
Seismic physical modeling I: acquisition of 2D and 3D surveys involving HTI targets	
Joe Wong*	84

Seismic physical modeling II: VVAZ and AVAZ effects observed on reflections from isolated HTI targets
Joe Wong..... 85

Instantaneous frequency computation: theory and practice
Matthew J. Yedlin*, Gary F. Margrave, and Yochai Ben Horin 86

Elastodynamic FWI in 2D with partial stacking
Vladimir Zubov*, Gary F. Margrave and Michael P. Lamoureaux..... 87

2013 CREWES Sponsors

Acceleware	BHP Billiton Petroleum (Americas) Inc.
CGG	Chevron Corporation
ConocoPhillips	Devon Energy Corporation
Exxon Mobil Corporation	Geokinetics Inc.
Halliburton	Husky Energy Inc.
INOVA Geophysical Equipment Ltd.	Nexen Inc.
Northwest Geology Institute, CNPC	Petrobras
PTT Exploration and Production Company	Saudi Aramco
Sensor Geophysical Ltd.	Shell Canada Limited
Suncor Energy Inc.	Talisman Energy Inc.
TGS-NOPEC	Tullow Oil p.l.c.
WesternGeco/GEDCO	Woodside Energy (USA) INC

Natural Sciences and Engineering Research Council of Canada (NSERC)
- Collaborative Research and Development Grant

CREWES Personnel

LEADERSHIP

Gary F. Margrave, Director

Professor, Department of Geoscience, University of Calgary

B.Sc. Physics, 1975, University of Utah

M.Sc. Physics, 1977, University of Utah

Ph.D. Geophysics, 1981, University of Alberta

- Work Experience: Chevron Canada Resources, Chevron Geoscience Company

Don C. Lawton, Associate Director

Professor, Department of Geoscience, University of Calgary

B.Sc. (Hons. Class I) Geology, 1973, University of Auckland

Ph.D. Geophysics, 1979, University of Auckland

- Work Experience: New Zealand Steel Mining Ltd., Amoco Minerals (N.Z.) Ltd.

Kristopher A. Innanen, Associate Director

Associate Professor, Department of Geoscience, University of Calgary

B.Sc. Physics and Earth Science, 1996, York University

M.Sc. Physics, 1998, York University

Ph.D. Geophysics, 2003, University of British Columbia

- Work Experience: University of Houston

Laura A. Baird, Business Manager

BA, History, 1992, University of Calgary

- Work Experience: Department of Geoscience, University of Calgary

Kevin W. Hall, Technical Manager

B.Sc. Geophysics, 1992, University of Calgary

M.Sc. Geophysics, 1996, University of Calgary

- Work Experience: Lithoprobe Seismic Processing Facility, University of Calgary

ADJUNCT DIRECTORS

Laurence R. Lines

Professor, Department of Geoscience, University of Calgary

B.Sc. Physics, 1971, University of Alberta

M.Sc. Geophysics, 1973, University of Alberta

Ph.D. Geophysics, 1976, University of B.C.

- Work Experience: Amoco Production Research, Tulsa University, Memorial University of Newfoundland

Robert R. Stewart

Cullen Chair in Exploration Geophysics, University of Houston
Adjunct Professor, Department of Geoscience, University of Calgary

B.Sc. Physics and Mathematics, 1978, University of Toronto

Ph.D. Geophysics, 1983, Massachusetts Institute of Technology

- Work Experience: Arco Exploration and Production Research Centre, Chevron Geoscience Company, Veritas Software Ltd., Gennix Technology Corp., University of Calgary.

ASSOCIATED FACULTY AND SCIENTISTS

John C. Bancroft

Adjunct Professor, Department of Geoscience, University of Calgary

B.Sc. Electrical Engineering, 1970, University of Calgary

M.Sc. Electrical Engineering, 1972, University of Calgary

Ph.D. Electrical Engineering, 1975, Brigham Young University

- Work Experience: Geo-X Systems Ltd., Veritas Software Ltd., Ulterra Geoscience Ltd.

Michael P. Lamoureux

Professor and Department Head, Department of Mathematics and Statistics, University of Calgary

Adjunct Professor, Department of Geoscience, University of Calgary

B.Sc. Mathematics, 1982, University of Alberta

M.Sc. Mathematics, 1983, Stanford University

Ph.D. Mathematics, 1988, University of California, Berkeley

- Work Experience: Farallon Computing, NSERC Canada

Roy O. Lindseth MC., FRSC

Technical Advisor, CREWES, University of Calgary

Doctor of Laws, Honoris Causa, 1978, University of Calgary

- Work Experience: Chevron; NSERC, Teknica Corporation; TCPL

Brian H. Russell

Adjunct Professor, Department of Geoscience, University of Calgary

B.Sc. Physics, 1972, University of Saskatchewan

Honours Certificate in Geophysics, 1975, University of Saskatchewan

M.Sc., Geophysics, 1978, University of Durham

Ph.D., Geophysics, 2004, University of Calgary

- Work Experience: Chevron Geoscience Company, Teknica Resource Development, Veritas Software Ltd., Hampson-Russell Software Ltd.

Matt Yedlin

Associate Professor, Department of Electrical and Computer Engineering, University of British Columbia

B.Sc. Honors Physics, 1971, University of Alberta

M.Sc. Physiology, 1973, University of Toronto

Ph.D. Geophysics, 1978, University of British Columbia

- Work Experience: Conoco

RESEARCH STAFF AND POST DOCTORIAL FELLOWS

Kevin L. Bertram

Electronics Technician Certificate, 2005, Southern Alberta Institute of Technology

- Work Experience: Aram Systems Ltd.

Malcolm B. Bertram

B.Sc. Geology, Auckland, New Zealand

- Work Experience: Allied Minerals NL (Western Australia), GSI (Western Australia), Western Geophysics (Western Australia), Auckland University, University of Calgary.

Patrick F. Daley

B.Sc. Mathematics, 1974, University of Alberta

M.Sc. Physics 1976, University of Alberta

Ph.D. Geophysics, 1979, University of Alberta

- Work Experience: Independent contractor associated with research centres of major oil companies

Eric V. Gallant

Journeyman Interprovincial Ticket in Electrical Construction, 1976, Cape Breton Institute of Technology

- Work Experience: IBEW, University of Calgary

Christopher B. Harrison

B.Sc. Physics, 1999, University of Calgary

B.Sc. Geophysics, 2001, University of Calgary

Ph.D. Geophysics, 2009, Curtin University of Technology, Perth, Western Australia

- Work Experience: University of Calgary, Total Depth Pty, Australia,

David C. Henley

B.Sc. Physics, 1967, Colorado State University

M.Sc. Physics, 1968, University of Michigan

- Work Experience: Shell Oil Co., Shell Canada Ltd

Helen Isaac

B.Sc. Mathematics, 1973, Imperial College, London

M.Sc. Geophysics, 1974, Imperial College, London

Ph.D. Geophysics, 1996, University of Calgary

- Work Experience: Phillips Petroleum, Hudson's Bay Oil and Gas, Canterra Energy, Husky, Fold-Fault Research Project

Rolf Maier

B.Sc. Chemical Engineering, 1978, Technikum Winterthur, ZH, Switzerland

M.Sc. Physical Chemistry, 1984, University of Calgary

Ph.D. Physical Chemistry, 1988, University of Calgary

- Work Experience: Lithoprobe Seismic Processing Facility, University of Calgary

Peter M. Manning

B.Sc. Mathematics, 1961, University of British Columbia

Ph.D. Geophysics, 2007, University of Calgary

- Work Experience: Mobil Oil Canada

Joe Wong

B.Sc. Physics/Mathematics, 1971, Queen's University

M.Sc. Applied Geophysics, 1973, University of Toronto

Ph.D. Applied Geophysics, 1979, University of Toronto

- Work Experience: Ontario Ministry of the Environment, University of Toronto, JODEX Applied Geoscience Limited

Vladimir Zubov

B.Sc. Mathematics, 2004, Rostov State University, Russia

M.Sc. Mathematics, 2006, Rostov State University, Russia

Ph.D. Mathematics, 2009, Southern Federal University, Russia

- Work experience: Computing Center of Southern Federal University, Russia

GRADUATE STUDENTS

Mohammed Alarfaj

B.Sc. Geophysics, 2007, Boise State University

- Work Experience: Saudi Aramco

Khaled Al Dulaijan

B.Sc. Geosciences, 2003, University of Tulsa, Oklahoma

M.Sc. Geophysics, 2008, University of Calgary

- Work Experience: Saudi Aramco

Babatunde Arenrin

B.Sc. Geophysics, 2005, University of Lagos, Nigeria.

M.Sc. Petroleum Geophysics, 2010, Imperial College London, UK.

- Work Experience: WesternGeco Norway.

Jessie Arthur

B.Sc., Geophysics, 2003, University of Alberta

M.Sc. Geophysics, 2013, University of Calgary

- Work Experience: ConocoPhillips

Roohollah Askari

B.Sc. Applied Physics, 2002, University of Hormozgan

M.Sc. Geophysics, 2005, University of Tehran

Ph.D. Geophysics, 2013, University of Calgary

- Work Experience: CGGVeritas, Calgary

Rafael Asuaje

B.Sc. Mechanical Engineering 2005

M.Sc. Mechanical Engineering 2006

- Work Experience: Faurecia Interior Systems.

Peng Cheng

- B.Sc. Applied Geophysics, 2001, Jilin University, China
M.Sc. Electrical Engineering, 2005, Peking University
Ph.D. Geophysics, 2013, University of Calgary
- ARCIS Seismic Solutions

David Cho

- B.Sc. Physics and Geophysics, 2007, University of Calgary
Ph.D. Geophysics, 2013, University of Calgary
- Work experience: Sensor Geophysical Ltd.

Raúl Cova

- B.Sc. Geophysical Engineering, 2004. Simon Bolivar University, Venezuela.
Graduate Diploma in Petroleum Studies, 2011. IFP School. Venezuela
- Work experience: PDVSA Intevep. Venezuela

Jean Cui

- B.Sc. Geophysics, 1998, Petroleum University
M.Sc. Geophysics, 2005, China University of Mining & Technology
- Work experience: Nexen Inc.

Tianci Cui

- B.Sc. Geophysics, 2013, China University of Petroleum (Beijing)

Jessica Dongas

- B.Sc. Hons. Geological Sciences, 2013, Queen's University
- Work experience: Alberta Geological Survey, Edmonton

Sina Esmaeili

- B.Sc.: Physics, 2009, Science and Research University - Iran
M.Sc.: Field Theory and Particle Physics, 2011, Science and Research University, Iran

Patricia Gavotti

- B.Sc. Geophysical Engineering, 2006. Simon Bolivar University, Venezuela
- Work Experience: Hampson-Russell Reservoir Characterization Services
Caracas, Venezuela, Encana Corporation

Marcelo Guarido de Andrade

- B.Sc. Physics, 2006, University of São Paulo, Brazil
M.Sc. Geophysics, 2008, University of São Paulo, Brazil
- • Work Experience: Petra Energia S.A., Brazil

Saul Guevara

- B.Eng. Civil Engineering, 1984, National University of Colombia
M.Sc. Geophysics, 2001, University of Calgary
- Work Experience: Ecopetrol ICP

Melissa Hernández

- B.Sc. Geophysical Engineering, 2006, Simon Bolivar University, Venezuela
M.Sc. Geophysics, 2012, University of Calgary
- Work Experience: ConocoPhillips

Shahin Jabbari

- B.Sc. Mathematics applied in Physics, 1992, University of Tehran, Iran
M.Sc. Medical Physics, 1997, Tabriz University of Medical Sciences, Iran
M.Sc. Medical Physics, 2010, University of Calgary
- Work Experience: Encana Corporation

Hassan Khaniani

- B.Sc. Petroleum Exploration Engineering, 2003, Petroleum University of Technology
M.Sc. Petroleum Exploration Engineering, 2006, University of Calgary & Petroleum University of Technology
- Work Experience: Terras Persia Seismic Company (TPS), Nexen Inc.

Steve Kim

- B.Sc. Geophysics, 2010, University of Calgary

Jesse Kolb

- B.Sc. Physics, Minor in Geophysics, 2013, University of Maryland, USA

Oliver Lahr

- B.Sc. Pure and Applied Mathematics, 1988, University of Calgary
- Work Experience: Hampson-Russell Software Ltd.

Heather Lloyd

- Diploma in Fashion Design and Technology, 2004, Kwantlen Polytechnic University
B.Sc. Geology, 2010, University of Calgary
B.Sc. Geophysics, 2010, University of Calgary
M.Sc. Geophysics, 2013, University of Calgary
- Work Experience: Schlumberger, Calgary

Li Lu

- BSc., Geophysics, 1989, Daqing Petroleum University, China
- Work experience: CGGVeritas, Canada

Faranak Mahmoudian

- B.Sc. Applied Physics, 2000, Khage Nassir Toosi University
M.Sc. Geophysics, 2006, University of Calgary
Ph.D. Geophysics, 2013, University of Calgary
- Work Experience: Shell Canada

Paul McGee

- B.A.Sc. Engineering Physics, 1999, University of British Columbia
M.C.S. Computer Science, 2003, Carleton University
M.A. Geosciences, 2005, Princeton University

Shahin Moradi

- B.Sc. Applied Physics, 2006, University of Razi, Iran
M.Sc. Geophysics, 2010, University of Tehran, Iran

Shahpoor Moradi

- B.Sc. Applied Physics, 2000, University of Razi, Iran
M.Sc. Theoretical Physics, 2002, University of Razi, Iran
Ph.D. Theoretical Physics, 2006, University of Razi, Iran

E. Andrew Nicol

B.Sc. Hons. Geophysics, 2010, University of Western Ontario

M.Sc. Geophysics, 2013, University of Calgary

- Work Experience: Devon Canada

Davood Nowroozi

B.Sc. Mining engineering, University of Tehran, 1996

M.Sc. Mining engineering, University of Tehran, 1999

- Work Experience: Geophysicist at National Iranian Oil Company

Pan (Penny) Pan

B.Sc. Geophysics, 2012, Xi'an Shiyou University, China

Wenyong Pan

B.Sc. Computer and Software Engineering, 2009, China University of Geosciences (Beijing)

M.Sc. Geophysics, 2012, China University of Geosciences (Beijing)

Chris Petten

BSc. Physics, 2011, University of Calgary

BSc. Geophysics, 2011, University of Calgary

- Work Experience: University of Calgary Research Assistant - Stable Isotopes

A.-Nassir Saeed

B.Sc. Geology, 1991, University of Salahaddin

M.Sc. Geophysics, 1998, University of Science Malaysia

- Work Experience: Ikon Science

Adrian Smith

B.Sc. Honours Geophysics 2012, University of Western Ontario

- Work Experience: Husky Energy Inc.

Jian Sun

B.Sc. Geophysics, 2009, Shandong University of Science and Technology, China

M.Sc. Geophysics, 2012, Shandong University of Science and Technology, China

Todor Todorov

B.Sc. Exploration Geophysics, 1994, University of Mining and Geology, Bulgaria

M.Sc. Geophysics, 2000, University of Calgary

- Work Experience: Suncor Energy

Ben Wards

B.Sc. Hons. Applied and Pure Mathematics, 2003, University of Calgary

M.Sc. Applied and Pure Mathematics, 2005, University of Alberta

Bona Wu

B.Sc., Applied Geophysics, 1999, Jianghai Petroleum Institute, China

M.Sc., Geophysics, 2006 China University of Petroleum

- Work Experience: CGGVeritas

Student Theses

The following theses are included with the CREWES 2013 Research Report:

Ph.D.	Mahdi H. Al Mutlaq	Surface-consistent matching filters for time-lapse processing
M.Sc.	Jessie M. Arthur	A seismic study of active faults, Canterbury, New Zealand
Ph.D.	Roohollah Askari	Surface Wave Analysis and its Application to the Calculation of Converted Wave Static Corrections
Ph.D.	Peng Cheng	Anelastic attenuation in seismic data: modeling, measurement, and correction
Ph.D.	David Cho	Elasto-static and -dynamic Analysis of Subsurface Fracture Phenomena
M.Sc.	Melissa Judith Hernandez Quijada	Internal multiple prediction: an application on synthetic data, physical modeling data and field data
M.Sc.	Byron Matthew Kelly	Processing and Interpretation of Time-Lapse Seismic Data from a Heavy Oil Field, Alberta, Canada
M.Sc.	Heather Jeanne Eileen Lloyd	An Investigation of the Role of Low Frequencies in Seismic Impedance Inversion
Ph.D.	Faranak Mahmoudian	Physical Modeling and Analysis of Seismic Data from a Simulated Fractured Medium
M.Sc.	Edward Andrew Nicol	A Multicomponent Seismic Investigation of Natural and Induced Fracturing, Saskatchewan, Canada
Ph.D.	Abdolnaser Yousefzadeh	High Resolution Seismic Imaging using Least Squares Migration

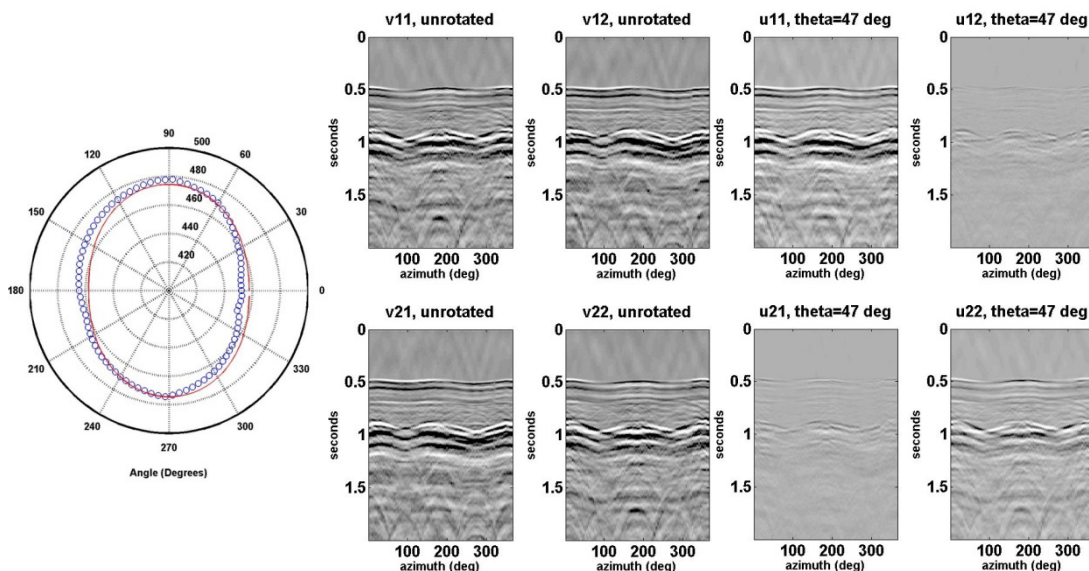
A physical model investigation of P and S wave azimuthal anisotropy on transmission

Khaled Al Dulaijan, Gary Margrave, and Joe Wong

ABSTRACT

Information related to fracture orientation and intensity is vital for the development of unconventional hydrocarbons, such as tight sand gas and shale gas. Numerical modeling provides a valuable tool for geophysicists to test and validate their methodologies that provide them with information about reservoirs. Fractures make numerical modeling more complicated and introduce complexities that might even require geophysicists to validate their numerical models before using them to test and validate their methodologies. Alternatively, physical modeling provides a unique opportunity to test, validate, and develop methods for characterizing fractured reservoirs. This report utilizes seismic physical modeling for fracture characterization, is a continuation to previous work conducted within CREWES, and is an in-progress work.

A two-layer model is built using vertically laminated Phenolic overlaid by Plexiglas to represent a fractured reservoir overlaid by an isotropic overburden. Three 9-component common-receiver gathers were acquired over that model in the laboratory. For each gather, 90 shot locations are distributed along a circle of radii 250 m, 500 m, or 1000 m and separated by 4° to cover all azimuths. P-wave first-arrival times were analyzed on all three gathers and fracture orientation was predicted. S-wave analysis suggests an error in the polarization direction of the horizontal transducers. An Alford rotation was applied to the four horizontal components and successfully minimized energy on components other than those two that have fast S wave and slow S wave.



Kinematic structural forward modeling for fault trajectory prediction in seismic interpretation

Mohammed Alarfaj* and Don C. Lawton

ABSTRACT

Deformation in the hanging wall of a normal fault is largely controlled by stratal movement along the fault surface. Hanging-wall beds rollover and collapse at fault-bends in the direction of active axial surfaces often seen as antithetic and synthetic secondary faults in seismic sections. The distinct relationship between a normal fault shape and its hanging-wall rollover allows for the construction of kinematic forward models which are used as an indicator of fault shape. The deformation geometry is affected by variables such as fault shape, amount of sedimentation, slip ratio and shear angles. We create balanced kinematic forward models to predict the shape of a master fault at depth and map the fault's surface from a 3D seismic survey.

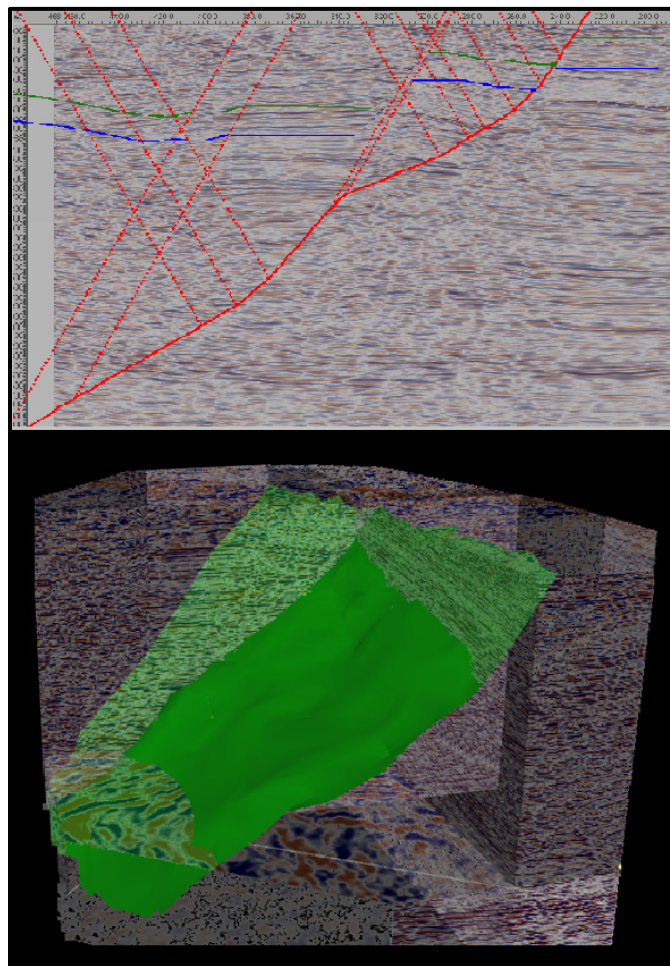


FIG. 1. a) Fault geometry prediction by kinematic structural forward modeling b) Modeled Fault surface.

Preliminary results using Acceleware's AxRTM API

Babatunde Arenrin, Gary Margrave, and Rolf Maier

ABSTRACT

We describe a seismic modelling program based on modules designed to perform forward modelling and reverse time migration, and show results derived from the code. The software we used demands that we provide a velocity model and necessary parameters, which must be fed to a central repository in predefined structures from which the forward modelling and migration software read the required information.

We perform forward modelling and reverse time migration on a simple velocity model consisting of three horizontal layers. To demonstrate the output to be expected from the software, we show a shot with a split spread configuration, with 800 receiver locations spaced 10 meters apart.

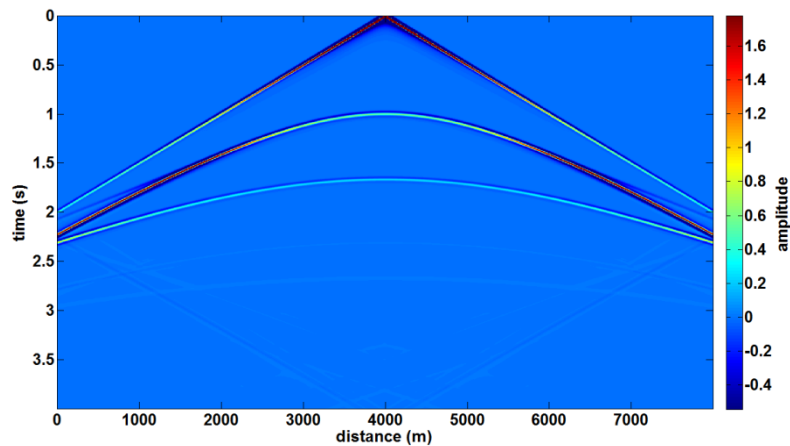


FIG. 1. A shot gather.

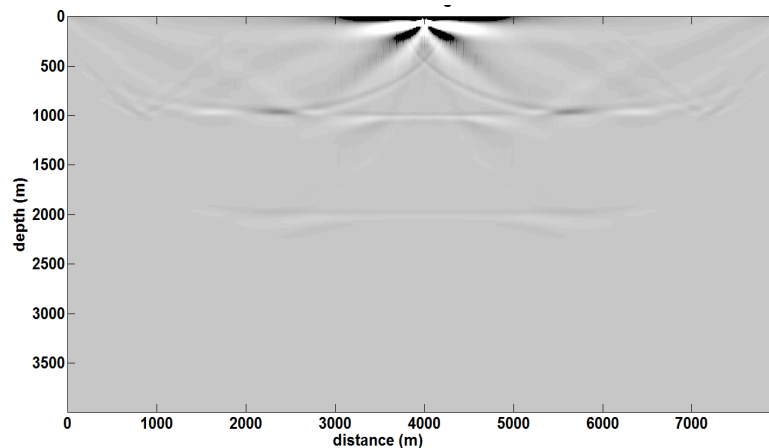


FIG. 2. The migrated shot gather.

Turning-ray tomography and tomostatics

Babatunde Arenrin*, Gary Margrave, and John Bancroft

ABSTRACT

Turning-ray tomography is a good tool for estimating near surface velocity structure, especially in areas where conventional refraction statics fails such as in the case of a hidden layer. The velocity model from turning-ray tomography can be used for static correction, wave equation datuming and prestack depth migration. In this research we apply turning-ray tomography to the statics problem of the Hussar 2D seismic line. This process is referred to as tomostatics. The travelttime tomography algorithm is similar to the constrained damped simultaneous iterative reconstruction technique (CDSIRT). The two-point problem for ray-tracing interpolation was used for forward modelling. To verify results from tomostatics, we compared datasets after tomostatics with datasets using the delay-time approach of a conventional refraction statics correction. The inversion result converged after 50 iterations and was used for statics correction. This inverted velocity model is reliable to a depth of about 750 meters, i.e. from the surface location to about one-fifth of the farthest offset (the recommended depth of sounding for turning rays). Our results show that the velocity model from turning-ray tomography reveals a hidden, slow velocity layer between two fast velocity layers that conventional refraction statics would not detect. The hidden layer is in agreement with the interval velocities from well logs. As we would expect, the stacked section, after applying tomostatics, shows better continuity of events compared to the stacked section from conventional refraction statics.

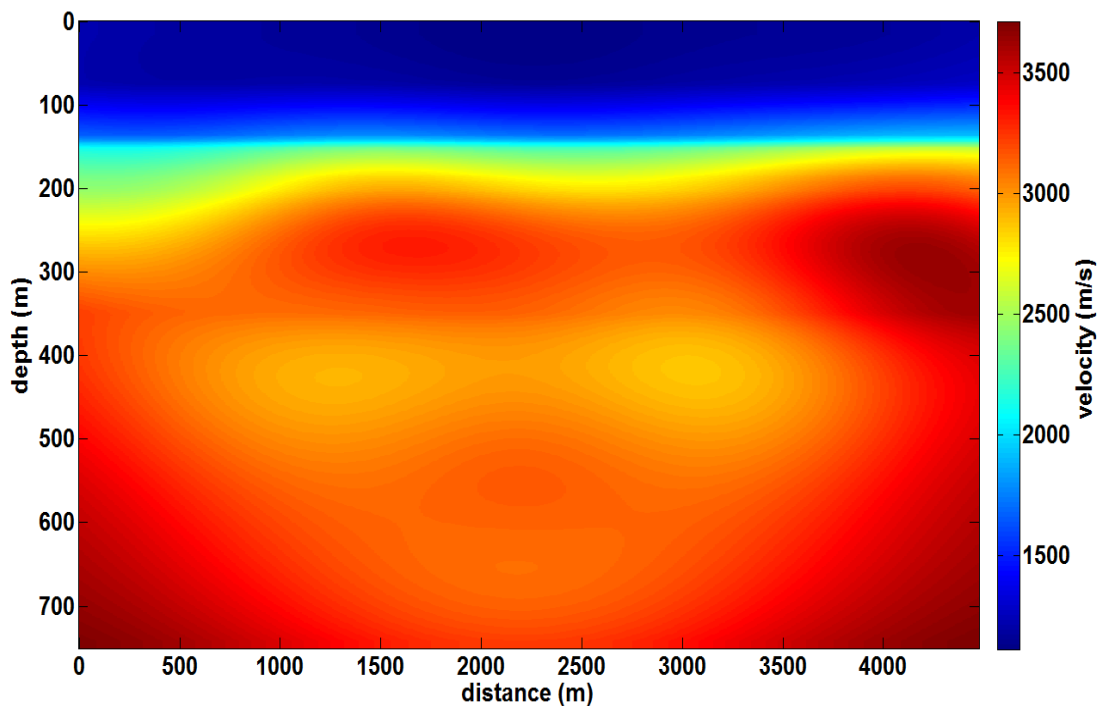


FIG. 3. Velocity model after 50 iterations.

Seismic interpretation of the Canterbury Plains, New Zealand

Jessie M. Arthur and Don C. Lawton

ABSTRACT

The 2010-2011 Canterbury earthquake sequence on the South Island of New Zealand occurred in a region where hidden faults systems were unknown, but were suspected. Following the 2011 Christchurch earthquake, 2D seismic reflection data was acquired in the Canterbury region. The seismic data, along with a regional tectonic and geologic overview, is used to image, interpret, and identify faults extending to basement structure beneath the Canterbury Plains.

Hidden fault structures have been suspected in the Canterbury Plains (Pettinga et al., 2001); however the region has been largely unstudied with very little well control and a lack of seismic data. This research contributes to constraining seismic hazard and risk assessment by identifying the presence of faults beneath the central Canterbury plains and within the city of Christchurch in newly acquired 2D seismic profiles.

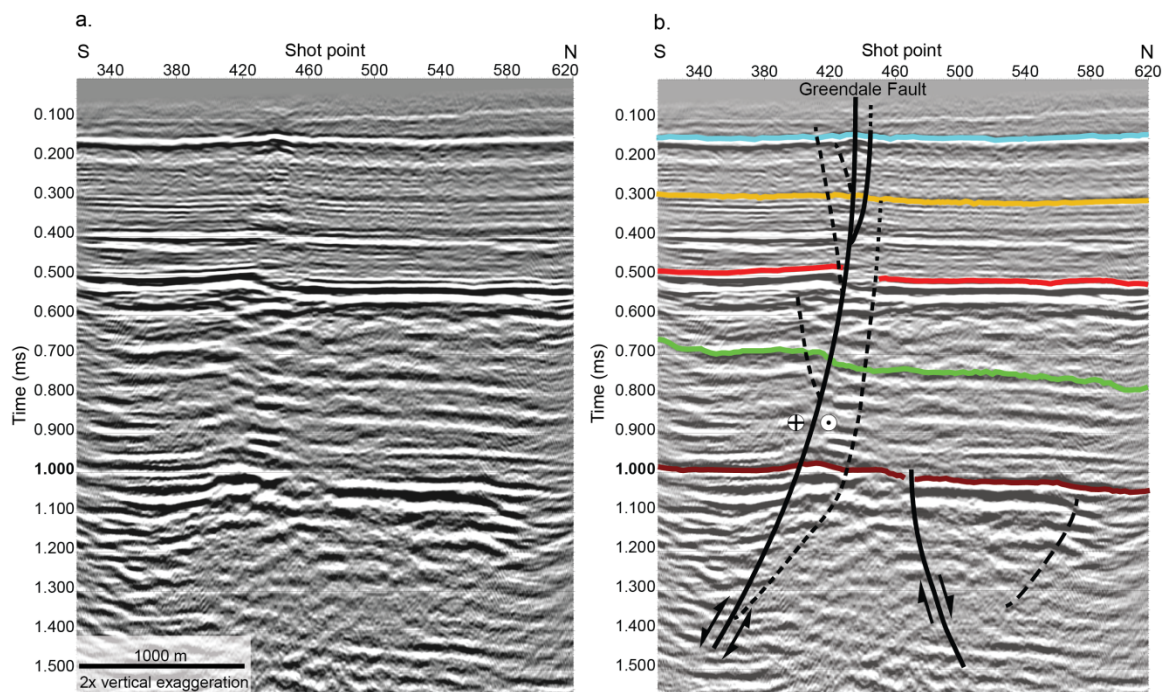


FIG. (a) Highfield Road seismic line without interpretation. (b) With interpretation. The 125,000 year gravels are represented by the light blue horizon, the Top of the Kowai formation is represented by the yellow horizon, the Miocene volcanoclastics/Mid-Tertiary limestone is represented by the red horizon, the Top of the Paleogene (?) is represented in green, and the undifferentiated Mesozoic basement is picked in brown. The Greendale fault is illustrated below station 440, where the fault ruptured the surface. Fault splays are indicated by short dashed lines off the main Greendale Fault.

Estimation of Converted Waves Static Corrections Using CMP Cross- Correlation of Surface Waves

Roohollah Askari, Robert J. Ferguson, J. Helen Isaac CREWES, Department of Geoscience, University of Calgary

ABSTRACT

We enlarge upon the idea of CMP Cross-Correlation of Surface Waves (CCSW) to obtain an S-wave velocity model for the calculation of PS receiver static corrections. In our approach, we cross-correlate each trace of a shot record with a reference trace that is selected from within the shot gather based on high signal to noise ratio. New midpoints that relate to the correlated traces are then calculated. We calculate the phase velocity for each CMP gather, and we convert the resulting dispersion curve to an S-wave model. Our approach is faster than the conventional CCSW because in the conventional CCSW all traces within a CMP gather are cross-correlated with each other. In this study we show that, in order to have a precise estimation of a dispersion curve, we only consider those traces that lie in a spatial window and we found that the optimum window length (aperture) should be close to (one to one and half times) the maximum wavelength in a CMP gather. When the aperture is optimum, we see a high resolution image of each mode within the dispersion curve that avoids modal interferences. We obtain 2D near surface S-wave velocity models for two real data sets. By decimating traces from the first dataset, we show that we can obtain a good trend of S-wave statics relatively similar to those obtained from the original dense array data. This demonstrates that CCSW has a capacity to address static correction of converted waves when geophone spacing is wide. Using the second data set, we show the importance of wavelength-dependent aperture for estimating the phase velocity. We obtain static corrections based on an S-wave velocity model obtained from CCWS and successfully apply them to the data.

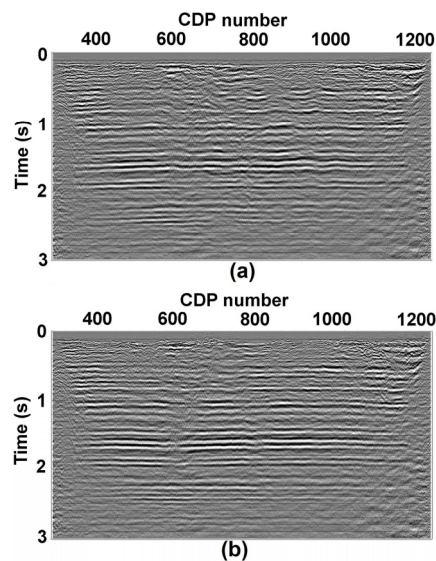


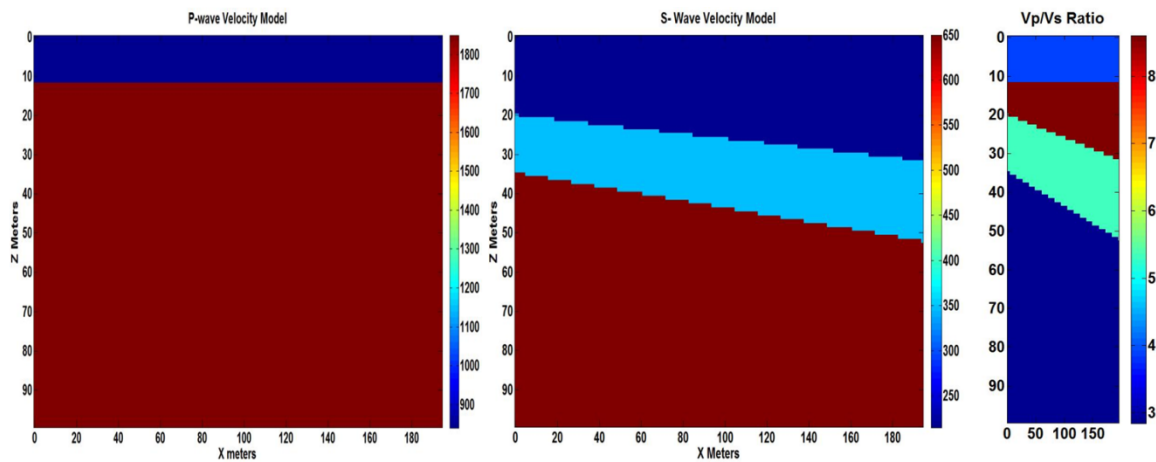
FIG. 1. (a) Stacked Hussar data before static correction, (b) the stacked data after applying the calculated S-wave receiver static.

Analysis of multicomponent seismic data recorded with a new hydraulic thumper source

Rafael Asuaje

ABSTRACT

This paper examines the performance of the new, multicomponent weight drop source built by CREWES. The source was tested on the University campus to generate P-wave and S-waves and to provide a detailed velocity structure of the near-surface. The source generates SH-waves by orienting the source mast ± 45 degrees from the vertical and subtracting records generated with opposite polarities of the source. This cancels P-waves and constructively adds SH mode.



Data collected shows that the uppermost layer of the shallow subsurface has a P-wave velocity of 840 m/s and the SH-velocity of 215 m/s, yielding V_p/V_s ratio of 3.90.



Comments on wavefield propagation using Reverse-time and Downward continuation

John C. Bancroft

ABSTRACT

Each iteration of Full-waveform inversion requires the migration of the difference between the real data and new data created from an updated model. The migration process has typically used the Reverse-time algorithm, though alternative algorithms are now being used to create the data for cross-correlation at the imaging condition. The cross-correlation data contains artifacts that are very low frequency and bias the reflectivity. The cause of these low frequency artifacts are identified and evaluated using Reverse-time and Downward-continuation wavefield propagation of energy using a wavelet on a one dimensional model. The model contains varying velocities that produce multiples that are displayed with a two dimensional array in space and time. The wavefields are propagated using finite difference and phase-shift algorithms, with various initial conditions and boundary values. The resulting cross-correlations and then processed to evaluate their potential for representing the reflectivity of the model.

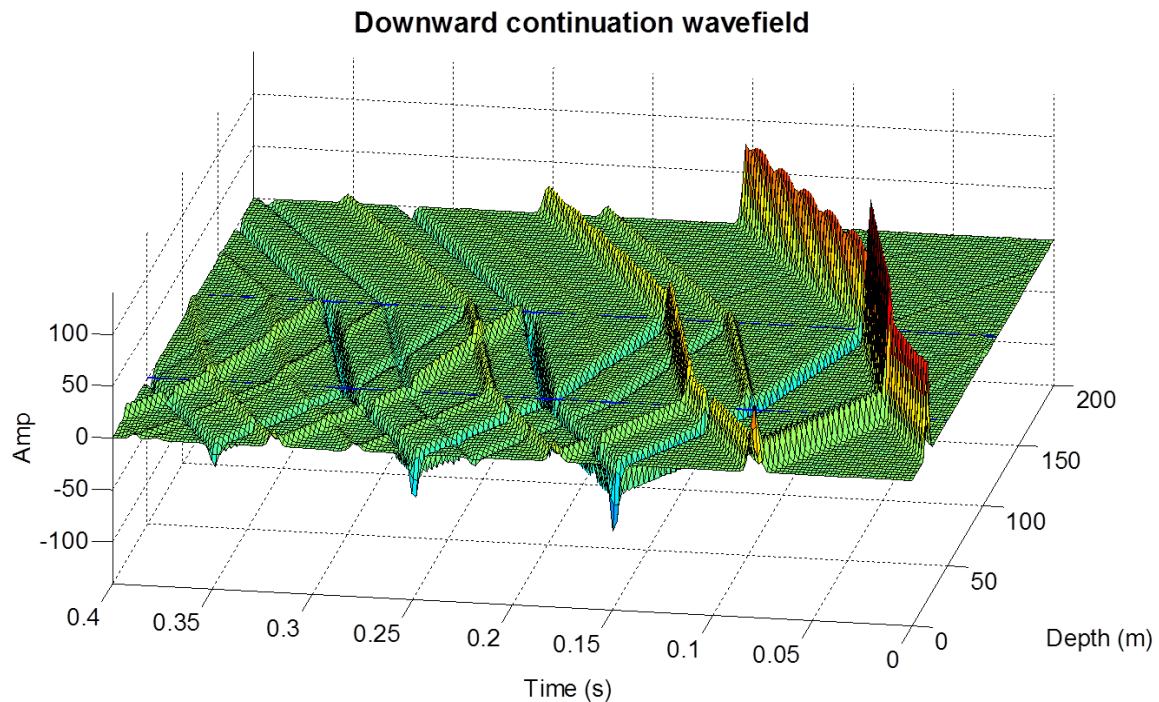


FIG. A full wavefield was created in (z, t) space from a source at zero time and forward propagated in time to the maximum time. Reflection and multiple energy was created from two velocity boundaries, an open reflectivity boundary at the surface, and an absorbing boundary at the basement. The above image is a recreation of the full wavefield using a downward continuation algorithm.

Modelling migration, and inversion using Linear Algebra

John C. Bancroft* and Rod Blais

ABSTRACT

Modelling, migration, and inversion, can all be accomplished using linear Algebra. Key to these processes is the diffraction array that is multidimensional. Two dimensional poststack migrations require a fourth order diffraction array. Current processing practices for Least-squares analysis require a diffraction array that is two dimensional (a matrix), with one dimensional vectors for the reflectivity and seismic data. These matrix and vectors can be derived from multidimensional data by helical unwrapping. The field of Multidimensional Linear Algebra may allow the data to retain their multidimensional arrays, but require defining processes such as a two dimensional transpose of a four dimensional array. Modelling, migration, and inversion are demonstrated with very small dimensions using MATLAB software.

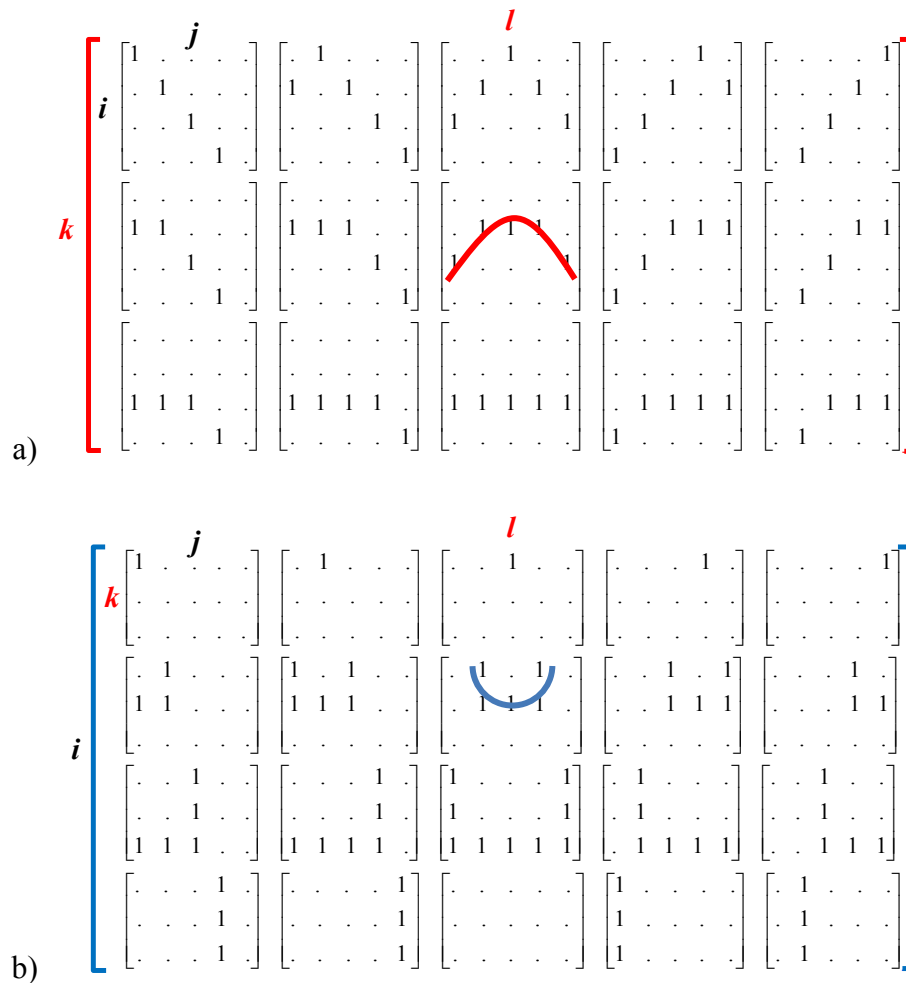


FIG. Simplified matrices for 2D data a) for the diffractions (hyperbolic shape), and b) the 2D transpose of (a) showing migration semicircles.

Resolution enhancement with deconvolution after migration

John C. Bancroft, Thais Guirigay, Naser Yousefzadeh, and Helen Isaac

ABSTRACT

Deconvolution is a process that is normally applied to seismic data before migration to enhance the resolution. We propose that deconvolution should also be applied to the data after a poststack or a prestack migration. We address the objections to this process, then present arguments for its use. The deconvolution process should be applied as a multidimensional process to the complete data. However, a typical trace process is usually sufficient to provide a significant enhancement in the resolution after migration. Two data examples are provided that show significant improvement in the resolution of the data by use of a simple spiking deconvolution, that was applied to each trace after migration. (Update of previous paper.)

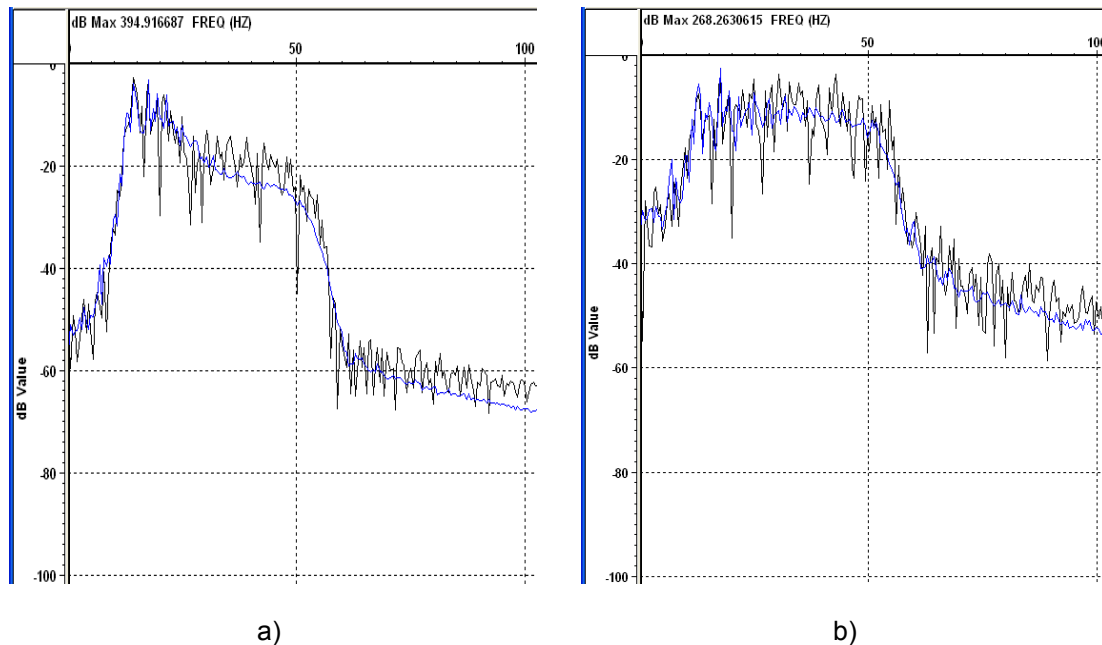


FIG. Amplitude spectra of a) the prestack migrated data, and b) the migrated data with deconvolution applied after the migration.

CREWES in the Field, acquisition and preliminary results

Kevin L. Bertram*, Malcolm B. Bertram, Kevin W. Hall, Eric V. Gallant, Don C. Lawton, Gary F. Margrave and Kristopher A.H. Innanen

ABSTRACT

CREWES is unique in that it has access to modern commercial grade seismic survey equipment. Every year this equipment is used to perform real world experiments as well as demonstrate how acquisition is done. In 2013 CREWES has completed the following acquisition projects: a) a GPS survey for new observation well installation at the Priddis test site; b) a small demonstration of the recording system to the new students of CREWES; c) a small test survey to test downhole geophones as well as some fibre optic sensors; d) resurveying the well location for permitting reasons; e) the 2013 GOPH549 undergraduate Field School project within the city of Calgary, Alberta; f) an experiment at the Priddis test site to test the response from the geophones installed in the well as well as various different sources.

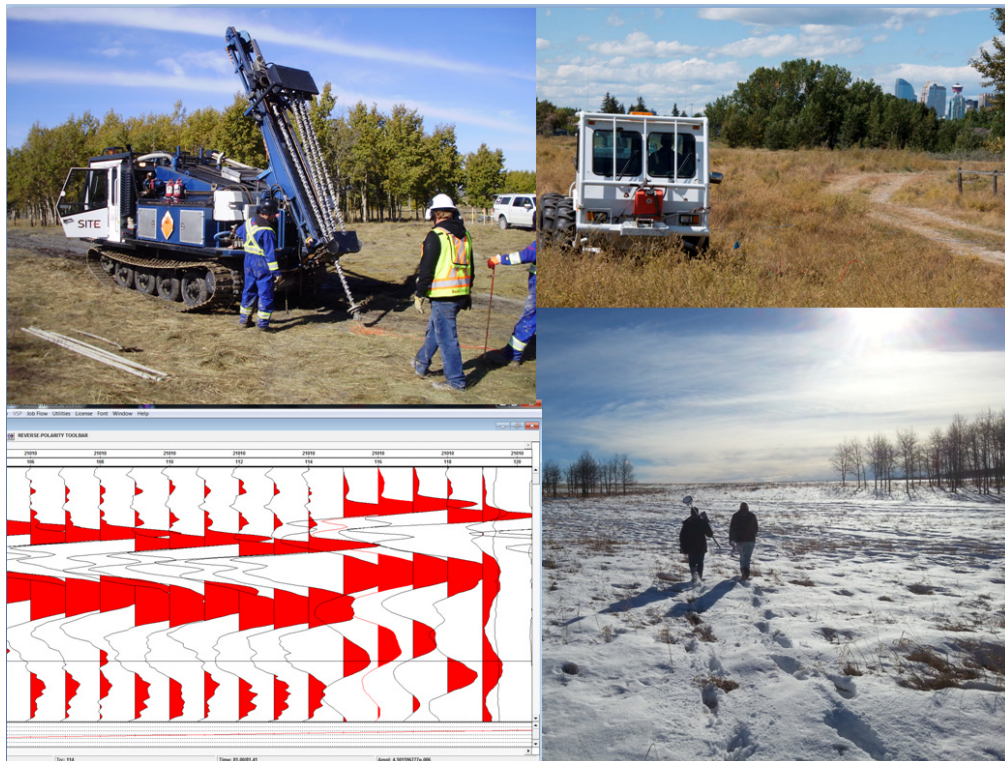


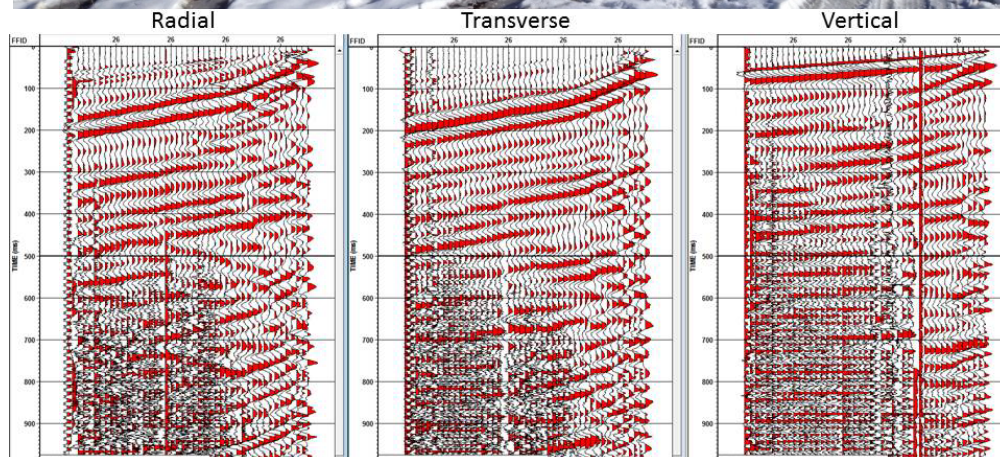
FIG. 1. CREWES working outside the office.

Recent data from the Priddis Geophysical Observatory

Malcolm B Bertram, Don C Lawton, Kevin W Hall, Kevin L Bertram, Eric V Gallant

ABSTRACT

An analysis of selected data from two surveys conducted using the recently completed shear wave accelerated weight-drop seismic source shows that there is good shear wave energy generated by this device. Data is presented from both surface and downhole geophones deployed at the new well location at the Priddis Geophysical Observatory in October 2013. The first survey used dynamite, an Envirovibe and the shear wave weight-drop as sources, while the second was a follow up survey to check completion of casing cementing and used just the Envirovibe and the shear wave weight-drop.



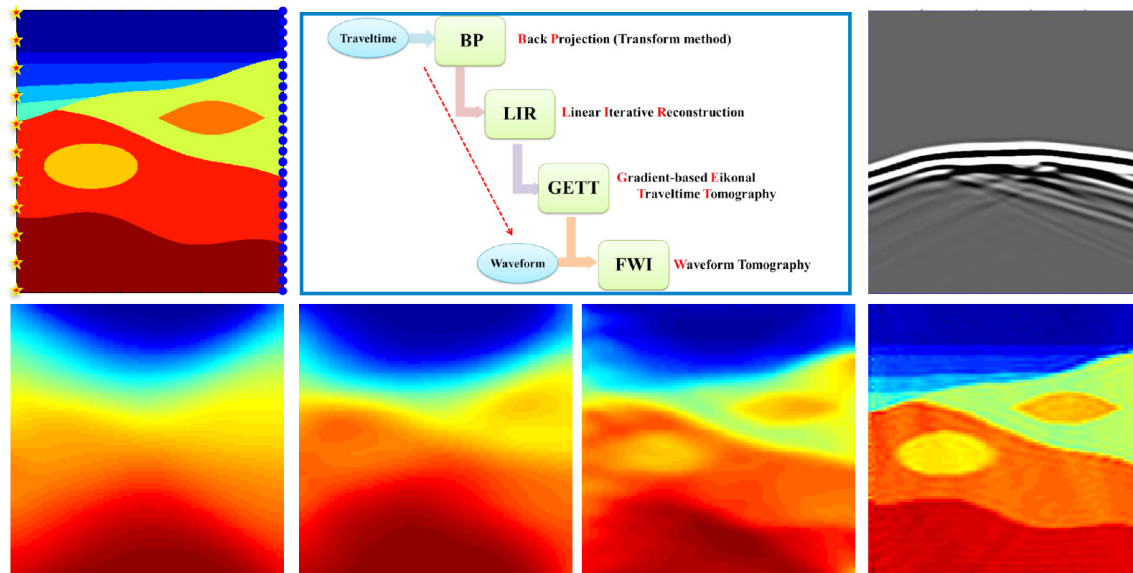
The Envirovibe and the shear wave accelerated weight-drop source at Priddis (top). Downhole geophone data from the new observation Well 1 (bottom). (3C GS14 geophones).

A hybrid tomography method for crosswell seismic inversion

Danping Cao and Wenyuan Liao

ABSTRACT

The waveform tomography, or full waveform inversion (FWI), is in general better than the ray tomography method; however a reliable initial model is usually required to ensure the success of seismic inversion. In this work we designed a cascade-like hybrid tomography technology to solve the crosswell seismic inversion problem. The new method is a combination of several widely used tomography technologies. We start from the Radon-transform based back projection (BP) method, which produces a smooth initial velocity model. Next, the Linear Iterative Reconstruction (LIR) method is adopted to update this initial model, then it is further improved by the nonlinear Gradient-based Eikonal Traveltime Tomography (GETT) method. The velocity model reconstructed from the previous multi ray tomography methods is sufficiently reliable to serve as the initial model for the computational intensive waveform tomography method, from which the accurate velocity model is obtained. The numerical example shows that this hybrid tomography method has great potential in reconstructing accurate acoustic velocity or other high-resolution reservoir characterization for crosswell seismic inversion. With this hybrid tomography method, the inversion result of three cascade ray tomography methods is used as the initial model for FWI that provide a perfect initial velocity model, which leads to a significant reduction for the computation time and the iteration number. It is noticeable that this hybrid tomography method is able to obtain an accurate velocity even when the recorded seismic data is in poor coverage at spatial and the signal-to-noise ratio is low.



Comparison of Q-estimation methods: an update

Peng Cheng and Gary F. Margrave

ABSTRACT

In this article, three methods of Q estimation compared: a complex spectral ratio method, the centroid frequency-shift method, and a time-domain match-filter method. Their performance for Q estimation is evaluated using synthetic data and real data in terms of accuracy and robustness to noise. Testing results shows that the complex spectral-ratio method, with phase information employed, can obtain improved estimation results. The centroid frequency-shift method is robust to noise and gives stable estimations, while the accuracy of estimated result is subject to the frequency band used to estimate centroid frequency and variance. The match-filter method is robust to noise and can give accurate estimation result for both VSP data and reflection data.

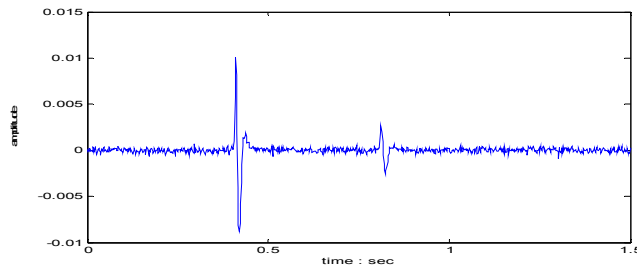


FIG. 1. An attenuated seismic trace with noise level of SNR=4 and constant Q of 80.

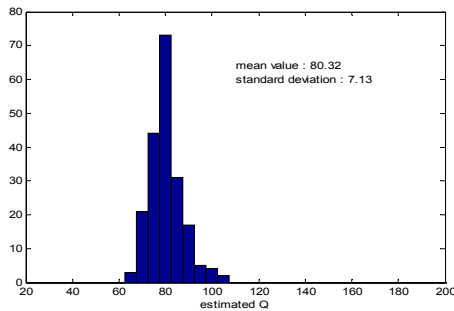


FIG. 2. Histogram of estimated Q values by complex spectral-ratio (only phase information is employed) method using 200 seismic traces similar to the one shown in figure 1.

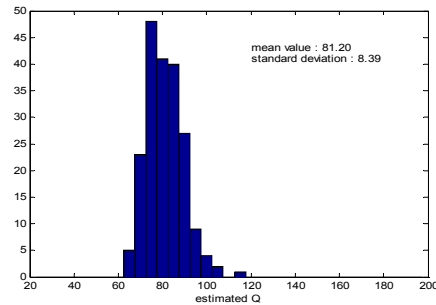


FIG. 3. Histogram of estimated Q values by centroid frequency-shift method using 200 seismic traces similar to the one shown in figure 1.

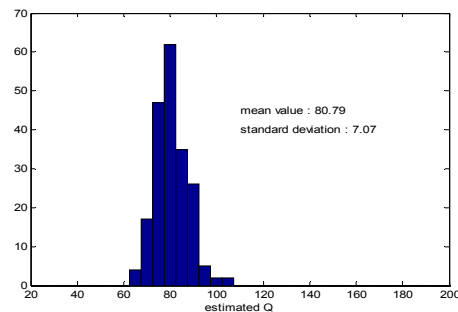


FIG. 4. Histogram of estimated Q values by the match-filter method using 200 seismic traces similar to the one shown in figure 1.

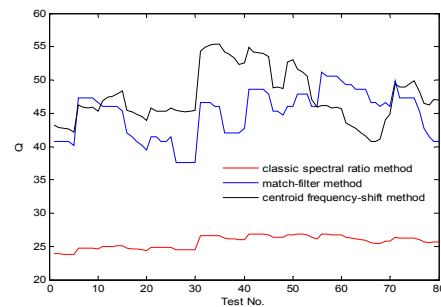


FIG. 5. Q estimation by centroid frequency-shift method and match-filter method using 80 pairs of real VSP data.

Cross-correlation based time warping of one-dimensional seismic signals

David Cho

ABSTRACT

The computation of a dynamic displacement field between pairs of seismic traces has numerous geophysical applications including the estimation of displacement vectors in time lapse seismic, P- to S-wave image registration and residual moveout correction. In this paper, I present a cross-correlation based methodology for the estimation of small time displacements between signals followed by stretching to match the signals. The utility of the algorithm was demonstrated through a synthetic time lapse example illustrating production effects and the associated time shifts between baseline and monitor surveys. The differencing of the baseline and monitor traces prior to warping results in apparent amplitude changes below the reservoir interval. Upon application of the warping algorithm, the undesirable amplitude changes below the reservoir interval are reduced.

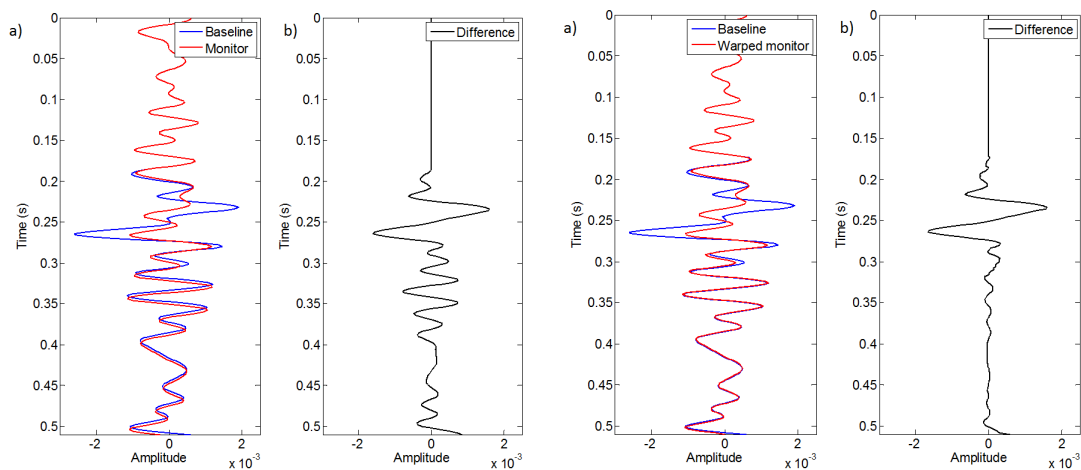


FIG. 1. Comparison of 4D a) baseline and monitor traces and their b) difference before and after the application of the proposed warping algorithm.

Approximate- vs. full-Hessian in FWI: 1D analytical and numerical experiments

Raul Cova and Kris Innanen

ABSTRACT

Feasibility of using Full Waveform Inversion (FWI) to build velocity models has been increasing as the computational power and more comprehensive forward modelling approaches have arose. Traditionally, the objective function used during the FWI process has been minimized by the means of steepest-descent methods by conditioning the gradient function. Quasi- and full-Newton methods use the Hessian, or an approximate to it, as a gradient conditioning. For a 1D scalar medium, we derived an analytical expression for the approximate-Hessian suggesting that it brings the model update to within a first order approximation of the exact reflection coefficient for a single interface. In its functional form the Hessian is represented by delta functions into the integration for computing the model update. Compared to the approximate-Hessian, we found that the full-Hessian provides additional scaling information at the depth of the interface, improving the accuracy of the inversion. These ideas were also tested using a numerical example displaying how both Hessians move very fast toward the actual velocity model. It is also shown that the full-Hessian leads to a very accurate inversion in the presence of large velocity contrasts superior to the approximate-Hessian. Hence, the full-Hessian may achieve a faster convergence and accurate inversion while providing amplitude information. For large velocity contrasts, or in a 2D case, where strong AVO effects may be present, the application of the full-Newton FWI might be a good candidate.

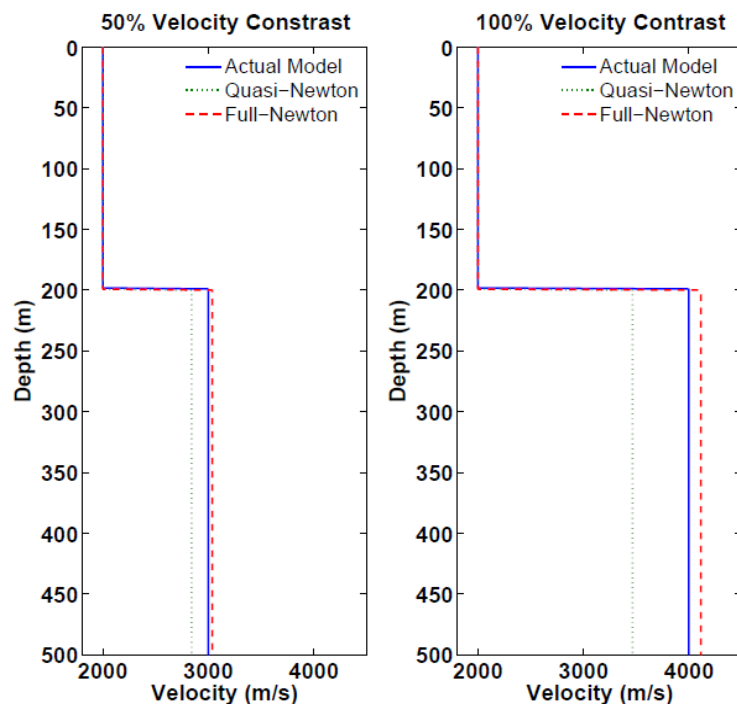


FIG. 1. FWI results using the approximate- and full-Hessian for a 50% (left) and a 100% (right) velocity contrasts.

An interferometric solution for raypath-consistent shear wave statics

Raul Cova*, David Henley and Kris Innanen

ABSTRACT

Converted-wave data processing requires the computation of shear-wave statics for the receiver side. Conventionally this is done under the assumption of surface consistency. However, if the velocity change between the low velocity layer (LVL) and the medium underneath is smooth, the vertical raypath assumption that supports the surface consistent approach is no longer valid. This feature results in a non-stationary change of the statics that needs to be addressed in order to properly solve the problem. In this paper the radial-trace (R-T) transform is used for moving the data to a raypath consistent framework where the statics change was showed to be approximately stationary. In this domain traveltime interferometry was applied to retrieve the delays caused by the near surface. Cross-correlation of the delayed traces with a model trace free of statics was showed to return a cross-correlation function that carries the statics information. These functions were convolved with the original traces to remove the delay caused by the near surface. Since all the operations are done in the R-T domain an inverse radial trace transform was applied to return the data to the space-time domain. Stacked sections computed using surface- and raypath-consistent solutions showed how the latter one effectively removed the statics by addressing the non-stationarity of the problem. The analysis of the trend of the cross-correlation functions for different receiver locations showed that there is a link between the delays captured by these functions in the R-T domain and the traveltimes through the near surface at different raypath angles. Such information could be used in an inversion algorithm to retrieve a velocity model for the near surface.

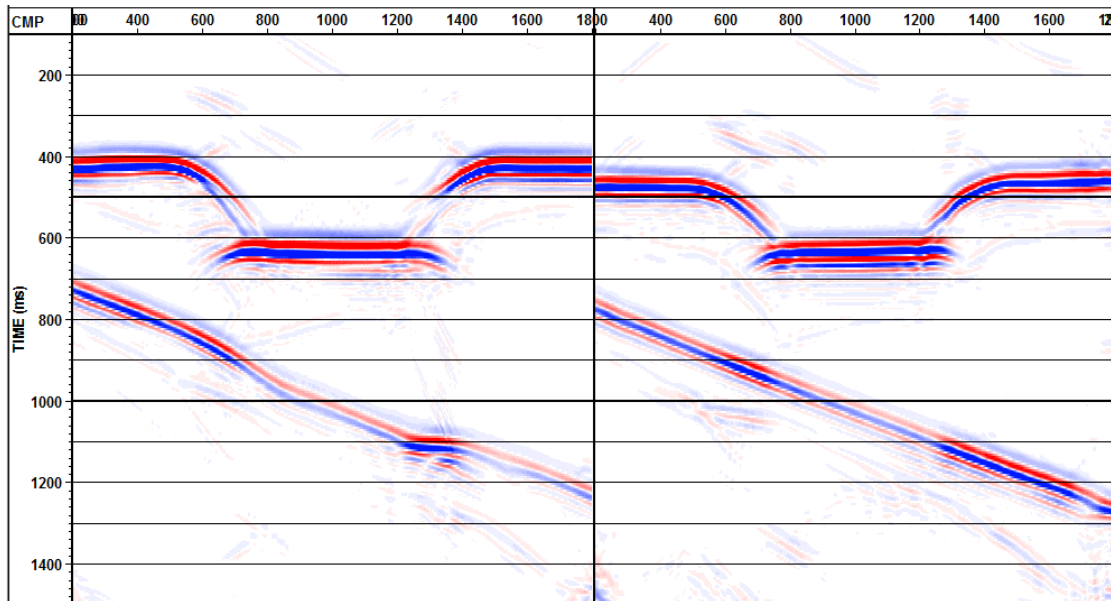


FIG. 1. Converted-wave stacks corrected by surface-consistent (left) and interferometric raypath-consistent (right) receiver statics.

Non-stationary S-wave statics

Raul Cova, David Henley and Kris Innanen

ABSTRACT

Shear-wave statics are one of the main problems in converted-wave processing. The lack of a good correlation between P- and S-wave velocities in the near surface introduces a whole new problem to be solved. Due to its very low velocity values the magnitude of the S-wave statics are several times larger than the P-wave statics, producing a very destructive effect when stacking traces. In this paper it is shown how S-wave statics may also show a non-stationary behaviour. This effect was studied in terms of variations in the transmission angle through the low velocity layer (LVL) due to changes in offset and as a result of the structure of the LVL. An analytic expression for computing deviated travel times through the LVL in terms of its dip, thickness and velocity is proposed here. This expression may be used as the engine for an iterative non-linear inversion algorithm that will allow us to compute velocity models for the near surface given a set of delay times and the ray-path angles associated with them.

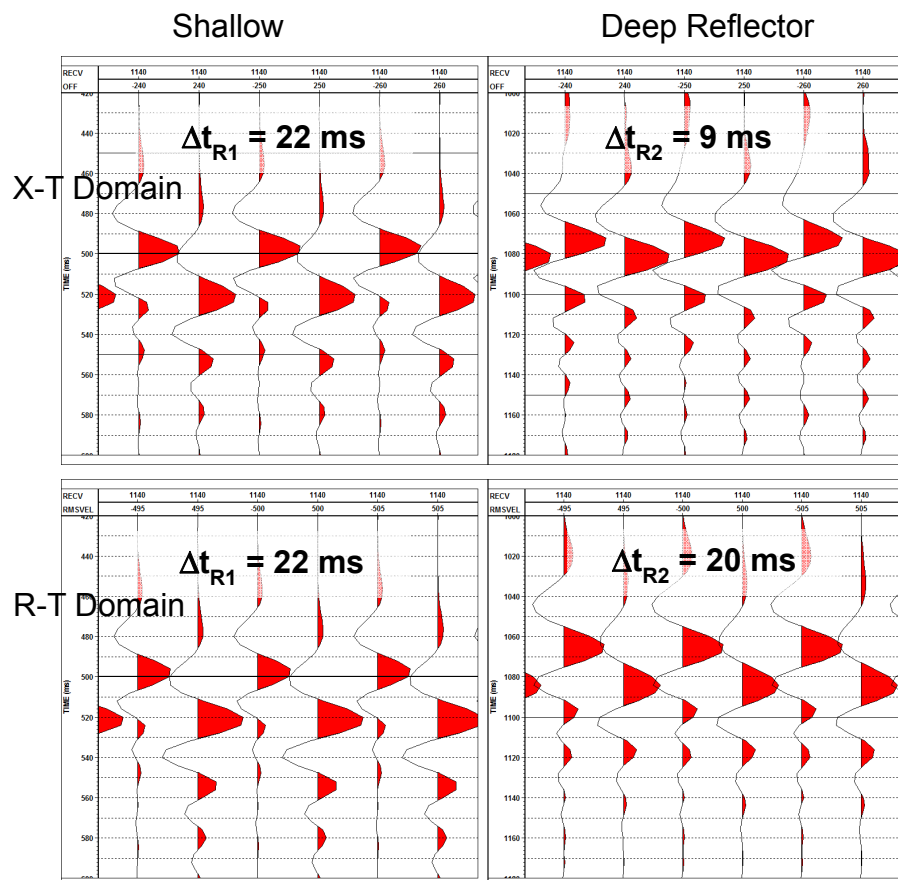


FIG. 1. Zoomed receiver gathers showing non-stationary statics in the X-T domain (top) and approximately-stationary statics in the radial trace (R-T) domain (bottom).

Seismic modeling and inversion for reflections from fractures

Xiaoqin (Jean) Cui*, Laurence R. Lines and Edward S. Krebs

ABSTRACT

We have studied a theory of linear slip nonwelded contact interfaces (Schoenberg, 1980) and extended the theory to simulate the subsurface fracture features by developing a 2D/3D numerical forward modeling method and a method of analysis of the PP and PS seismogram characteristics regarding the responses of the fractures (Cui, Lines and Krebs, 2012). In this paper we present a new AVO inversion equation that depends upon the theory of the linear slip nonwelded contact interfaces. We use the assumption that the two half spaces are in imperfect contact due to the presence of fractures, meaning that only the stresses produced by the wave are continuous across a fracture, and that the displacements are discontinuous across the fracture. The new equation can be inverted not only to estimate the subsurface elastic parameters contrasts, but also to estimate eight parameters related to the fractured media. This paper analyses fracture models and compares the results of numerical forward modeling between media with interfaces in perfect welded contact (no fractures) and with interfaces in imperfect linear slip nonwelded contact (with fractures) (Figure 1). Inversion results of three models are also compared (Figure 2).

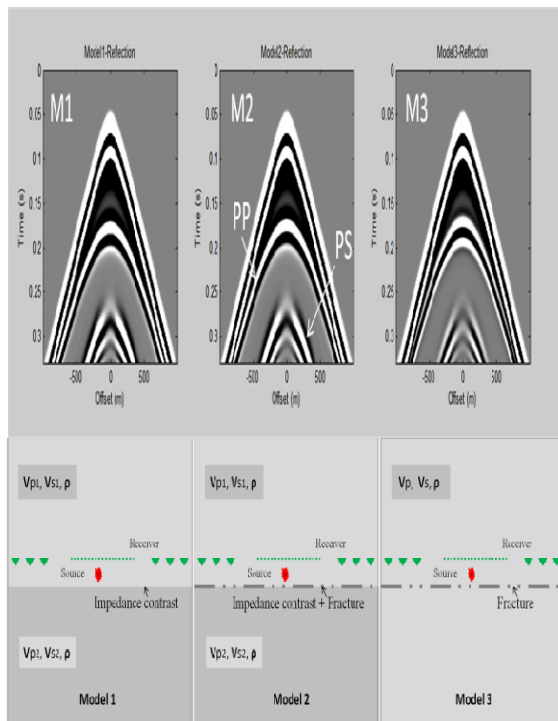


FIG. 1. Three shot records (the top) of the three models (the bottom) are normal impedance contrast (M1), the combination of the impedance contrast plus a fracture (M2) and a fracture embedded in single medium (M3).

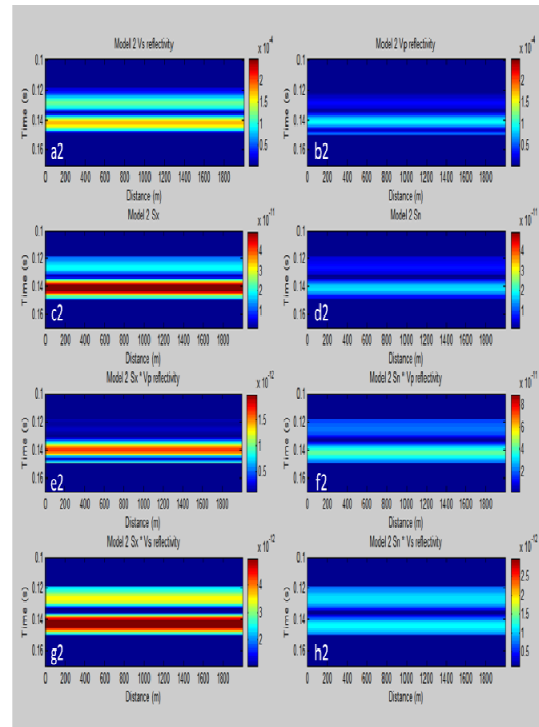


FIG. 2. Inversion results for the model 2. a2, b2 are V_s and V_p reflectivity. c2, d2 are fracture tangential and normal compliances S_x , S_n . e2, f2, g2 and h2 are V_p , V_s reflectivity multiplying S_x , S_n respectively.

Anelastic (poroviscoelastic) medium – the S_H – wave problem

P.F. Daley

ABSTRACT

When considering the problem of extending seismic wave propagation in an elastic medium to a poroviscoelastic medium, replacing real quantities by complex equivalents has been the accepted way to proceed. Given the number of works dealing with, what could be called the inadequacy of this method of this approach, another line of reasoning might be in order. Starting with Biot's equations for a poroviscoelastic medium, employing a simplification route, results in the S_H (modified) potential related to the vector equation of motion. Biot's theoretical development of wave propagation in a medium comprised of a fluid within a porous solid may be overly complicated for the pursuit of an alternate methodology for addressing this problem in its most basic form. As a consequence, the *telegraph* equation might be a more modest, yet informative analogue to consider, as it is a well studied problem from mathematical and physical perspectives. In what follows an S_H potential wave equation is considered with attenuation introduced in a manner similar to that inherent in the telegraph equation. Additionally, the difficult situation will again be revisited, as it might be rationalized that a 1 – 2% modification of a real quantity such as velocity produces imperceptible effects in, say a reflection coefficient, while the same amount of perturbation introduced to make velocity a complex quantity results in significant dissimilarities between nearly similar initial input data. This is difficult to comprehend and seemingly at least as problematic to explain.

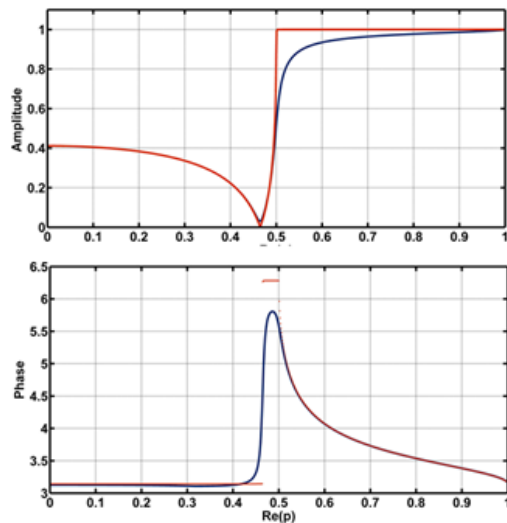


FIG. 1. An example of the S_H reflection coefficient when Q in the second layer is less than Q in the incident layer (difficult case).

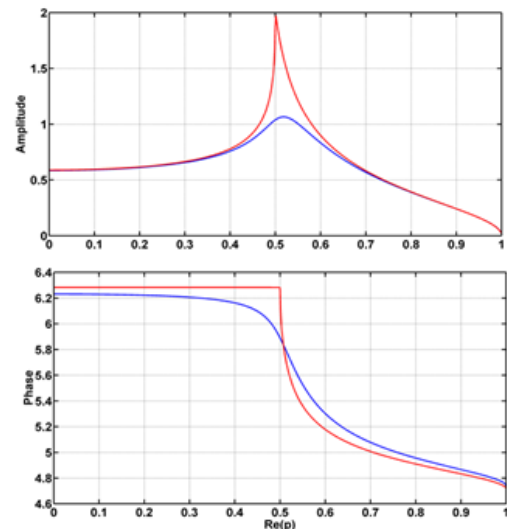


FIG. 2. An example of the S_H transmission coefficient when Q in the second layer is less than Q in the incident layer (difficult case).

Higher order analytic approximations to the $\check{P}\check{P}$ and $\check{P}\check{S}$ reflection coefficients – numerical methods and results

P.F Daley

ABSTRACT

The high frequency solution to the problem of a $\check{P}\check{P}$ and $\check{P}\check{S}$ reflected wave at a plane interface between two isotropic homogeneous halfspaces at near vertical and grazing incidence developed. In reflection seismology sub-critical reflections are often all that is required in data processing. A distorted (compared to the zero order geometrical optics approximation to the arrival) wavelet is seen on the traces in these areas. The correction terms derived as a result of the saddle point associated with a ray being close to branch point, together with other related quantities, are graphically presented.

$\check{P}\check{P}$ reflected wave, is considered in Červený and Ravindra (1970) and Brekhovskikh (1980). In each of these works a different conformal mapping is introduced so as to incorporate a real parameter in the solutions by high frequency methods involving the evaluation of integrals of the Sommerfeld type. After stating this, it should be noted that the motivation for considering the $\check{P}\check{S}$ reflected arrival is partly due to the fact that in the $\check{P}\check{P}$ reflected case the saddle point location may be obtained analytically, while in the $\check{P}\check{S}$ case this must be done numerically.

Another reason for revisiting this problem type is to introduce, in as simple a manner as possible, software for displaying the effects described above, which may be useful in the area of geophysical interpretation. To obtain analytical expressions for wave types such as the reflected $\check{P}\check{P}$ and $\check{P}\check{S}$ a thorough understanding of the formalism required to obtain solutions for these problems in the elastic case is an important and useful precondition.

Higher order approximations are required when the spherical nature of the incident (P – wave) must be considered. Although plane wave reflection coefficients are what are of interest here, some aspects of spherically wave incidence must be introduced. Again, to keep the implementation of the theory as simple as possible, only 3 additional parameters, beyond those for the computation of plane wave reflection coefficients are required. These are the distance of both the source and receiver above the reflecting interface and some reference frequency, usually associated with the source wavelet being used in the acquisition of the seismic data being processed.

More numerical experiments in high frequency edge diffraction

P. F. Daley

ABSTRACT

Formulae related to the diffraction of seismic waves by linear edges in elastodynamic media, based on an extension of the high frequency, zero order Asymptotic Ray Theory (ART) formulation are presented. Theoretical aspects of the problem have been minimized, as these have been developed in numerous notable works. The intention here is to present the basic methodology for numerical implementation into synthetic seismogram software. Schematics indicating relevant details such as the shadow boundary and the boundary ray are have been included. The identification of the boundary ray is required as the argument of the diffraction coefficient is dependent on the angle between the shadow boundary ray and the diffracted ray or equivalently the difference between the diffracted and direct arrival times. The direct geometrical arrival does not exist in the shadow region and its travel time is required to determine the argument of the diffraction coefficient which is done within the context of analytic continuation and the aforementioned limits of minimal theoretical discussion. A basic problem is considered to give a brief overview of the theory of edge diffractions. The geometry of this problem involves a wedge embedded in a halfspace in a manner such that the plane of incidence is the (r, z) plane and the wedge is such that its leading edge is perpendicular to this plane, i.e., parallel to the y axis. Both the source and receivers are located in the (r, z) plane.

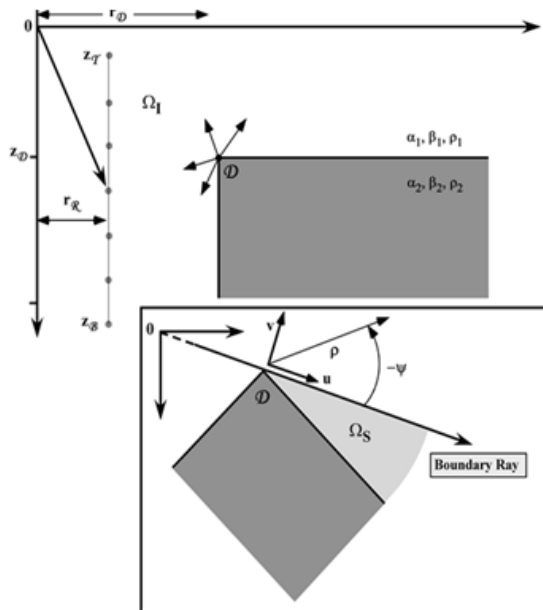


FIG. 1. Schematic of Model 2.

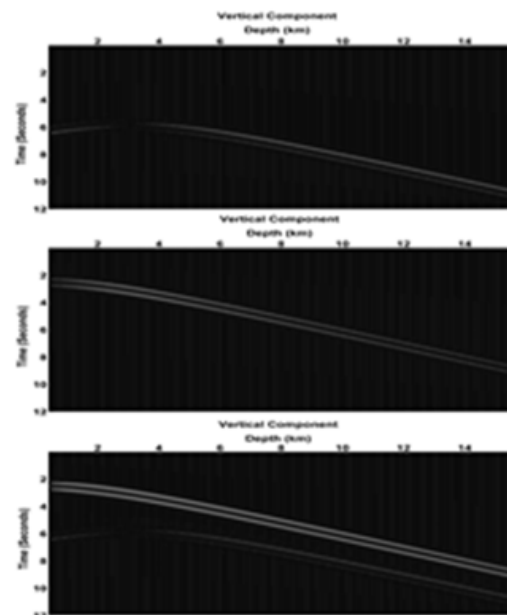


FIG. 2. Vertical component of displacement for Model 2 showing the direct, diffracted and combination of the two arrivals.

Recovering low frequency for impedance inversion by frequency domain deconvolution

Sina Esmaili and Gary F. Margrave

ABSTRACT

Acoustic impedance is a rock property that can be derived from seismic data and contains important information about subsurface properties. Direct measurements of acoustic impedance are available from acoustic and density well logs but these well data can provide the acoustic impedance only at the well's location. Mathematically, it is true that acoustic impedance can be calculated from earth's reflectivity function and this function could be estimated from seismic data. Additionally, estimation of reflectivity from seismic data is always bandlimited and affects acoustic impedance significantly. Acoustic impedance inversion can easily be computed by standard impedance inversion algorithm which uses well logs to fill in the low-frequency information that is missing in bandlimited seismic data.

In this study we investigate the performance of standard deconvolution and its ability to recover low frequency directly from seismic data. We find that standard deconvolution does not perform well at low frequencies and this is a limiting factor in impedance inversion. Using frequency domain deconvolution, we show that improving the spectral smoothing process and applying a minimum phase spectral color operator to the deconvolved seismic trace can improve the performance of impedance inversion and reduce the bandwidth necessary from well control.

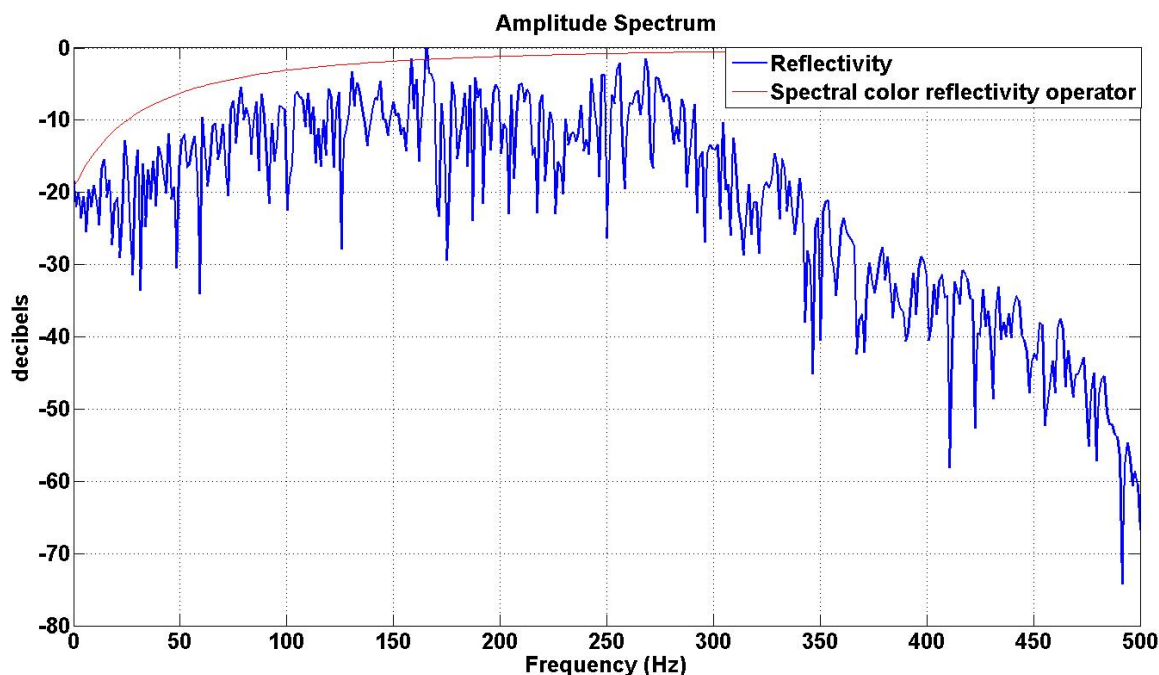


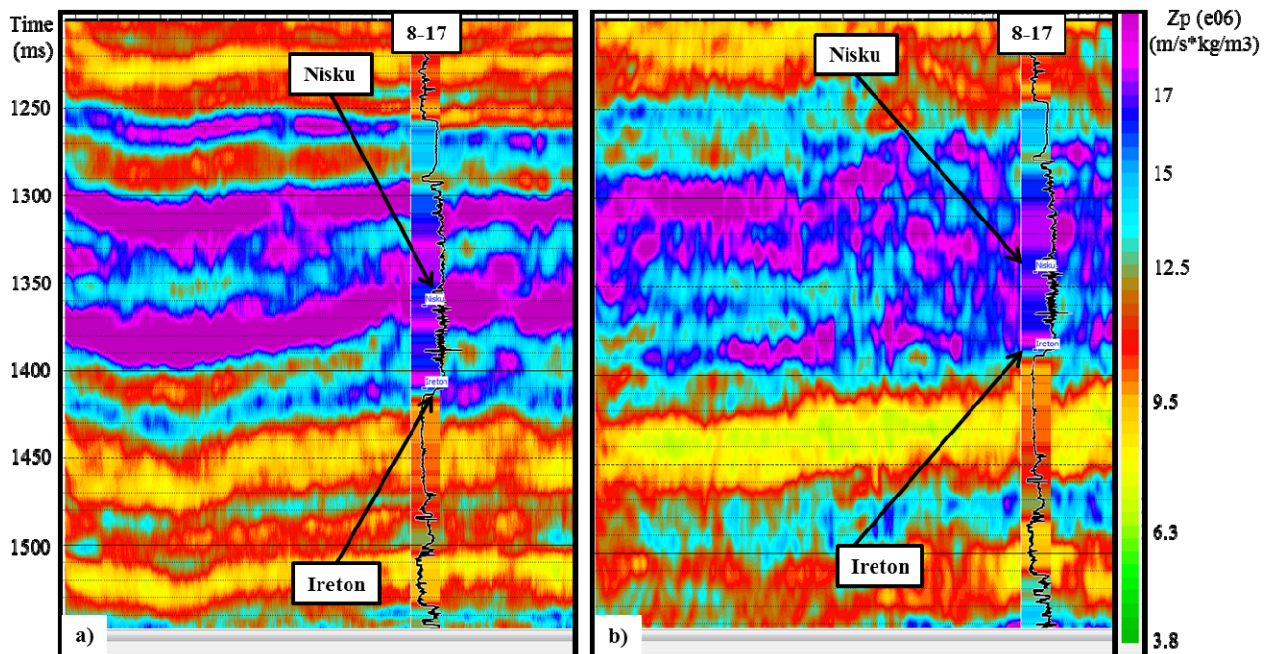
FIG. Amplitude spectrum of colored reflectivity and spectral color operator.

Inversion of seismic data for assessing fluid replacement in the Nisku Formation

Patricia E. Gavotti* and Don C. Lawton

ABSTRACT

The seismic response of the Nisku Formation in Alberta was evaluated in terms of its impedance variations with the surrounding formations. The methodology compares the effect of using a dataset processed with different approaches in an inversion study. These approaches are based on a previously conditioned dataset with a conventional processing sequence (a) versus a new specialized processing sequence (b) focused on attaining coherent noise without compromising low-frequency signal. A model-based inversion was performed with these datasets. In both cases, the inverted impedance showed good results at the well location and yielded a similar general trend and lateral variations. The figure below shows the inverted impedance in case (b) with a broadband result possibly related with the presence of more low frequency content in the seismic data. In case (a) the result yielded a cleaner section and the units look more continuous without much lateral variation. A 2D seismic modelling was undertaken to simulate a CO₂ injection scenario in the Nisku Formation. The time-lapse study was performed by comparing seismic amplitudes and impedance changes before and after the CO₂ injection. The post-injection seismic section shows a time delay of 1.8 ms of the basal reservoir reflector and amplitude change of ~30% with respect to the baseline case. After performing the inversion, a decrease in the impedance values of ~7% was observed in the post-injection scenario.



Seismic processing workflow for suppressing coherent noise while retaining low-frequency signal

Patricia E. Gavotti and Don C. Lawton

ABSTRACT

Two different processing workflows were applied to the same dataset to evaluate the effect of noise attenuation methods while attempting to preserve low-frequency signal. The approach was based on a previously conditioned dataset with a conventional processing sequence versus applying a specialized processing sequence focused on suppressing coherent noise. The conventional sequence used surface wave noise attenuation and spiking deconvolution processes, whereas the specialized sequence used radial filter and gabor deconvolution processes. The specialized processing flow resulted in better attenuation of low-frequency noise while succeeding in retaining the low frequency signal. In comparison with the previously processed stack (Figure 1 (a)), new results showed more low-frequency content at the target zone (~ 5-9 Hz) than the previous processing (~ 9-14 Hz) (Figure 1 (b) and (c)); but showed a structural depression in the middle part of the section possibly related with a shallow channel caused by an old meander of the North Saskatchewan River. However, no velocity or statics anomalies were determined during the processing of this dataset.

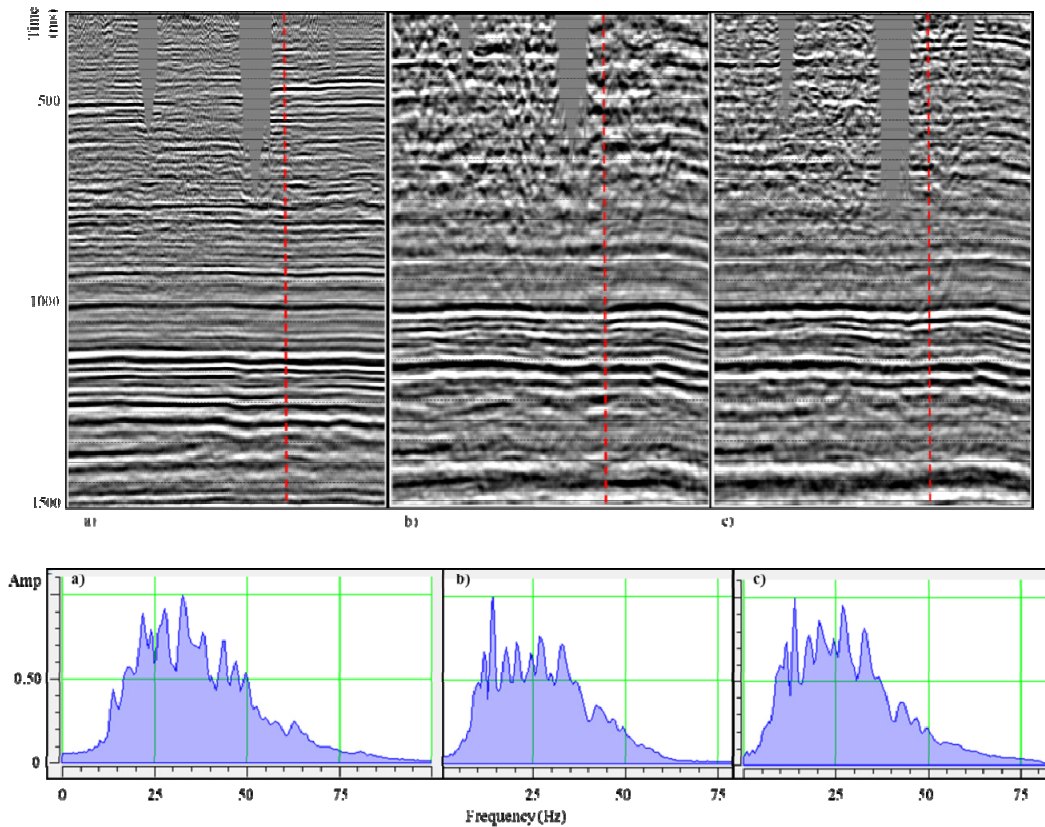


FIG. 1. Comparison of processed sections: a) previous processing b) new specialized sequence and c) new conventional sequence. The amplitude spectrum for each case is also shown.

Analysis of S-waves generated by explosive sources in boreholes: modeling and the Priddis experiment

Saul E. Guevara*, and Gary F. Margrave

ABSTRACT

An explosive charge in a borehole is a common energy source in seismic exploration. Frequently it is assumed to be a pure dilatational source, generating only compressive waves. However S-waves generated in boreholes is predicted by theoretical work, but not frequently identified in experimental data.

The Priddis field experiment, carried out this year by CREWES, included explosive sources in boreholes. This report presents analysis of this source of S-waves using synthetic data generated by a finite difference method, and also shows how these analyses can be related to the experimental data. The resulting synthetic data in the horizontal component, corresponding to the same source location and velocity model, are illustrated in Fig. 1: (a) an explosive source without borehole, (b) with a vertical borehole and (c) with a tilted borehole. Fig. 2 illustrates the real case of a source tilted to the right in Priddis, and Fig. 3 shows the S-wave velocity model obtained from data generated by explosive sources in this experiment using tomography.

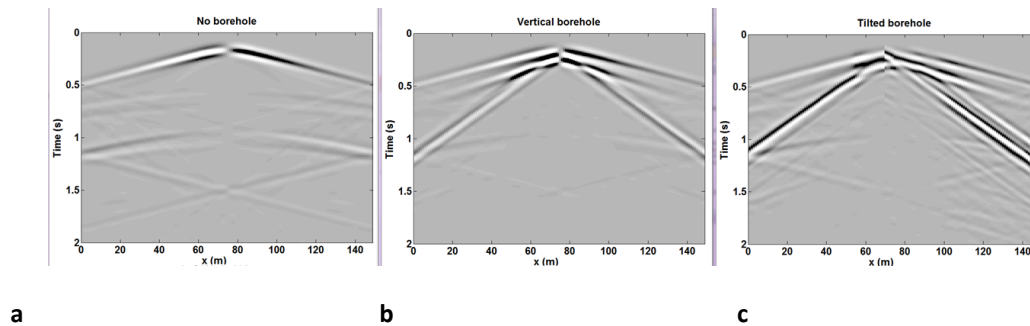


FIG. 1. Modeling of the borehole effect: left, without borehole, middle with a vertical borehole and right with a tilted borehole.

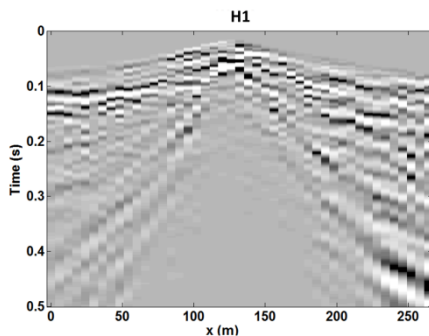


FIG. 2. Field data from a tilted source, H component.

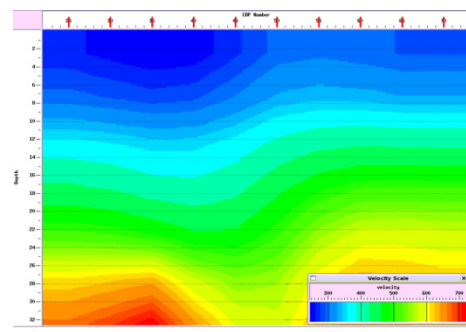


FIG. 3. S-wave velocity from the uphole.

Converted-wave processing in a complex area: near surface and depth imaging challenges

Saul E. Guevara, Gary F. Margrave, Babatunde Arenrin, John C. Bancroft, and William M. Agudelo.

ABSTRACT

Converted waves could have a more extensive application, if some processing challenges were overcome. Some of them are specific to complex areas. An interesting case to study these issues is a multicomponent seismic data set from Colombia, corresponding to a valley with a mild topography and geological structure. A 2-D seismic line is used for this study. The near surface heterogeneity is a serious issue for C -waves here. A seismic section after statics from receiver stacks is shown in Fig. 1. Data from an uphole experiment acquired there and from S -refractions can be used to improve the statics correction. The near surface S -wave velocity model obtained from the uphole data using tomography is shown in Fig. 2. Improvements in the depth velocity model are also required. In order to investigate this issue, a model using finite differences was generated, which is illustrated by the P -wave velocity in Figure 3. Figure 4 shows a stack section of the synthetic data using the CCP approach. Test and analysis of these data and processing methods are presented in this report.

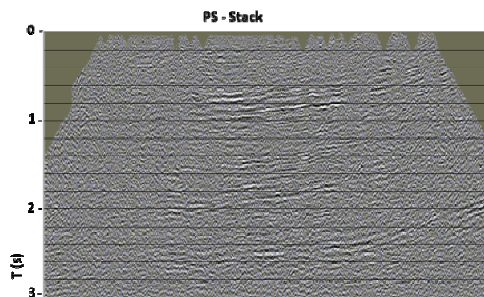


FIG. 1. Stack section of the PS-wave real data after static correction using Common Receiver Stacks.

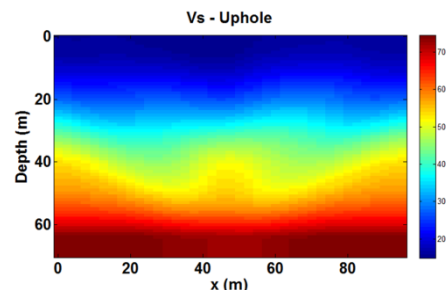


FIG. 2. Velocity of S-wave in the near surface from an uphole experiment.

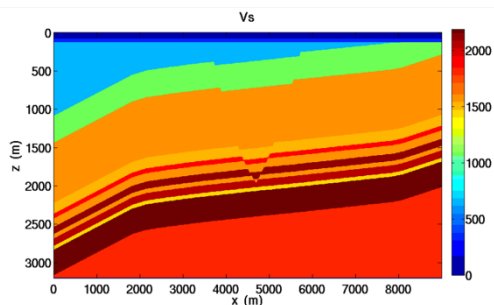


FIG. 3. Geological model, S-wave velocity, to generate synthetic data.

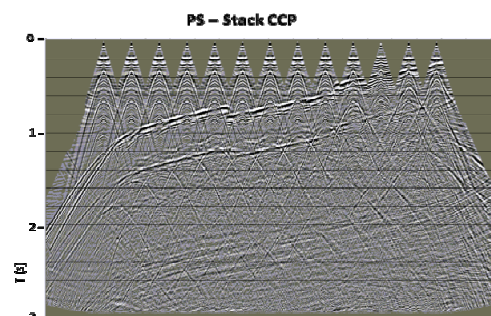


FIG. 4. Stack of the synthetic converted wave using the CCP approach.

The role of source modeling in prestack depth migration for AVO estimation

Saul E. Guevara and Gary F. Margrave

ABSTRACT

Migration is very successful in obtaining information about the location of geological structures. In principle migration methods can also obtain information about the properties of the rocks, provided that true amplitude of the seismic reflections is recovered. The deconvolution imaging condition for reflectivity was defined by Claerbout (1971) as:

$$R = \frac{U}{D}$$

where R is the Reflectivity, U is the up-going wave (Data) and D is the down-going wave (Source).

This work explores the effect of source modeling on the reflectivity, using modeling and shot-profile prestack depth migration with the PSPI approach. A simple geological model, with only one horizontal reflector, was used. The input data were calculated using an finite difference method. The migration source was modeled as a 2D Green's function. The two wavefields (source and data) for the PP imaging condition are compared in Fig. 1, and the corresponding migrated common angle gather is shown in Figure 2. Also the AVA (Amplitude versus Angle) response for the migrated data are presented in Fig. 3, compared with the theoretical result calculated from the Zoeppritz equations for PP and PS waves. Resemblance to the theoretical Zoeppritz results is apparent, as there are clear differences, especially for larger angles. This work can contribute to improvement in the imaging condition for PP and PS waves, and to better AVO analysis.

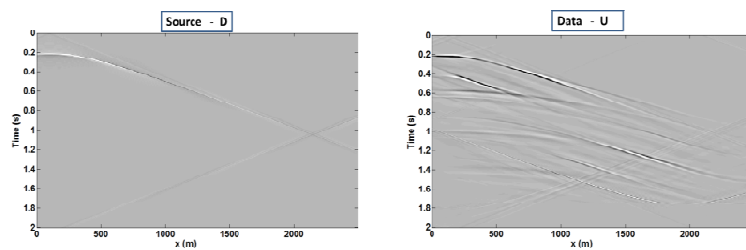


FIG. 1. Source (D) and Data (U) at the imaging condition.

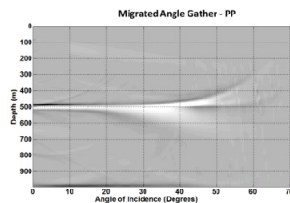


FIG. 2. Migrated gather PP

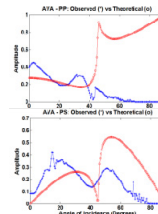


FIG. 3. AVO observed vs. theoretical.

Wave mode separation for a surface with slope using the free-surface response

Saul E. Guevara, Gary F. Margrave and Don C. Lawton

ABSTRACT

Elastic P and S- wave modes can be mixed on the field records recorded with multicomponent receivers. The separation of these two wave-modes makes easier to handle and process each one of them, so it is considered an important first step analyzing these data. If the data are recorded on the earth's surface, the free surface has an effect on both wavefield phase and frequency. Methods for wave-mode separation taking into account the free surface effect have been proposed by some authors, such as Dankbaar (1985), assuming a flat horizontal free surface and with receivers normal to it.

However, if there is a slope, such as the case of rough topography, the receivers are placed vertically. This work extends the method to the case of a free surface with slope. A test of wave mode separation in the presence of slope using synthetic data is presented. Figure 1 shows the velocity model, Figure 2 shows common receiver gathers for the vertical and the horizontal components, obtained from the ray trace method. Finally, Figure 3 presents the two wave modes after separation.

This method could be applied to land multicomponent data acquired in complex areas.

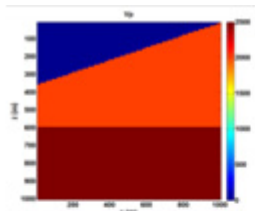


FIG. 1. Geological model. The sources and receivers are on the sloping surface.

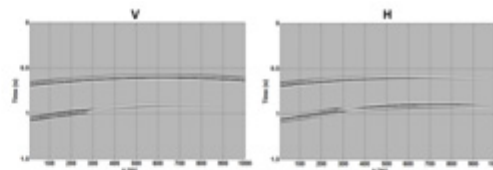


FIG. 2. Common receiver gathers for the vertical and horizontal components resulting from ray tracing. The receiver is located at $x=1000\text{m}$.

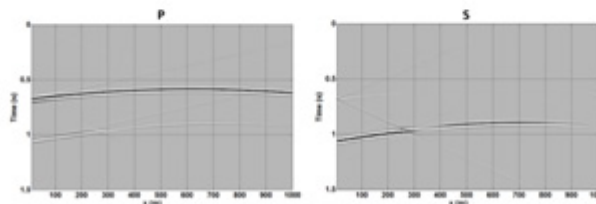


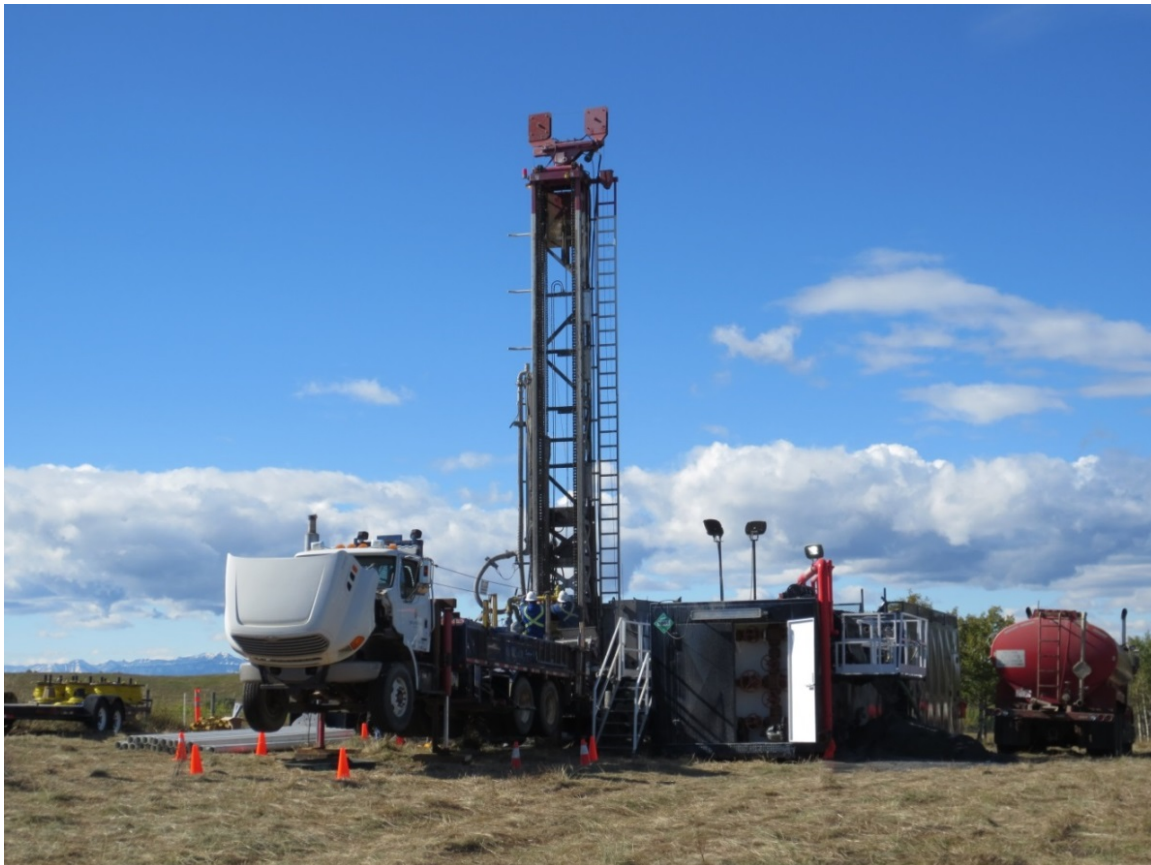
FIG. 3. P- wave (left-hand side) and S-wave (right-hand side) after wave mode separation taking into account the slope.

Installation of new observation wells at the Priddis Geophysical Observatory

Kevin W. Hall*, Kevin L. Bertram, Malcolm B. Bertram, Eric V. Gallant, Gary F. Margrave, Don C. Lawton

ABSTRACT

The Consortium for Research in Elastic Wave Exploration Seismology (CREWES) has had two new wells drilled on University of Calgary land near Priddis, Alberta, bringing the total number of wells available for geophysical projects on the property to three. The new wells were permitted as geophysical test wells with a maximum depth of 149 m. One of the wells was successfully instrumented with forty-five 3C geophones at 3.06 m receiver spacing, as well as multi- and single-mode optical fibres. The wells will be used for geophysical teaching and research, including well-logging, vertical seismic profiles, cross-well seismic and microseismic. Work was completed October 30, 2013.

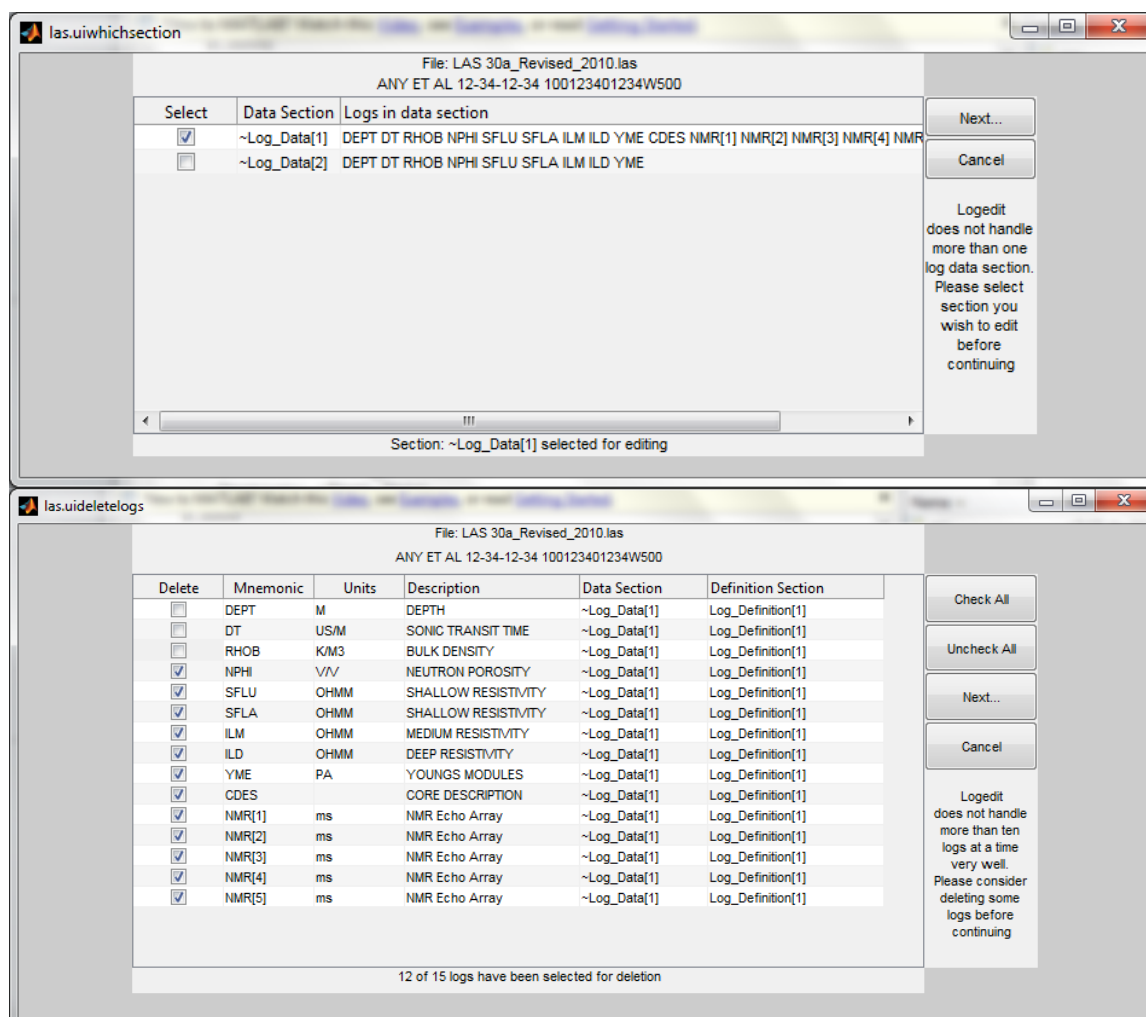


Updates to readlas

Kevin W. Hall and Gary F. Margrave

ABSTRACT

The CREWES Matlab toolbox contains a script called *readlas* that has long had the ability to read version 1.2 and version 2.0 Log ASCII Standard (LAS) files. A new Matlab class called *las* that can handle all LAS versions has been written. The constructor reads an entire LAS file into memory and splits it into a Matlab cell string array using regular expressions. The *readlas* script is now a wrapper that creates a new *las* object and returns version 2.0 inputs suitable for *logedit* and *synggram* regardless of the LAS version of the input file. Since *logedit* and *syngram* cannot handle the multiple log data sections or logs containing character data (eg. lithology) that are allowed in LAS 3.0 files, or more than ten logs effectively, *readlas* provides graphical user interface (GUI) windows that prompt users to pick which log data section they would like to work on, and decide which logs within that section they want to edit. It also replaces any log character data with log null (numeric) values. The original *readlas* (pre 2013) is still available in the toolbox as *readlas_old*.



Harnessing harmonics for imaging thin shallow reflectors

Christopher B. Harrison, Gary Margrave, Michael Lamoureaux*, Arthur Siewert, Andrew Barrett and Helen Isaac

ABSTRACT

Harmonics as generated during vibrator seismic surveys have traditionally been considered noise for attenuation. Acquisition techniques, processing algorithms, and vibrator system engineering have been developed to suppress these harmonics since the vibrators introduction in the 1960's. The harmonics cause a correlation-ghost forerunner or tail, depending on type of sweep, at positive and negative correlations times. However, it is only because these harmonics are not sampled properly nor conditioned suitably that these correlation-ghost have been understood as “destructive” and not constructive.

In this paper we show that with proper acquisition and processing, higher order harmonics can readily be used to image thin shallow reflectors. Using time dependent Gabor decomposition (TDGD) and frequency dependent Gabor decomposition (FDGD), we decomposed 75080 harmonics and recombined sweeps from 3754 sweeps recorded at 1877 shot points. We show that the second (H2), third (H3) and H2+H3 harmonics (Figure 1) as decomposed from the baseplate recorded sweep reveal an abundance of thin shallow reflectors.

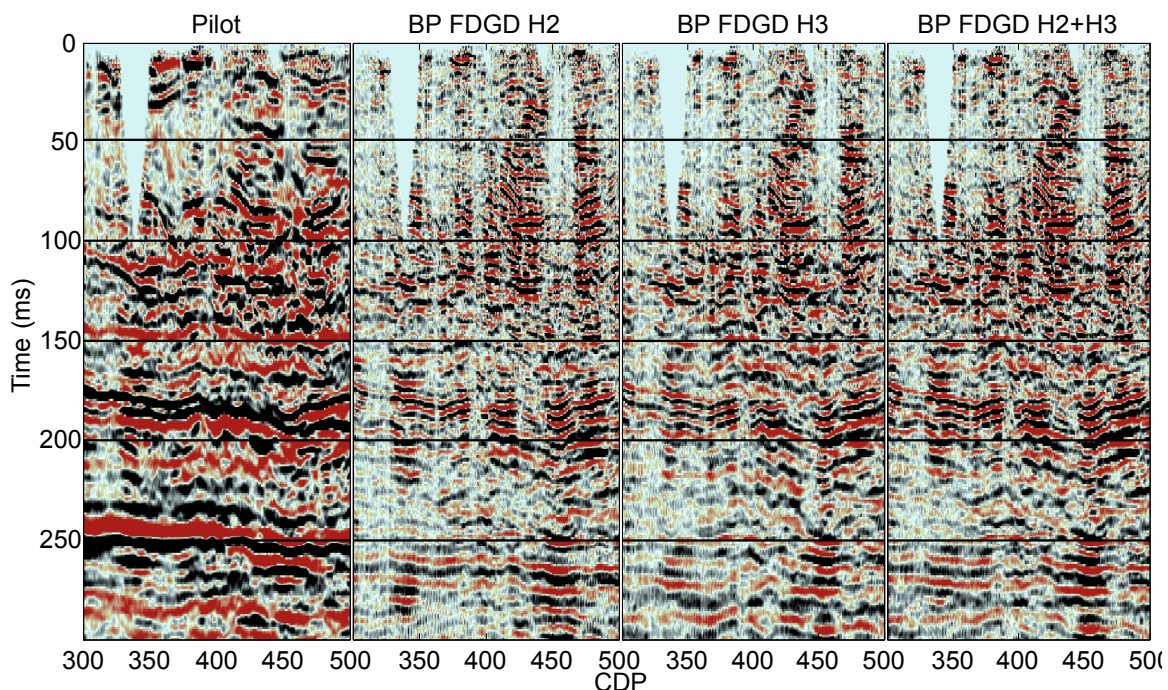


FIG. 4. Imaging results from using H2, H3 and H2+H3 as correlation operators. These harmonics were decomposed using frequency dependent Gabor decomposition. The pilot image is plotted on the left for comparison.

Through the looking glass: using X-T plane distortions for wavefield separation

David C. Henley and Joe Wong

ABSTRACT

In exploration seismology, we record the response of the earth to various controlled seismic energy sources applied at or near the earth's surface. Since the earth is an imperfect elastic half-space, usually containing many internal boundaries and irregularities, the seismic response recorded at the surface consists of many different modes of wave propagation, some related to the surface of the half-space, others generated by the internal structure. Typically, we are primarily interested in using various back-scattered modes, like reflections, to construct images of the internal structure of the earth, so we need to separate one or more of these modes from the full seismic response for further processing. The separation is often accomplished using various mathematical transforms which take advantage of some unique characteristic of one or more of the modes.

In this work, we show how to apply some relatively simple geometric distortions to the X-T plane in which we usually display seismic data, to separate wavefield components for further processing. Since these distortions are all implemented as point-to-point re-mapping and interpolation in the plane, they can be reversed, with relative fidelity depending only upon the interpolation method. We thus avoid integral transforms, since these can exhibit undesirable artifacts related to the transform aperture, caused by operations applied in the transform domain, or caused by irregularities in the original data domain.

We use physical model data for our demonstrations. Hence, techniques which perform well on these data should be effective, as well, on actual seismic field data.

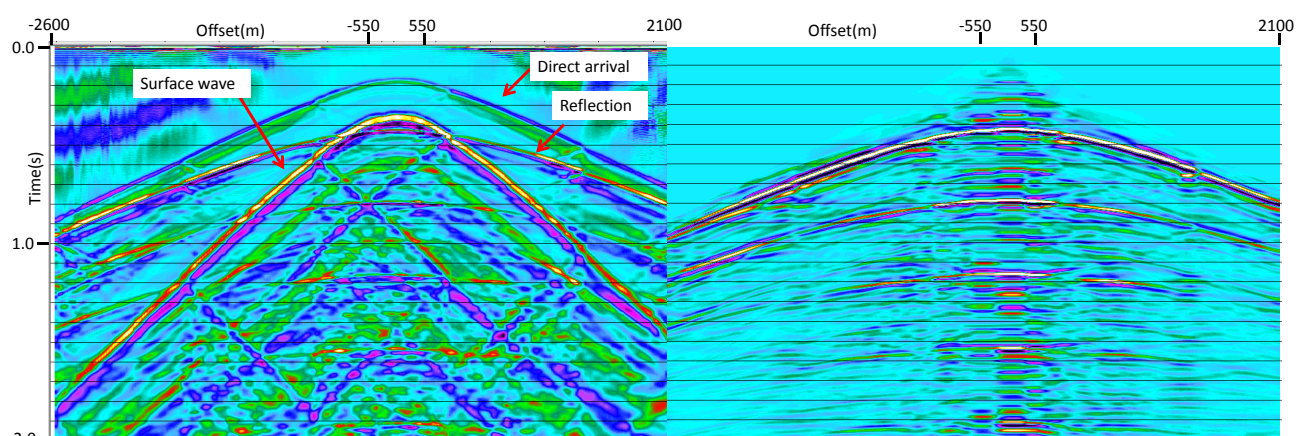


FIG. 1. Raw 3D receiver line gather for a two-layer physical model (left), showing full elastic wavefield response, can be processed using X-T plane distortions to extract the PP wavefield (right), consisting of the primary reflection and its surface-related multiples.

Undoing wavefield interference for AVAZ measurements

David C. Henley and Faranak Mahmoudian

ABSTRACT

There is a lot of interest in measuring the amplitudes of reflections from anisotropic rock layers in the earth. Such measurements can be used to estimate the rock layer's anisotropic elastic parameters. In the case of fracture-induced anisotropy, fracture orientation and intensity can be determined from these parameters. Most methods for estimating anisotropic elastic parameters require a set of reflection amplitude measurements as a function of both source-receiver offset and survey azimuth (AVAZ). A large problem with many of these measurements, however, is the interference between the targeted reflection event and other, shallower seismic events, or 'noise'. This interference can result in large amplitude disturbances of the target event, making accurate amplitude measurements impossible.

We show here how to remove most of this interference using radial trace (RT) filtering techniques. The RT filter method is attractive because it estimates and subtracts coherent components along various dip directions directly observed on the input trace gathers. Careful parameter selection ensures that amplitudes in the frequency band of the target reflection are unaffected by the noise subtraction. The resulting amplitude trend on each trace gather is much smoother, and a better fit to the theoretical trend. We demonstrate on a set of AVAZ survey data acquired at the CREWES physical modeling facility. Elastic parameters estimated from these measurements were verified elsewhere by an independent technique.

EXAMPLE

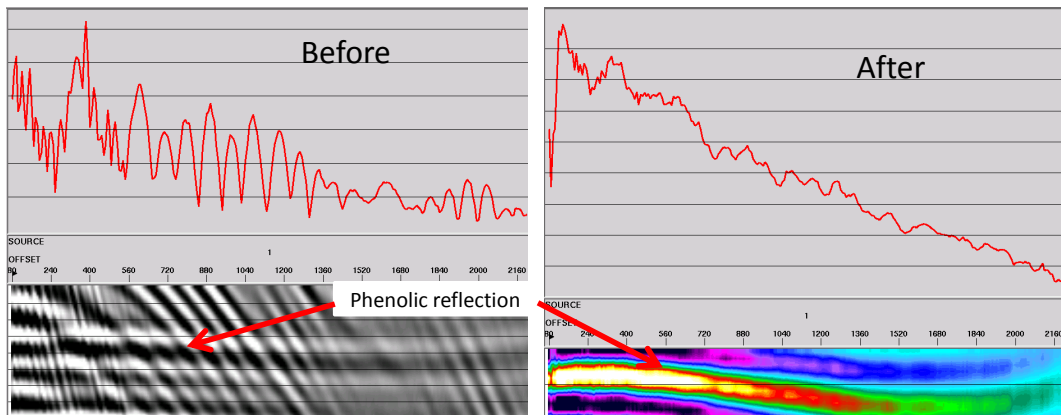


FIG. 1. Phenolic layer reflection before and after removal of interference from shallower reflection event. Red plot in each case is picked reflection amplitude.

Which way is up?—experiences with processing physical modeling data

David C. Henley* and Joe Wong

ABSTRACT

In the initial stages of an exploration project, a seismic data processor is often presented with a set of seismic data acquired over a geological prospect whose subsurface features and properties are either partially or completely unknown. It is then the processor's job to extract as much of this detail as possible through appropriate data processing. To simulate and illustrate the process, two data sets from the CREWES physical modeling facility were acquired by Wong (henceforth known as the Modeller) and presented to Henley (termed the Processor) for imaging, but *with no information conveyed about the physical model structure or materials*, except that the two surveys simulated 'baseline' and 'time-lapse' realizations of the *same* model. Each set of seismic data was processed independently, and algorithm parameters were deduced only from the data characteristics. Features of the processed data were then used to evaluate three different proposed 'models' supplied by the Modeller. Only one of these was consistent with images and other information obtained from the processed seismic data. This experiment was a very instructive illustration of the seismic exploration process.

The 'time-lapse' version of the model created a family of strong multiple reflections in the corresponding seismic data. As part of our analytic processing, we used this opportunity to test a multiple-elimination technique applied in the common-ray-parameter domain. Two variations of the technique were found effective on surface-related multiples in this geometrically simple model.

DEMONSTRATION

1	PVC	25.4mm	2350	1120	1300		
2	WATER	TEFLON	6.7mm	1360	470	2200	WATER
3	PLX	50.8mm	2750	1380	1190		
4	PHN	66.9mm	3500	1700	1350		
5	PLX	25.4mm	2750	1380	1190		
6	WATER	12.7mm	1485	0	1000		
7	PLX	25.4mm	2750	1380	1190		

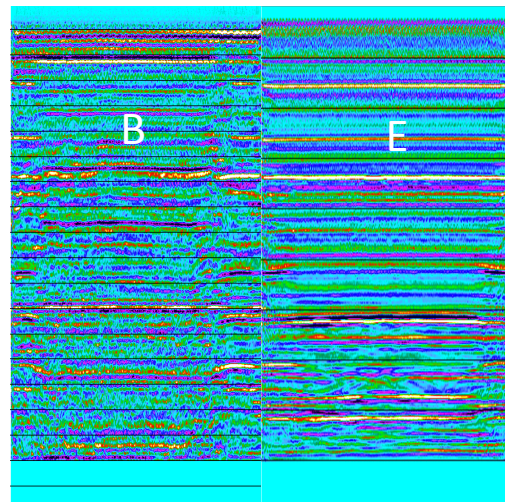


FIG. 1. Does either image B or image E correspond to the physical model portrayed schematically on the left? How can you tell?

Identifying internal multiples using 1D prediction: physical modelling and land data examples

Melissa Hernandez and Kris Innanen

ABSTRACT

Internal multiples, if not properly identified, are a significant impediment to seismic reflection data analysis. It has been suggested that some of the obstacles this overall problem presents, especially on land, can be addressed by applying 1D prediction algorithms to near offset or post-stack data. We examine this possibility by carrying out 1D predictions on a zero-offset physical modelling data set and a post-stack land data set, both of which are likely to contain significant multiple energy. Our results confirm the kinematic accuracy of the predictions by comparing them against synthetic traces, and flesh out the problem of optimally choosing the integration limit parameter ϵ in the algorithm. The prediction output may constitute a sort of “multiple probability map”, useful for identifying both multiples themselves, and primaries whose amplitudes are likely to have experienced interference from them.

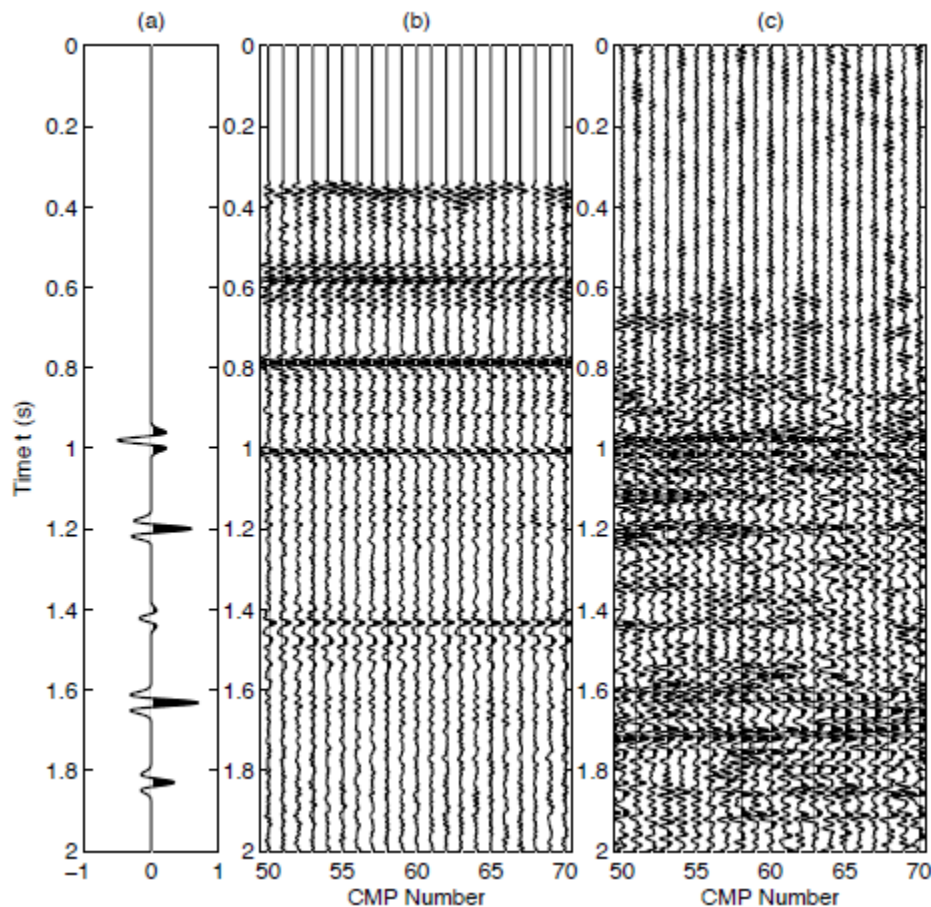


FIG. 1. (a) Synthetically modelled internal multiple trace plotted versus (b) input NEBC zero offset section, and (c) prediction output.

A collision theory of seismic waves applied to elastic VSP data

Kris Innanen and Kevin Hall

ABSTRACT

In previous CREWES reports we have been assembling a theory for seismic wave propagation which is based on particles with well-defined momenta and masses colliding inelastically. Here we discuss some early arguments towards this collision picture to elastic VSP data, such that it describes elastic processes, such as conversions. We choose a candidate reflection in the Husky Cold Lake 3C walkaway VSP data set, as discussed by Hall et al. in the 2012 CREWES Report, which has clear evidence of P-P interactions and P-S conversions, and report on the beginning of our attempts to validate the collision model.

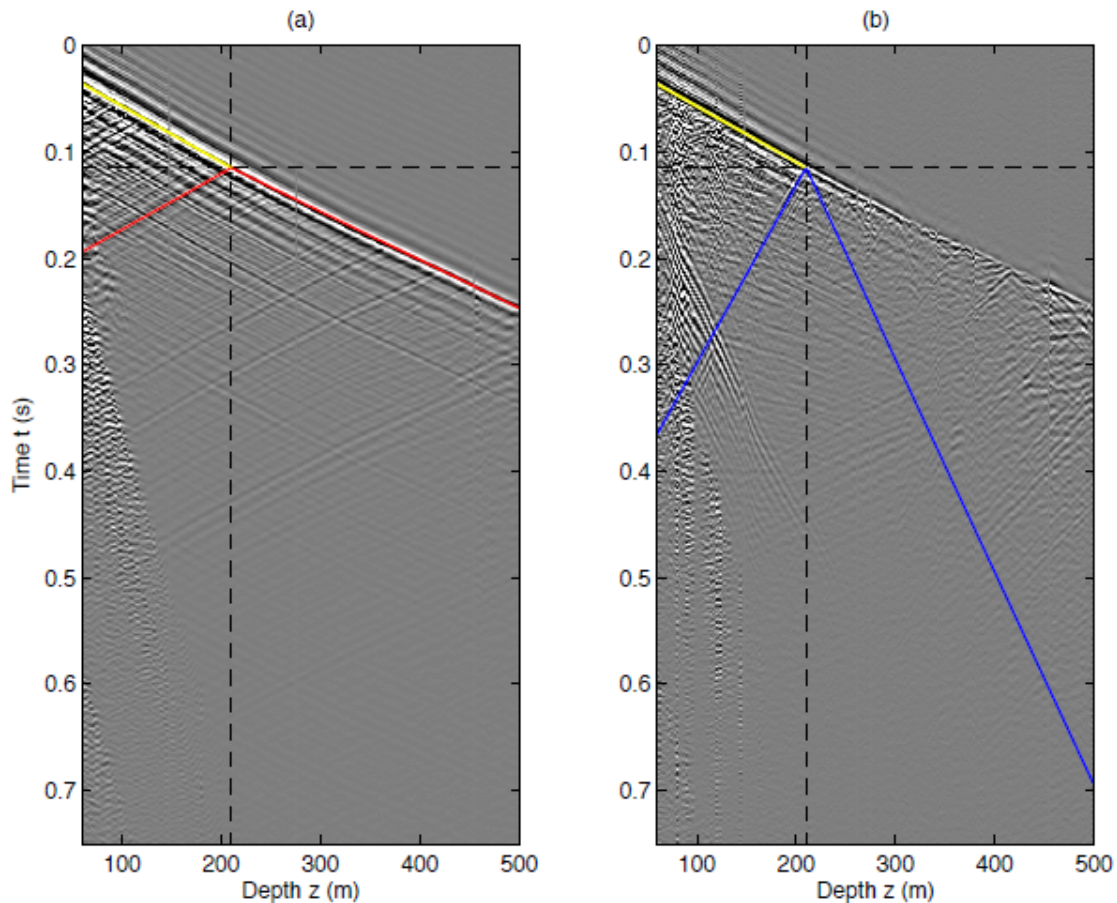


FIG. 1. A candidate reflection point in the Husky Tucker Lake VSP data set, near offset case. (a) Vertical component data, highlighting a P-P interaction; (b) Radial component data, highlighting a P-S interaction.

A framework for multiparameter full waveform inversion of precritical reflection seismic data

Kris Innanen

ABSTRACT

Formulas for computing full and quasi-Newton steps in seismic full waveform inversion, specifically designed for pre-critical reflection experiments, are derived. The formulas are partly continuous and partly discrete. The discrete aspect of the problem is connected to the multiplicity of parameters, whereas the continuous aspect is connected to the distribution in space of the unknowns. We analyze the opportunities this formulation provides for forming quasi-Newton steps. There are two different kinds we can invoke, which we refer to as parameter-type and space-type. The parameter-type approximation appears to retain the ability of reflection FWI to correctly update one parameter when several are responsible for the amplitude content of the data. A third approximation can be created by invoking both simultaneously. All three are simple to implement, since they each amount to the setting of different, and well-defined, off-diagonal Hessian operator elements to zero.

$$\begin{aligned}
 \begin{bmatrix} \delta s_{\kappa}(\mathbf{r}) \\ \delta s_{\rho}(\mathbf{r}) \end{bmatrix} &= \int d\mathbf{r}' \mathcal{H}_2^{-1}(\mathbf{r}, \mathbf{r}') \int d\mathbf{r}'' \begin{bmatrix} -H_{\rho\rho}(\mathbf{r}', \mathbf{r}'') & H_{\rho\kappa}(\mathbf{r}', \mathbf{r}'') \\ H_{\kappa\rho}(\mathbf{r}', \mathbf{r}'') & -H_{\kappa\kappa}(\mathbf{r}', \mathbf{r}'') \end{bmatrix} \begin{bmatrix} g_{\kappa}(\mathbf{r}'') \\ g_{\rho}(\mathbf{r}'') \end{bmatrix} \\
 \mathcal{H}_2(\mathbf{r}, \mathbf{r}') &= \int d\mathbf{r}'' [H_{\kappa\kappa}(\mathbf{r}, \mathbf{r}'')H_{\rho\rho}(\mathbf{r}'', \mathbf{r}') - H_{\rho\kappa}(\mathbf{r}, \mathbf{r}'')H_{\kappa\rho}(\mathbf{r}'', \mathbf{r}')]
 \end{aligned}$$

FIG. 1. A map of the formula for a two-parameter full Newton step.

How AVO information can be practically incorporated in full waveform inversion

Kris Innanen

ABSTRACT

We consider the claim made in a companion paper, namely that certain formulas for multiparameter reflection full waveform inversion are easy to analyze as well as implement. We ask the question we think is, in fact, a central matter in the future of FWI. If FWI automatically converges to the right answer for a particular parameter, through operations on data which are mixtures of the effects of several parameters, it must do some kind of “unmixing” akin to that in AVO inversion. If it cannot, there is no solution to what FWI practitioners refer to as parameter cross-talk. How does this happen? We ultimately conclude that the quasi-Newton update formula we refer to as the parameter-type approximation is properly equipped to incorporate our basic ideas of AVO inversion into FWI.

$$\begin{aligned}
 \text{(a)} \quad & \begin{array}{c} \text{determinant} \\ \text{Hessian functions} \\ \text{gradients} \end{array} \\
 & \begin{bmatrix} \delta s_{\kappa}(\mathbf{r}) \\ \delta s_{\rho}(\mathbf{r}) \end{bmatrix} \approx - \frac{1}{\Gamma_{\kappa\kappa}(\mathbf{r})\Gamma_{\rho\rho}(\mathbf{r}) - \Gamma_{\rho\kappa}(\mathbf{r})\Gamma_{\kappa\rho}(\mathbf{r})} \begin{bmatrix} \Gamma_{\rho\rho}(\mathbf{r}) & -\Gamma_{\rho\kappa}(\mathbf{r}) \\ -\Gamma_{\kappa\rho}(\mathbf{r}) & \Gamma_{\kappa\kappa}(\mathbf{r}) \end{bmatrix} \begin{bmatrix} g_{\kappa}(\mathbf{r}) \\ g_{\rho}(\mathbf{r}) \end{bmatrix} \\
 \text{(b)} \quad & \begin{array}{c} \text{amplitude correction} \\ \text{cross-talk suppression} \\ \text{cross-talk suppression} \\ \text{amplitude correction} \\ \text{angle-dependence suppression} \end{array} \\
 & \begin{bmatrix} \delta s_{\kappa}(\mathbf{r}) \\ \delta s_{\rho}(\mathbf{r}) \end{bmatrix} \approx - \frac{1}{\Gamma_{\kappa\kappa}(\mathbf{r})\Gamma_{\rho\rho}(\mathbf{r}) - \Gamma_{\rho\kappa}(\mathbf{r})\Gamma_{\kappa\rho}(\mathbf{r})} \begin{bmatrix} \Gamma_{\rho\rho}(\mathbf{r}) & -\Gamma_{\rho\kappa}(\mathbf{r}) \\ -\Gamma_{\kappa\rho}(\mathbf{r}) & \Gamma_{\kappa\kappa}(\mathbf{r}) \end{bmatrix} \begin{bmatrix} g_{\kappa}(\mathbf{r}) \\ g_{\rho}(\mathbf{r}) \end{bmatrix}
 \end{aligned}$$

FIG. 1. (a) The components of the parameter-type quasi-Newton update formula. (b) The tasks carried out by the components of the formula, including suppression of angle dependence and update balancing; amplitude correction; cross-talk suppression.

Internal multiple prediction in the continuous wavelet transform maxima domain

Kris Innanen*

ABSTRACT

We test a possible application of seismic processing in the continuous wavelet transform maxima (CWTM) domain, which is the prediction of internal or interbed multiples. Both the use of the algorithm in the CWTM domain itself and the use of CWTM preprocessed data in the nominal (time or pseudodepth) domain are considered. In this initial study it is established that the outcome of the use of the prediction algorithm in the CWTM domain is close to that produced in the nominal domain, opening this domain up to examination, in particular with respect to scale dependent integration limit parameters. It is also established using a particularly noisy poststack land data trace that aggressive denoising in the CWTM domain, while potentially harmful in action on traces whose amplitude information will be interpreted, could be very effective if used on the data ingredients of the prediction operator.

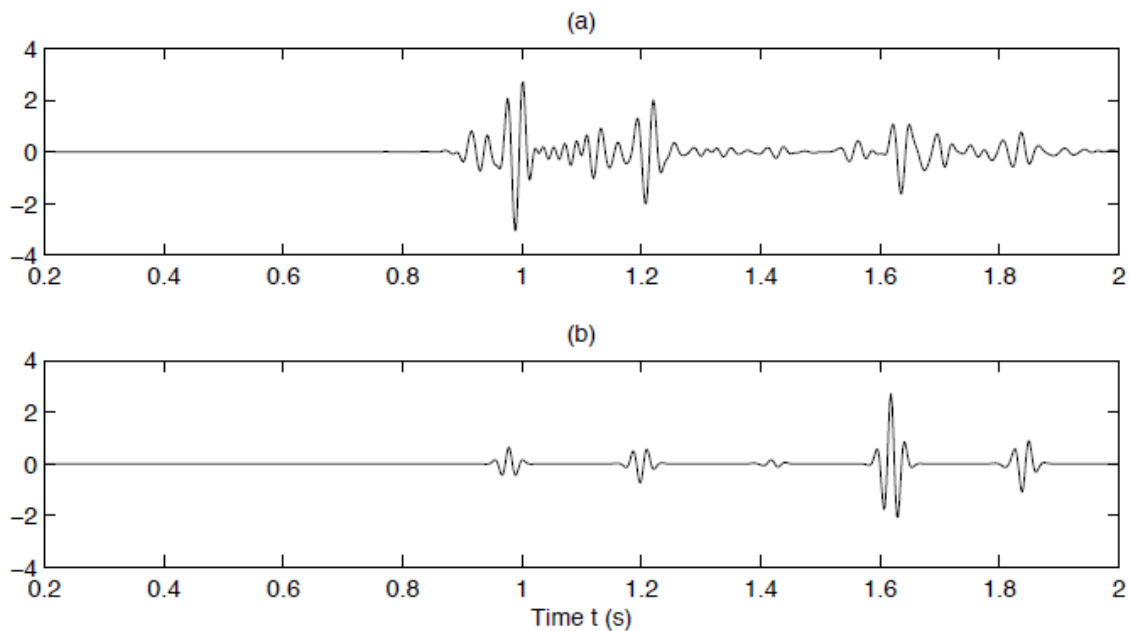


FIG. 1. (a) Prediction using the CWTM-denoised NEBC trace in the prediction operator. (b) Prediction using the synthetic trace derived from blocked well log data in the prediction operator.

Seismic processing with continuous wavelet transform maxima

Kris Innanen

ABSTRACT

Analysis of continuous wavelet transform maxima (CWTMs) has been applied in exploration seismology, but *processing* of these data have not. Simple methods exist to do this, and we discuss and implement one—the model of Mallat and Zhong—in this paper. The approach requires a bit of conceptual explanation, as it has not appeared in the exploration geophysics literature before, and we devote most of this paper to that task; our primary goal is logically develop the implementation, and leave relatively open the many possible applications to the seismic trace it seems to have in potentia. However, we end the paper with a simple example of *thresholding* of CWTMs, and the resulting reduction in noise. In a companion paper we use such data to produce internal multiple prediction operators.

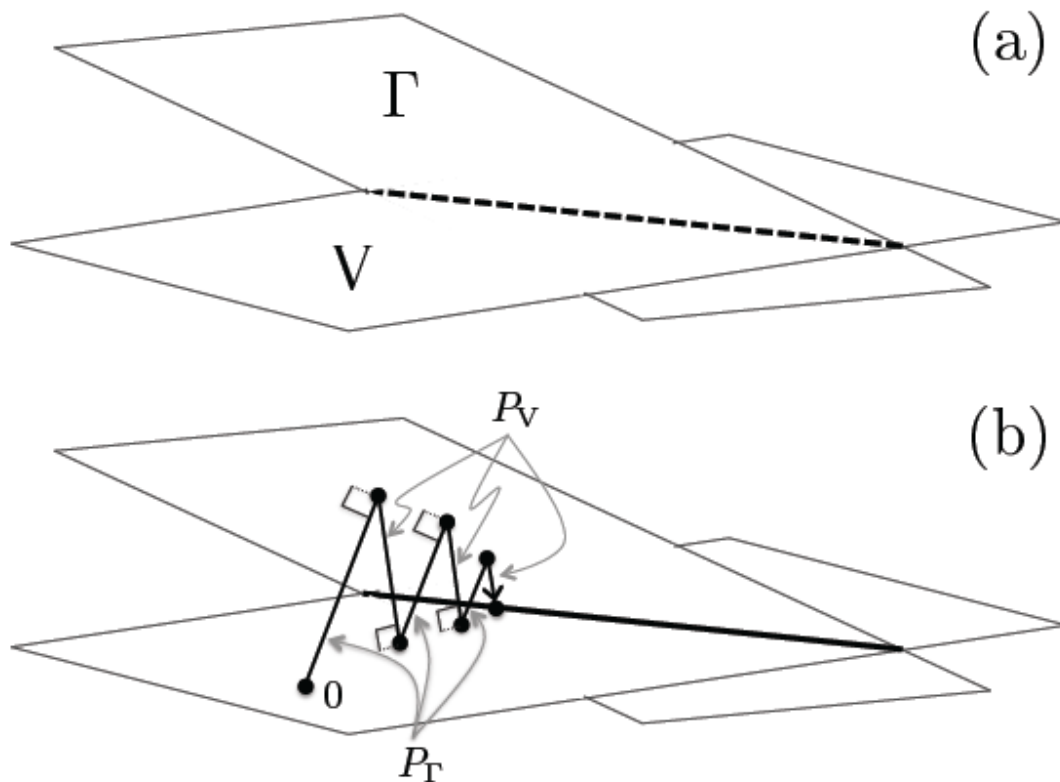


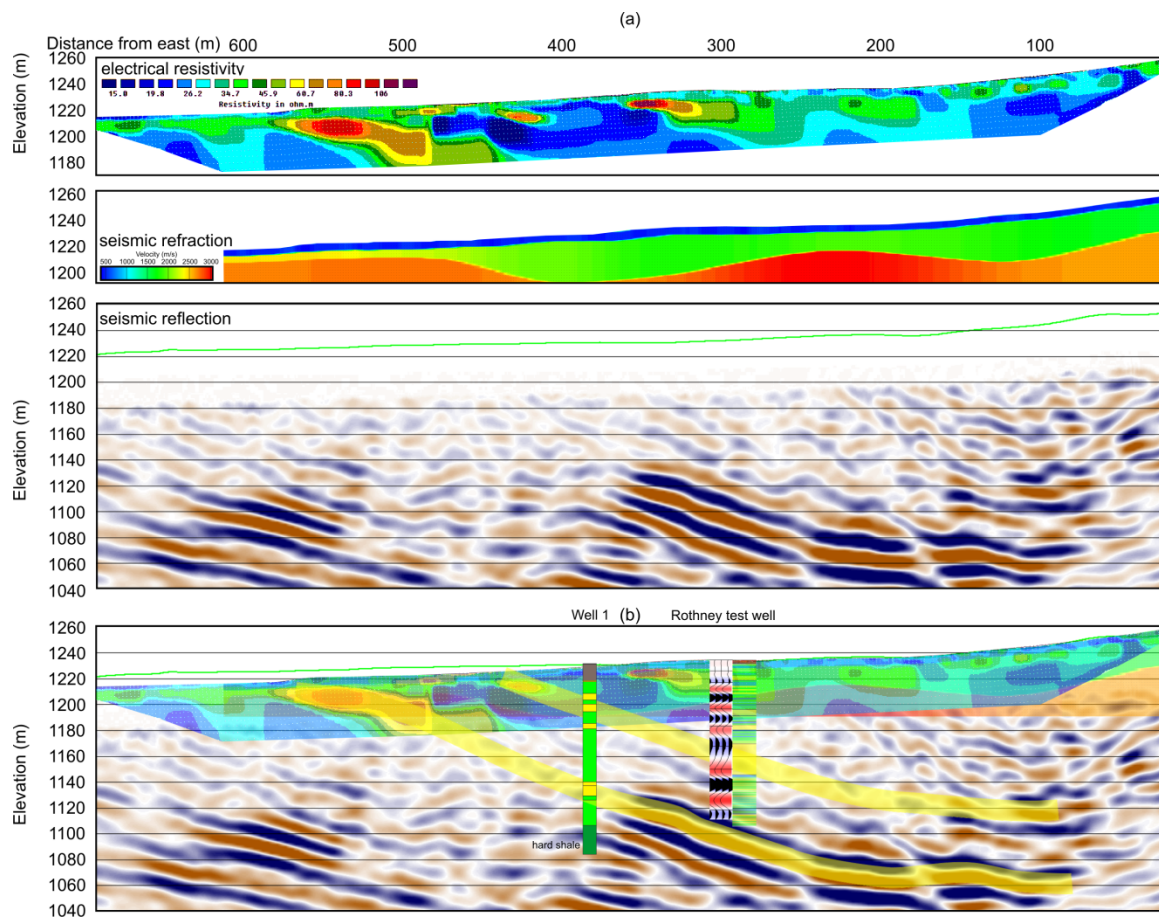
FIG. 1. (a) Γ is the space of matrices with the same maxima as we generate. V is the space of legitimate continuous wavelet transforms. P_Γ and P_V are operators mapping to these spaces. Reconstruction after processing involves sequentially applying these (b) until an acceptable convergence is obtained.

Geophysical characterization of the near-surface at Priddis, Alberta

J. Helen Isaac, Lei Zhi, Malcolm Bertram, Don C. Lawton, and L. R. Bentley

ABSTRACT

We integrated shallow well data with seismic reflection and refraction, and electrical resistivity data acquired at Priddis. The purpose was to derive a model of the near-surface to predict the lithology to be encountered in new wells that were planned to be drilled in the autumn of 2013 for the installation of a permanent downhole seismic recording and monitoring system. A major electrically resistive unit, interpreted to be a sandstone, correlates to strong reflectors on the reflection seismic data and a relatively high velocity on the seismic refraction data. We predict that the top of this unit would be encountered at about 95 m depth in the new Well 1. According to the drilling report, a sandstone was penetrated between 91-102 m. A hard shale with sandstone ledges, which was penetrated at 124 m in Well 1 and slowed the drilling, projects onto the original well deeper than the total depth and correlates to a high amplitude reflector on the seismic data.



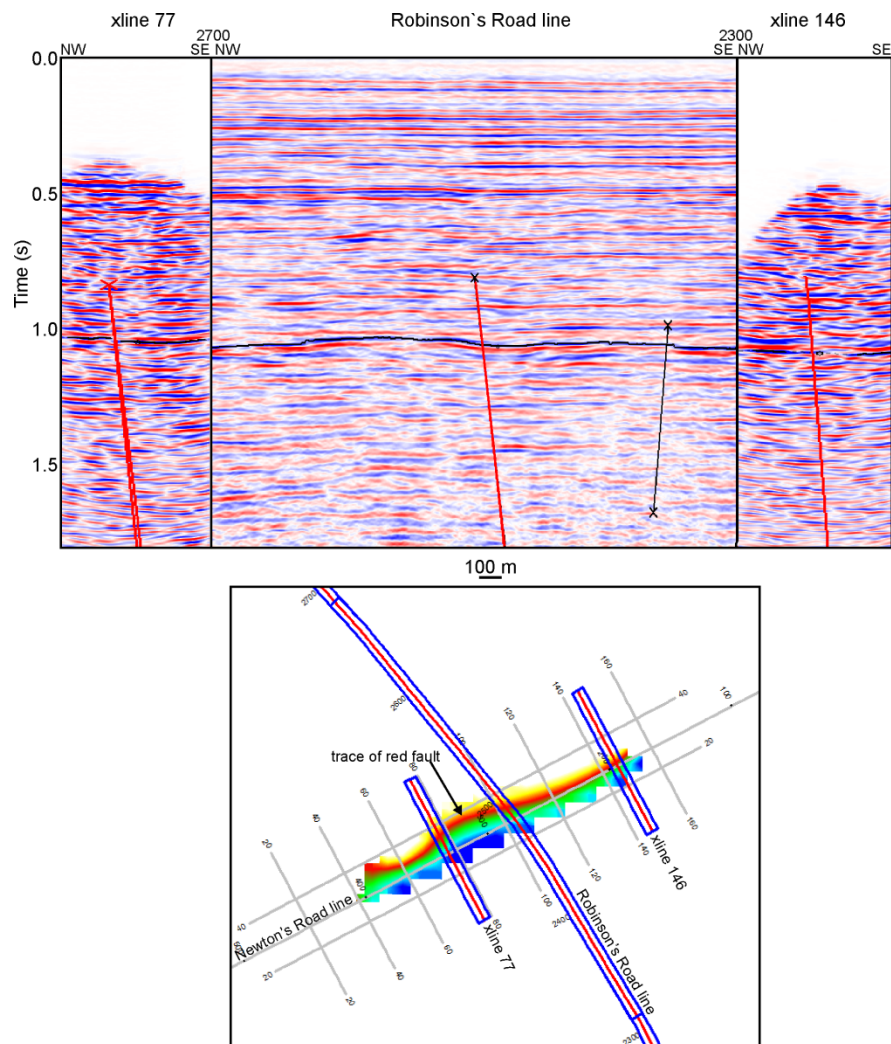
Electrical resistivity profile, seismic refraction near-surface velocity model and seismic reflection data plotted separately (a) and then superimposed (b). The refraction and electrical resistivity data were shifted laterally to align locations along strike. The lithology and synthetic seismogram in depth from the first Rothney well are overlain, along with the lithology of Well 1.

Squeezing more out of 2D seismic data: Processing and interpretation of a pseudo-3D seismic survey from New Zealand

J. Helen Isaac and Don C. Lawton

ABSTRACT

During the acquisition of seismic data near Christchurch, New Zealand, in 2011, some receivers along a 2D line were left live to record data from sources located on an orthogonal 2D line. We created a pseudo-3D seismic survey from these data. We processed the data using unconventional techniques to remove shot-generated noise, and stacked the data into bins having the same dimension as the receiver spacing in order to increase the fold. We interpreted faults on the pseudo-3D data and were able to update the regional fault trend interpreted previously using 2D data alone.



Three semi-parallel lines: crossline 77, Robinson's Road 2D line from cdps 2700 to 2300, and crossline 146. The red fault on the crosslines is interpreted to be the same one as the red fault interpreted on Robinson's Road line and its trace is displayed on the map.

An analysis of time-lapse phase shifts using perturbation theory

Shahin Jabbari and Kristopher A. Innanen

ABSTRACT

Scattering or perturbation theory has been widely used in many applications in seismology, including time-lapse problems. One of the main challenges in using scattering theory to predict the model for the difference data in a time-lapse problem is, the reference medium, the baseline survey, being a medium as complicated as the perturbed medium, the monitoring survey. We produce the linear and higher order terms in the forward scattering series for the difference data for the phase-shift changes between the baseline and monitor surveys in a reservoir. The baseline surveying is taken to be a homogenous single layer for simplicity, but can be extended for a more complicated medium in future research. Green's function for characterizing the wavefield in this reference medium has a term describing the wave reflected from the interface at the time of the baseline survey. This leads to extra terms in the first and higher order approximations of the difference data when compared with a standard scattering problem. These extra terms are a function of the reflectivity of the single interface in the baseline survey and the perturbation due to production in the reservoir. Our perturbation theory for nonlinear time-lapse seismic inversion, which is the future steps in this research, will accommodate multidimensional and multi parameter problems which will lead to more complete and general versions.

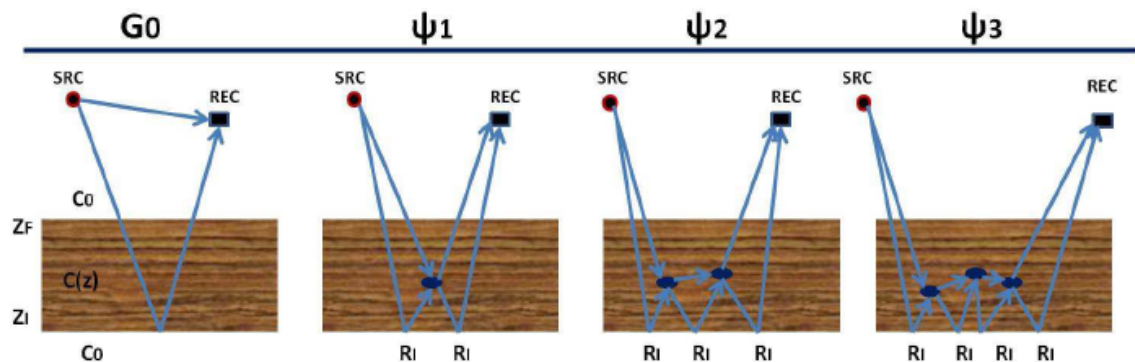


FIG. 1. Illustration of the geometry of the time-lapse difference field for the Green's function, ψ_1 (first order term), ψ_2 (second order term), and ψ_3 (third order term), in the scattering series for time-lapse difference data.

A framework for linear and nonlinear S-wave and C-wave time-lapse difference AVO

Shahin Jabbari and Kristopher A. Innanen

ABSTRACT

Multicomponent time-lapse amplitude variation with offset (AVO) may improve approximating time-lapse difference data. The difference data during the change in a reservoir from the baseline survey relative to the monitor survey are described for shear wave, and converted waves. We defined a framework for the difference reflection data, $\Delta R_{SS}(\theta)$, $\Delta R_{SP}(\theta)$, and $\Delta R_{PS}(\theta)$, in order of physical change or baseline interface contrast and time-lapse changes. A framework for linear and non linear time-lapse difference data are formulated using amplitude variation with offset (AVO) methods. The higher order terms represent corrections appropriate for large contrasts. We conclude that in many plausible time-lapse scenarios the increase in accuracy associated with higher order corrections is non-negligible for shear wave and converted wave as well as P-wave.

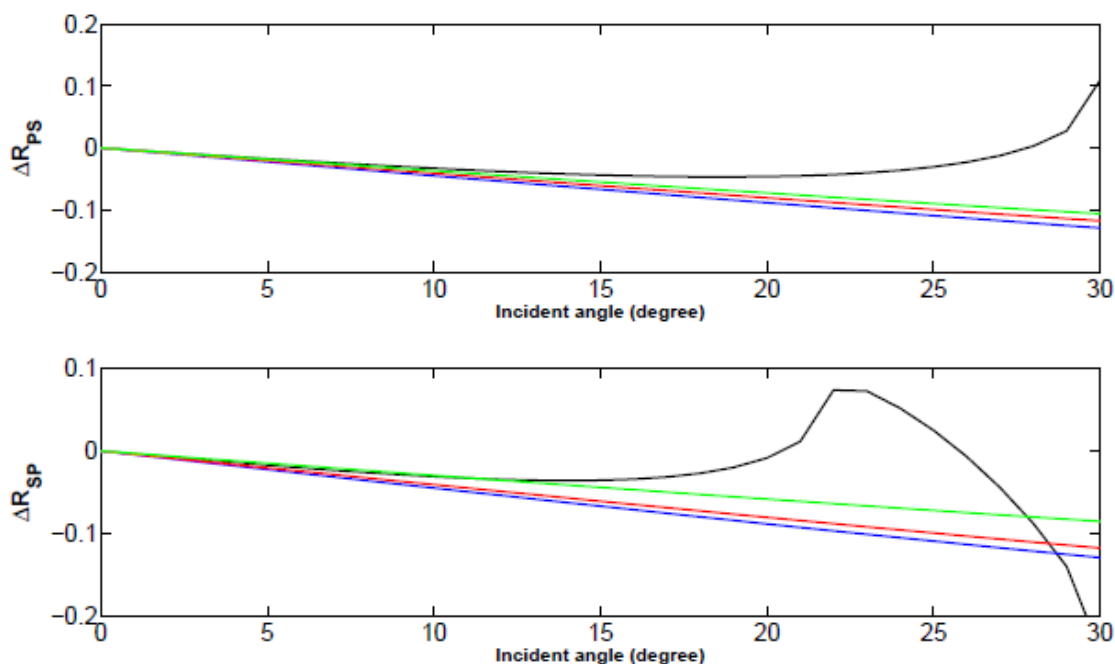


FIG. 1. ΔR_{PS} , and ΔR_{SP} for the exact, linear, second order, and third order approximation. Elastic incidence parameters: $V_{P0} = 2000\text{m/s}$, $V_{S0} = 1500\text{m/s}$ and $\rho_0 = 2.0\text{g/cc}$; Baseline parameters: $V_{PBL} = 3000\text{m/s}$, $V_{SBL} = 1700\text{m/s}$ and $\rho_{BL} = 2.1\text{g/cc}$; Monitor parameters: $V_{PBL} = 4000\text{m/s}$, $V_{SBL} = 1900\text{m/s}$ and $\rho_{BL} = 2.3\text{g/cc}$.

Black: Exact difference data, Blue: Linear approximation, Red: Second order approximation, and Green: Third order approximation.

Iterative multiparameter elastic waveform inversion using prestack Kirchhoff approximation

Hassan Khaniani*, John C. Bancroft and Eric von Lunen

ABSTRACT

For the inversion of elastic properties from seismic data, we developed an iterative scheme that simultaneously combines the standard AVO inversion with the full waveform inversion algorithm to update the model parameters. The non-iterative AVO inversion method assumes that P- and S-waves velocity of the medium are known which is not realistic all the times. Our method improves the forward and inversion operator (migration) at each step of the inversion to improve the stability and accuracy of the results compared to non-iterative methods.

To obtain the inversion results of Figure (1), we used 51 shot record from a real data acquired by Nexen from NEBC region. Both of the forward and inverse operators use prestack time imaging methods that map the migrated P-to-S traveltimes to be P-to-P traveltimes. We obtain two registered volumes on a pseudo depth that eliminates the need of ray tracing for registration issues. For complex structures, one can add ray tracing to the algorithm. Without the loss of generality, the approach is adaptable for different combination of modes such as P-to-P, P-to-S, S-to-S and S-to-P for different mediums such as anisotropic, anelastic, poroelastic and viscoelastic.

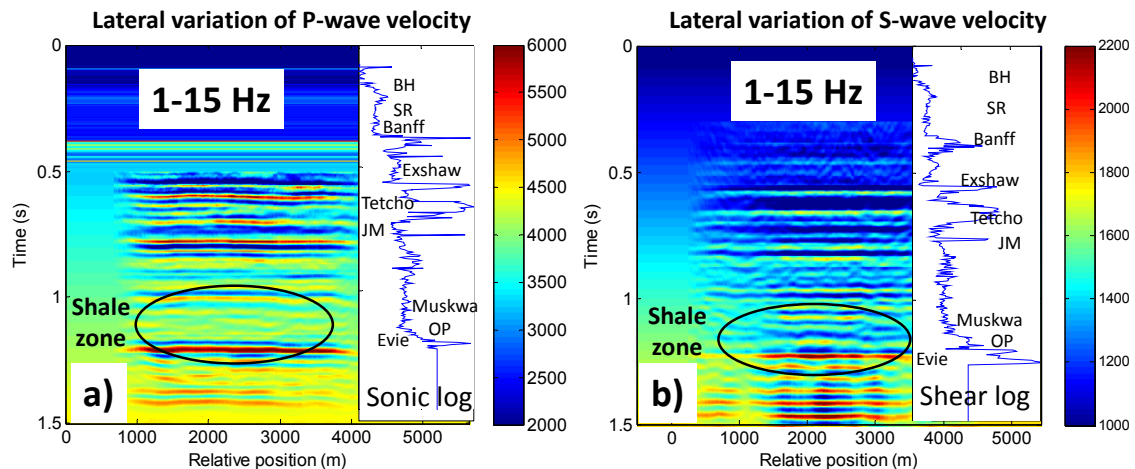


FIG. 1. Iterative waveform inversion of P-to-P and P-to-S data. a) P-wave velocity inverted from 1-15 Hz frequency content of P-to-P data starting from 0.5s. b) S-wave velocity inverted from 1-15 Hz P-to-S data starting from 0.3s.

Linear and nonlinear poroelastic AVO

Steven Kim and Kris Innanen

ABSTRACT

The purpose of our research is to merge the results of two recent theoretical and practical studies. First, Russell, and his fellow co-authors, has argued for a parameterization of the linearized AVO problem which highlights jumps in poroelastic properties across a reflecting boundary. The parameterization brings the Biot fluid term to the foreground. Second, Innanen has recently introduced an approach to analyzing linear and nonlinear AVO which mirrors the more general problem of scattering, and which accounts for low order nonlinearity in an intuitive way. This paper summarizes a project in which the poroelastic AVO problem is cast in terms of this nonlinear formalism. We derive first, second, and third order terms in an expansion for Rpp. The expansion is in terms of changes in density, shear modulus, and the Biot fluid term. We confirm mathematically the role second and third order fluid terms play in determining Rpp amplitudes. We comment on future directions the work can take, including moving towards a general poroelastic scattering picture, and incorporating dynamic poroelastic models also.

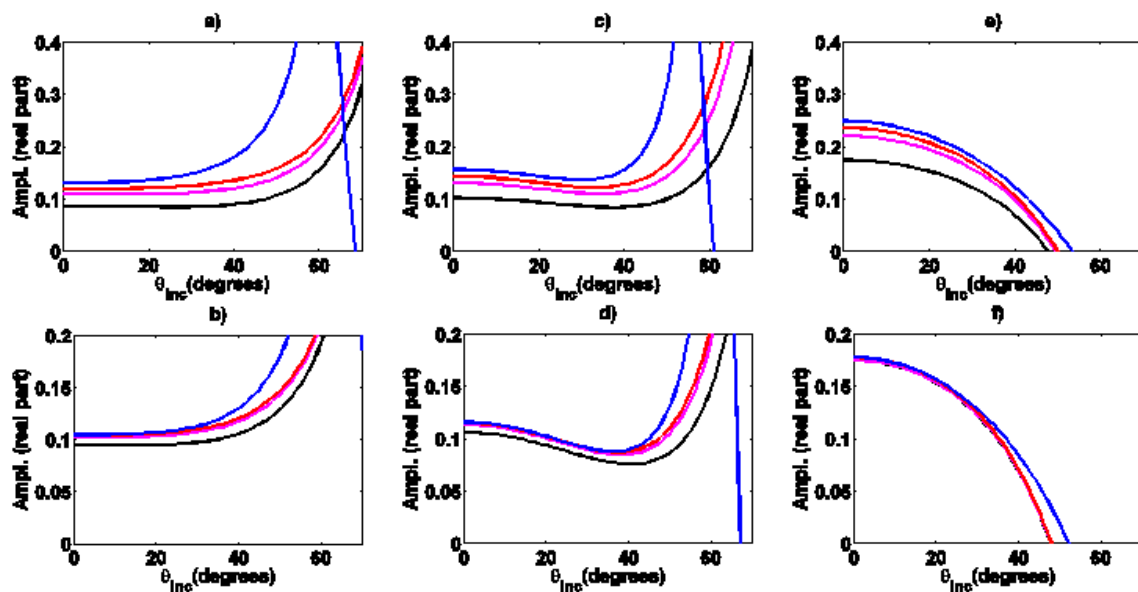


FIG. 1. (a), (c), and (e) represent the perturbation based (a_f , a_μ , a_ρ) poroelastic AVO approximations of 1st, 2nd, and 3rd order and are shown by the black, magenta, and red curves respectively. (b), (d), and (f) represent the reflectivity based ($\Delta f/f$, $\Delta\mu/\mu$, $\Delta\rho/\rho$) poroelastic AVO approximations of 1st, 2nd, and 3rd order and are shown by the black, magenta, and red curves respectively. The exact amplitudes are shown by the blue curve.

Detection and characterization of anelastic AVF with the Gabor transform

Jesse M. Kolb, Kristopher A. H. Innanen

ABSTRACT

Amplitude variation with frequency (AVF) inversion can be used to estimate Q given anelastic frequency-dependent reflection coefficients. While AVF signal is generally analyzed event-by-event, traces are usually populated with many events at different arrival times. This creates the need to perform time-frequency analysis in order to isolate the reflectivity from a single event. We choose the Gabor transform as the instrument for our analysis and use it to estimate frequency-dependent reflectivities from synthetic traces. These reflectivities are then inverted to obtain accurate Q estimates. In order to test limits of this method, we also tested its performance under increasing noise levels, as well as with a reflection from a second interface that is close to the interface in which we are interested.

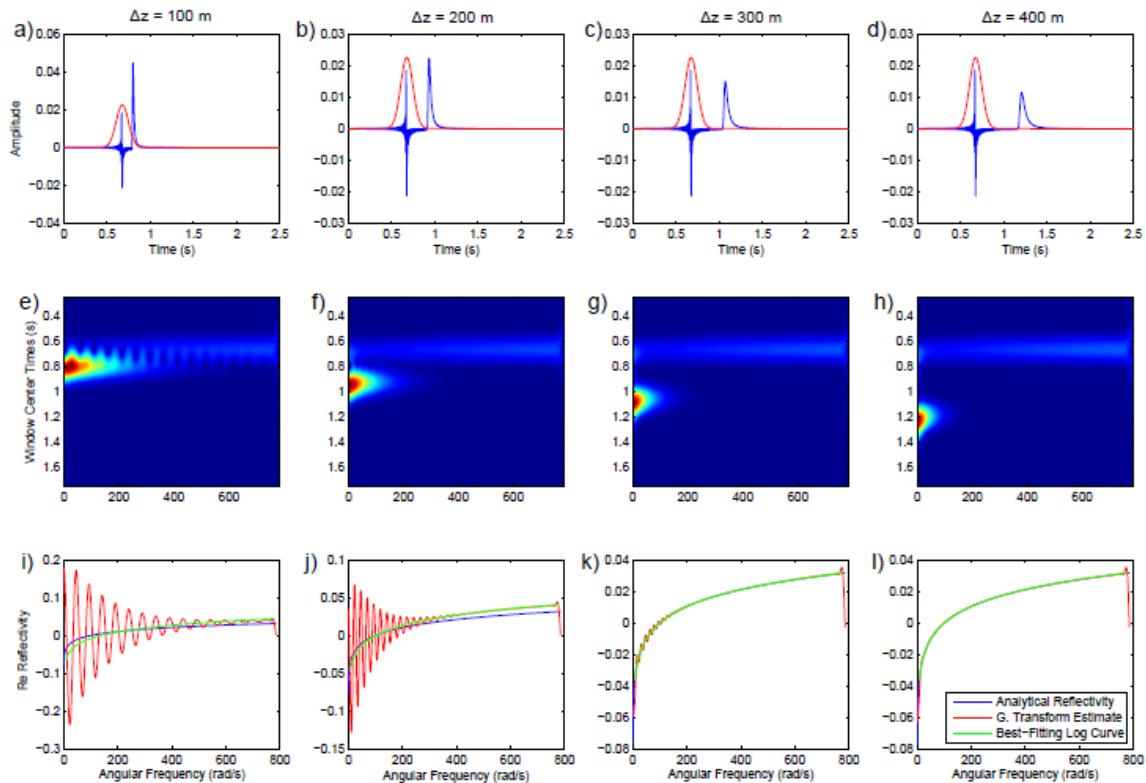


FIG. 1. Analysis using our standard Gaussian window size for closer reflectors. (a-d) show traces for two reflections separated by distances of 100, 200, 300, and 400 m. In red is the size of the Gaussian window used in our Gabor transforms for this analysis. (e-h) show the Gabor transforms and (i-l) show the $R(\omega)$ estimates, and their best-fit curves, for the traces above them.

Can we see a velocity ramp in reflection seismic data

Michael P. Lamoureux, Peter C. Gibson, Gary F. Margrave

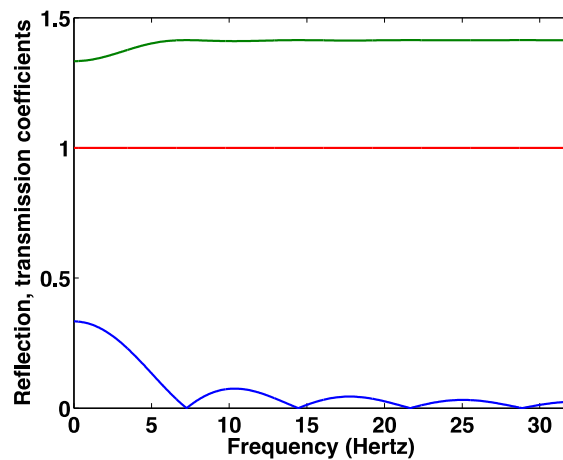
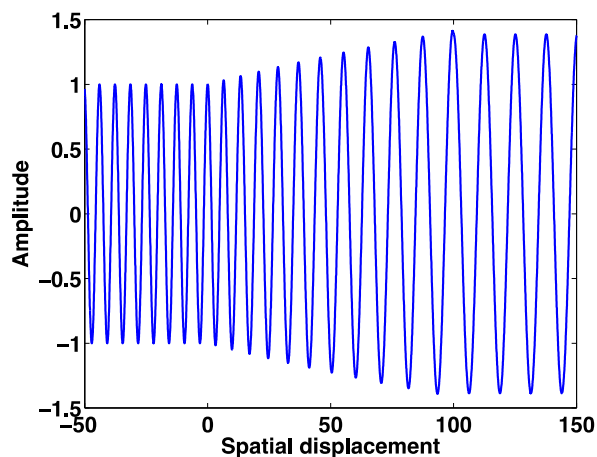
ABSTRACT

We answer the question: what happens when a seismic wave propagates from one region of constant velocity to another region of different velocity, through a smooth transition zone – and can we detect this with seismic reflection data?

This work presents an exact analytic solution for the case of a linear ramp velocity in the transition zone, and demonstrates that for long wavelengths, the ramp looks essentially like a jump discontinuity in the medium, with the corresponding reflection and transmission coefficients. For short wavelengths, the ramp provides essentially 100% transmission and no reflection.

We describe the mathematical details of this frequency-dependent reflection and transmission, and derive an estimate of the feature size of the transition zone that should be detectable. If we can detect zero crossing in the middle of the frequency range of our seismic measurements, for instance at 50Hz, we expect to be able to detect transition zones with length on the order of $L = c/100s^{-1}$, where c is the velocity of propagation.

We also present the numerical result for the transmission and reflection of a delta spike through the velocity ramp, and observe the reflection is a broadened “boxcar” response, whose width is directly related to the width of the transition zone. The transmission of the spike, however, also results in a spike.



Wave propagation in a velocity ramp.

Reflection response from the ramp.

A new S-wave seismic source

Don C. Lawton*, Eric V. Gallant, Malcolm B. Bertram, Kevin W. Hall, Kevin L. Bertram

ABSTRACT

Over the past year, CREWES designed and built a new shear-wave seismic source for multicomponent near-surface seismic studies. The source component of the system is a model A200 accelerated weight drop device manufactured by United Service Alliance Inc from Texas City, Texas. This source is mounted on a 2000 kg tandem axle trailer. The trailer, source configuration and all of the operational components were designed by CREWES and built in Calgary by CREWES and a fabricating shop. At the heart of the source is a 100 kg hammer that is accelerated by compressed nitrogen over a pressure range from 500 to 2000 psi. A pivot system was designed to enable the source to generate both P-wave and S-waves. The source mast can be operated in a vertical mode for generating P-waves and it can rotate ± 45 degrees transverse to the longitudinal axis of the trailer, in order to generate down-going P-wave and S-waves simultaneously. The photograph below shows the source in operation in the S-wave configuration, with stabilizers mounted on the rear of the trailer to minimize rotation of the trailer when the source fires. Pure-mode down-going S-waves are generated by subtracting records taken with the mast rotated in the positive and negative tilt modes. A triggering system was designed to allow vertical stacks at the source location.

Test data generated by this source show that good quality P-wave and S-wave data have been obtained, with surface seismic and vertical seismic profile examples given in other papers in this research volume. We plan to use this source to better understand the P-wave and S-wave velocity structure of the near-surface.



Viscosity estimation using seismic inversion

Laurence R. Lines*, Fereidoon Vasheghani and R. Phillip Bording

ABSTRACT

In the analysis of enhanced heavy oil production, it is crucial to have some knowledge of fluid viscosity in order the flow of oil in reservoir simulation. While viscosity can be measured using fluid samples taken from the borehole, it would be advantageous to have some measure of viscosity between wells. We develop a methodology for doing this by using seismic travelttime tomography to estimate velocity, followed by attenuation tomography to estimate seismic-Q. Tomographic inversion methods have been applied to crosswell seismic data from a heavy oil field in Northern Alberta. The Q values are transformed to viscosity values using the Biot Squirt theory (BISQ). Although this transformation can be ambiguous, the ambiguity problem can be obviated if we have some borehole information about viscosity to within an order of magnitude. A viscosity tomogram from a Laricina heavy oil field in Northern Alberta is show in Figure 1 below.

The estimates of Q could presumably be further improved by the use of full waveform inversion. One of the concerns with full waveform inversion is its sensitivity to noise. We have tested full waveform inversion on noisy model data and have found it to be robust for signal-to-noise ratios of 5, with convergence to a model fit within three iterations. The next steps in this research should involve the application of the inversion methods to time-lapse crosswell seismic data in order to monitor the changes in viscosity with time. This greatly enhance our ability to characterize dynamic changes is a heavy oil reservoir.

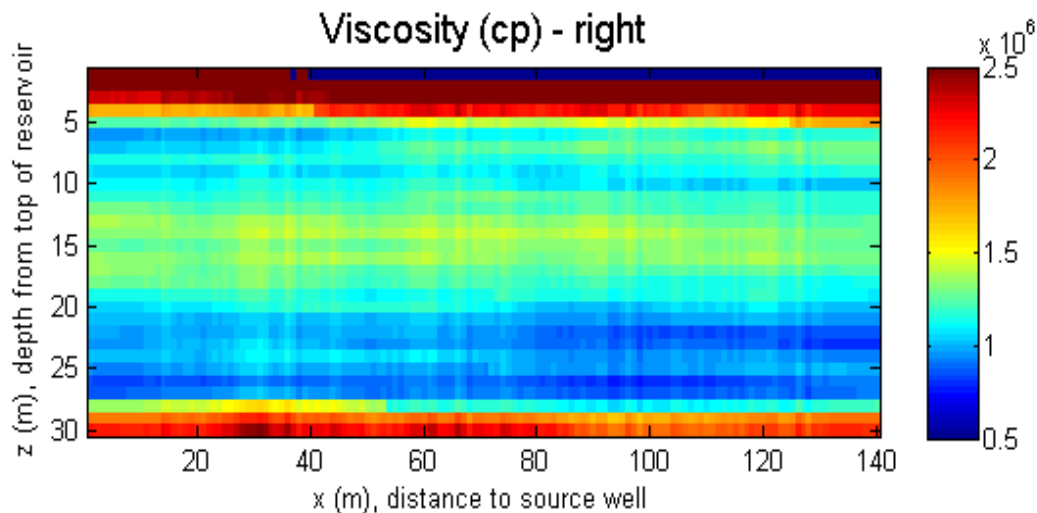


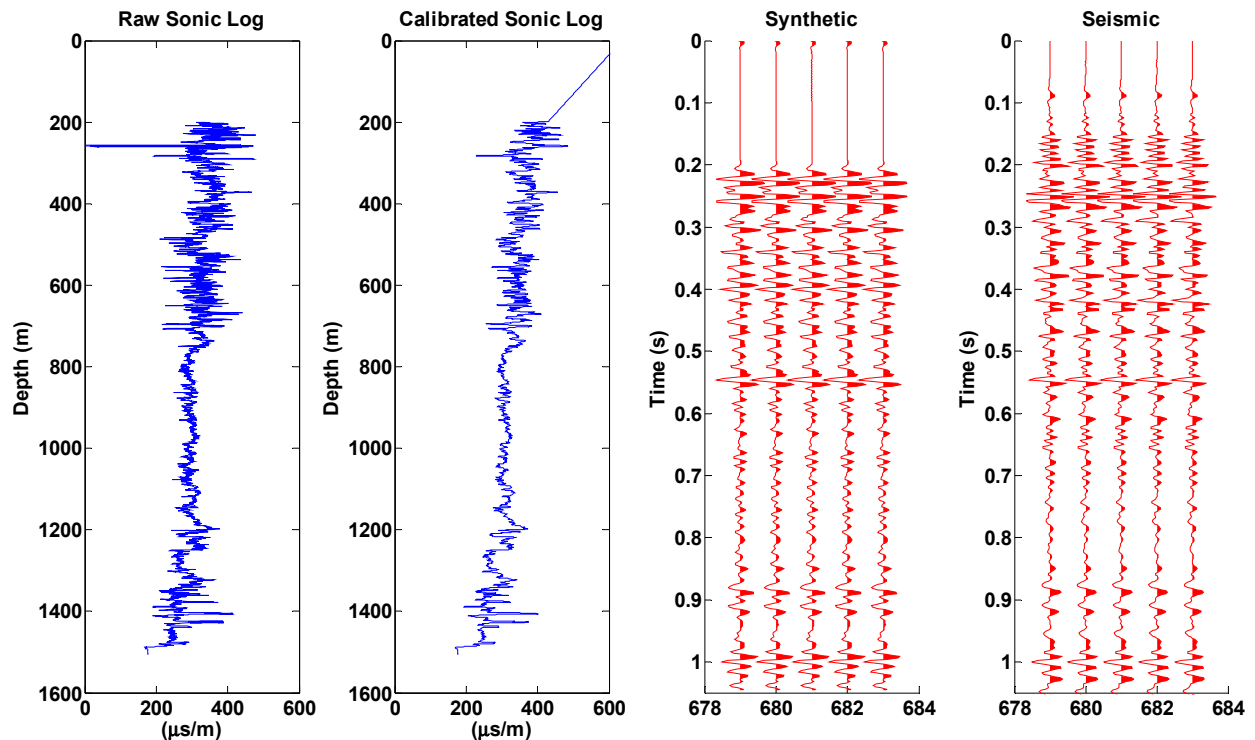
FIG. 1. This figure shows the viscosity tomogram for 30 m of the Grand Rapids heavy oil reservoir from a crosswell survey between two Laricina wells spaced 140 m apart. (Vasheghani and Lines (2012 Journal of Seismic Exploration, v21, 247-266).

The art of well tying with new MATLAB tools

Heather J.E. Lloyd* and Gary F. Margrave

ABSTRACT

To tie seismic data to well logs, four steps are required. The first step involves editing the sonic and density well logs, including de-spiking the logs, truncating any anomalous values and smoothing the logs to account for stratigraphic attenuation. Since the velocities that seismic data experience are different then the velocities sonic tools measure a calibration step is needed. The most common way to do this is to use checkshot data, however when this data is not available the calibration can be computed from an attenuation (Q) estimate or by matching seismic events to events on the synthetic. The third step includes the calculation of the time-depth relationship using the calibrated sonic and the calculation of reflection coefficients from the sonic and density. In the last step the wavelet is estimated from the seismic data and phase rotations are applied to get good correlation between the seismic and the synthetic. A series of MATLAB tools have been developed to make the well-tying process easier and good synthetics obtainable in a short amount of time.



Phase and group velocity measurements from physically modeled transmission gathers

Faranak Mahmoudian, Gary Margrave, and Joe Wong

ABSTRACT

Physical model data have been used for many years to simulate exploration targets, as in the example of a fractured medium. Yet, physical modeling is challenging for at least two reasons, (1) the initial characterization of the medium is difficult, and (2) the large highly-directional transducers used as sources and receivers cause distortions. The initial characterization of an anisotropic physical model is done by determination of elastic stiffness coefficients from the phase or group velocity measurements along various directions. We present a review on how to measure phase and group velocities from physical model transmission gathers acquired using piezoelectric transducers with different sizes. Group velocity measurements are found to be straightforward, reasonably accurate, and independent of the size of the transducers used. In contrast, the accuracy of phase velocities derived from the (τ, ρ) transform analysis was found to be very sensitive to small differences in picked arrival times and to transducer size. Compared to the phase-velocity procedure, the technique involving group velocities is much less prone to error due to time-picking uncertainties, and therefore is more suitable for analyzing physical model seismic data.

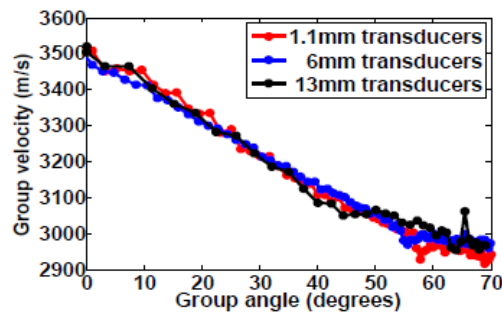


FIG. 1. Group velocity estimated from transmission data, (x_1, x_3) plane, acquired with three transducer sizes using the edge-to-edge distance correction.

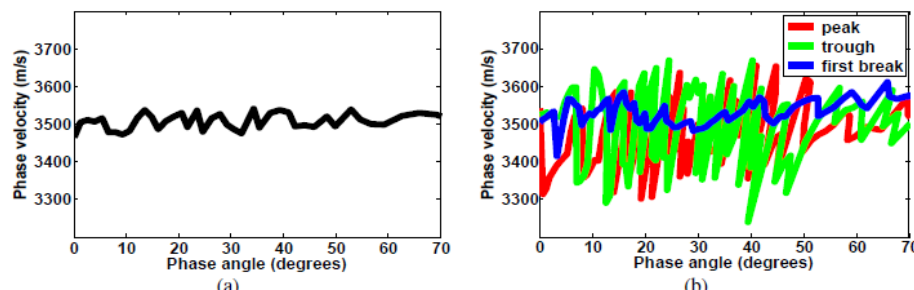


FIG. 2. Phase velocity measured from finite-difference data gathered over an isotropic layer with the constant velocity of 3500m/s. (a) Point source and receiver data. (b) 13mm transducer data, comparing the phase velocity when picking on first-break, peak or trough of the event on the (τ, ρ) transform.

Finite-difference models with an internal water-bottom boundary condition

Peter M. Manning and Joe Wong

ABSTRACT

The rationale for generating comparable physical and computer models is given. The requirement for a finite-difference model with one of its internal horizons conforming to a physical boundary condition is explained. The boundary condition is that of a water-bottom, where the acoustic waves in the water interact with the elastic waves in the solid material below. The condition is developed for use within the staggered-grid representation. Examples are given for a model that matches a physical model in water, and for some simple offshore seismic type models.

FIGURES

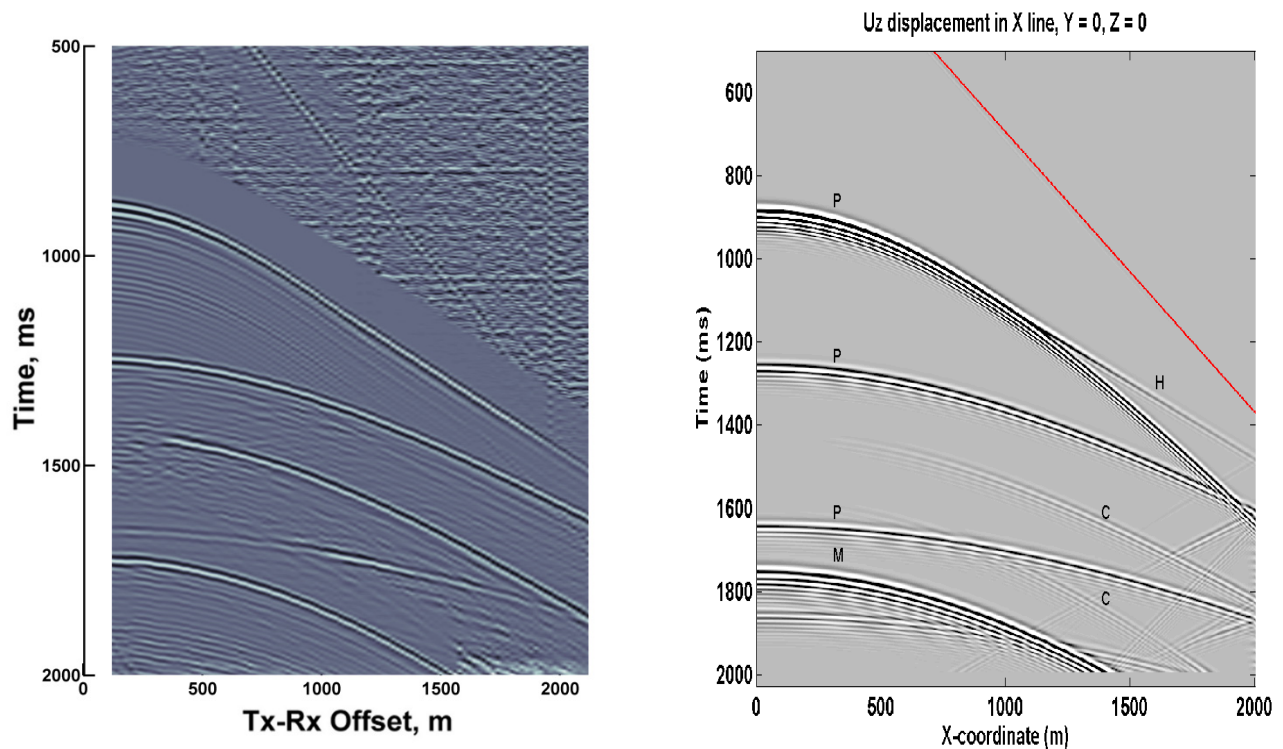


FIG. 1. Left: Physically modeled seismicogram for a model with a water-solid reflecting interface, displayed with a 200 ms. AGC. Right: Numerically modeled seismicograms for a structure similar to the physical model, displayed without AGC. Primaries are marked P, a multiple is marked M, a head-wave is marked H, and converted and reconverted wave events are marked C. The most obvious difference is the almost complete conversion of the first primary reflection into a head-wave in the physical model.

CREWES 5-year research plan: Towards broadband multicomponent seismology and practical iterated inversion

Gary Margrave, Kris Innanen, Don Lawton, John Bancroft, Michael Lamoureux, and Larry Lines

ABSTRACT

Seismic images provide the best possible views of the earth below its surface; but, despite an 80 year history, they are still far from optimal. Today, the computer methods used to create such images are transitioning from a standard methodology (SM), which incorporates an evolved blend of physical theory and practical experience, to the very modern full-waveform inversion (FWI) that is much more firmly rooted in mathematical

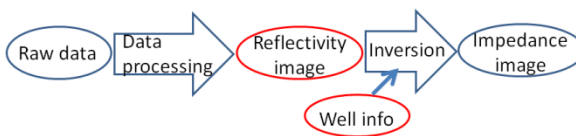


FIG. 6. The Standard Methodology (SM)

physics. However, this transition is hindered by insufficient low-frequency content in seismic data, by the inherently unknown seismic source waveform, by incompletely understood physics, and by the extreme computational effort required. As a consequence, SM is the dominant approach while FWI is rarely attempted outside of dedicated research labs. SM uses a sophisticated data processing sequence to create a reflectivity image of the subsurface. Then, incorporating well information, an inversion process converts the reflectivity image to earth properties such as impedance. FWI is a fundamentally iterative process that converges on an impedance model by minimizing the difference between real and predicted seismic data. FWI never creates a reflectivity image and does not use well control; while SM does not predict synthetic data and is not iterated. We will create a new class of seismic inversion methods that combines the most robust features of SM with the most promising concepts from FWI. From SM, we will retain most of the data processing steps, the creation of a reflectivity image, and the matching to well control. In particular, matching to well control facilitates the source waveform estimation and provides the needed low frequency information. From FWI, we will incorporate the concepts of iteration, prediction of synthetic seismic data, and imaging of the data residual. The proposed approach, which we call IMMI (Iterated Modelling, Migration, and Inversion), will produce estimates of subsurface properties that both match measurements in wells and also predict most features in the recorded seismic data. Such estimates should be much more reliable than those presently achieved by SM. This will have significant benefits to resource exploration and to subsurface environmental studies.

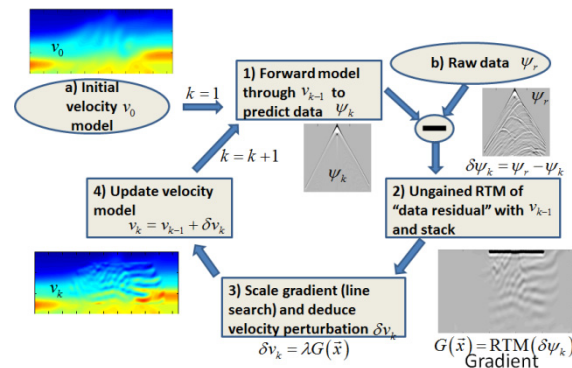


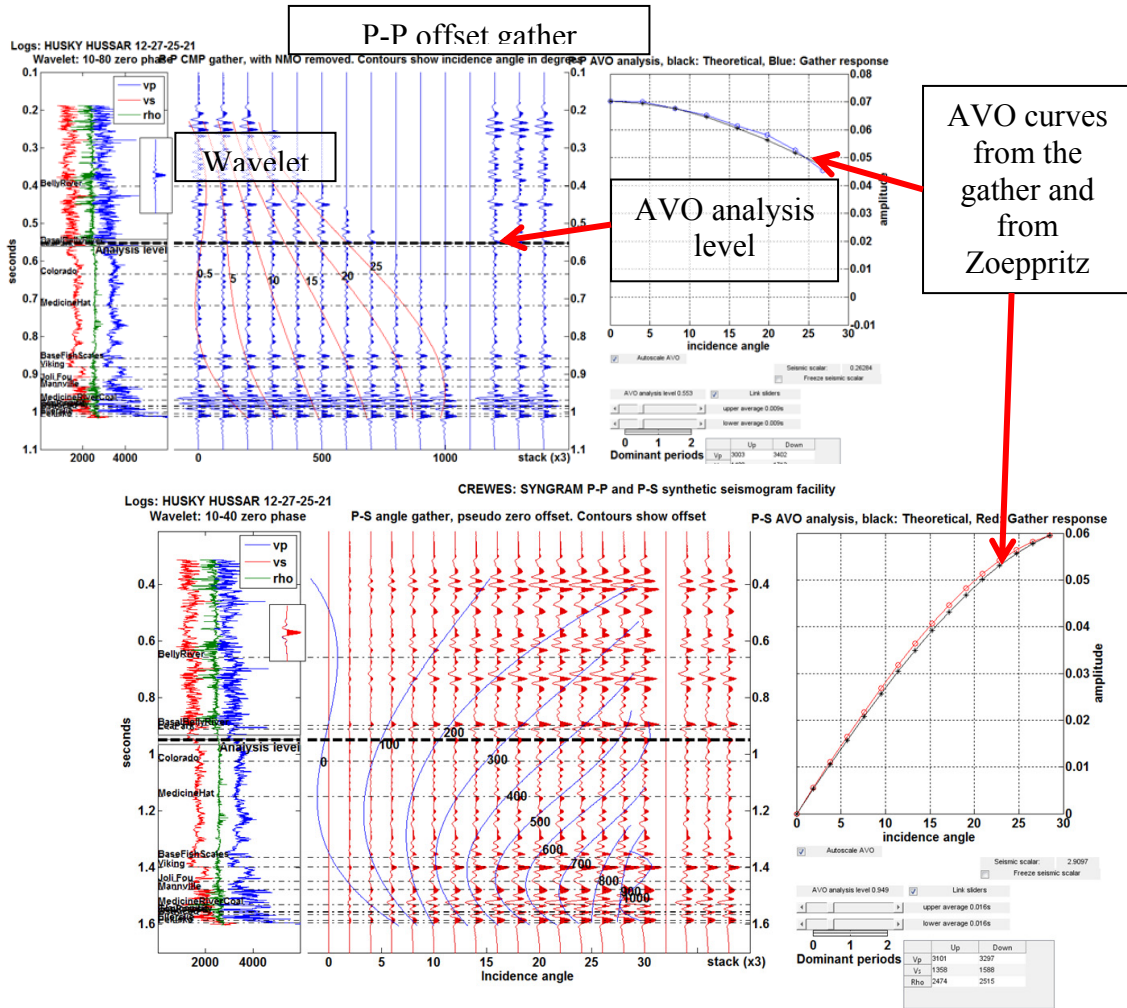
FIG. 5. Full Waveform Inversion (FWI)

New features in SYNGRAM

Gary F. Margrave

ABSTRACT

The CREWES AVO synthetic seismogram facility, SYNGRAM, has been upgraded to include several new features. These are (1) An interactive AVO analysis tool, (2) The option to create angle gathers as well as the traditional offset gathers, and (3) a wavelet display axis. The AVO analysis panel allows the interactive selection of an analysis level and then compares the AVO in the gather with that from a simple Zoeppritz calculation. These tend to agree on strong reflectors but not on subtle ones. The angle gathers are created by tracing rays from each reflector to the source and receiver at constant incidence angle regardless of the ultimate offset. Angle gathers are contoured with offset values while offset gathers are contoured with angle values. Finally the wavelet display panel provides a visual reminder of the selected wavelet and is plotted at the same scale as the seismogram and logs. This provides a direct assessment of resolution in either time or depth.

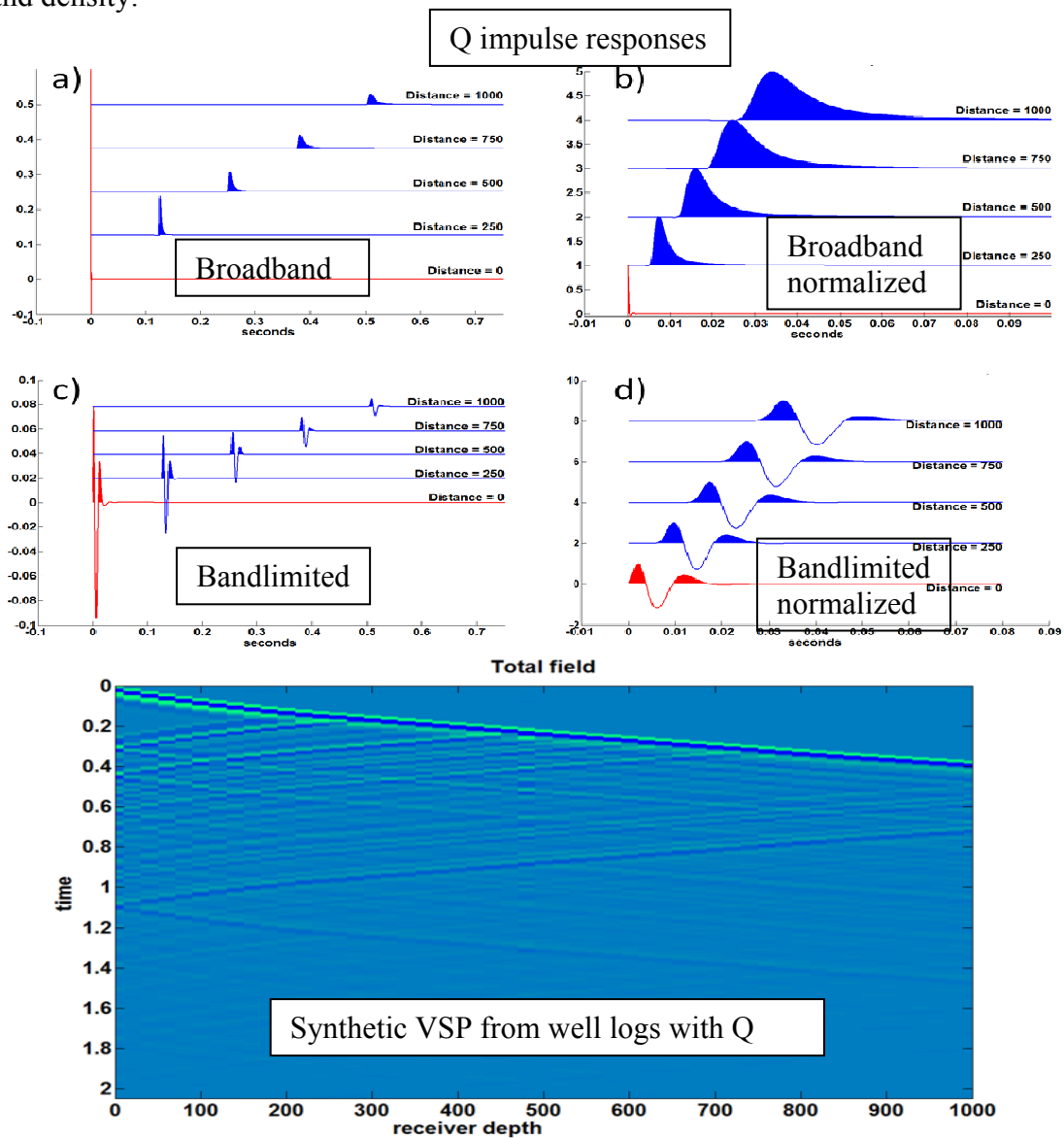


Q tools: Summary of CREWES software for Q modelling and analysis

Gary F. Margrave

ABSTRACT

CREWES has a number of tools in our Matlab toolbox for modelling constant Q attenuation and analysis of the results. The analysis tools can also be applied to real data. This paper presents an overview of those tools and illustrates their use in a few simple cases. We have tools to (1) generate the theoretical impulse response of 1D anelastic propagation, (2) to build a Q matrix that applies first-order Q transmission effects to a stationary signal, (3) to create an inverse Q matrix that removes Q effects, (4) to calculate the drift time given a Q model, (5) to drift correct a synthetic seismogram, (6) to estimate Q from a seismogram, (7) to build an empirical Q model from standard P-sonic and density logs, and (8) to create a theoretical zero-offset VSP given models of Q, velocity, and density.

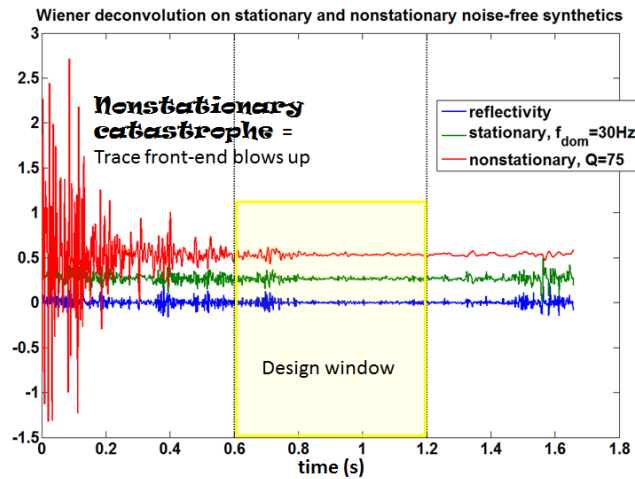


Why seismic to well ties are difficult

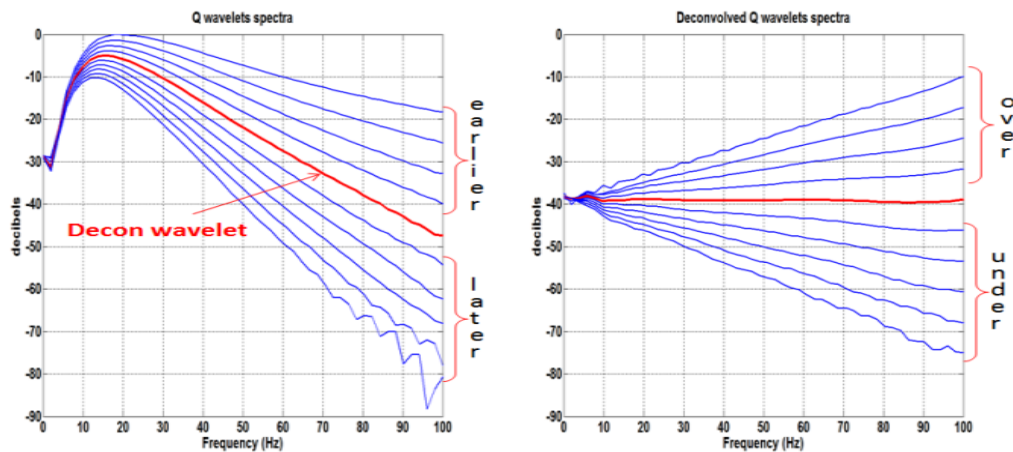
Gary F. Margrave*

ABSTRACT

Tying seismic data to well control is a crucial step in seismic inversion and interpretation. This is where key ambiguities that prevent the interpretation of a seismic image as bandlimited reflectivity are resolved. Reflectivity can be calculated directly from suitable well logs while the estimation of reflectivity from seismic requires the unambiguous determination of the seismic wavelet and the removal of the same. However, due to the unavoidable presence of anelastic attenuation, the very notion of a single seismic wavelet is not robust. Instead, constant-Q theory predicts that the source waveform evolves continuously as it propagates in the subsurface. It progressively loses frequency content and undergoes continual phase changes. This evolution means that each reflecting structure in the subsurface is illuminated by a unique waveform. The use of stationary (standard) deconvolution methods leads to a trace with unbalanced amplitude, in both time and frequency, and time-variant residual phase. Attempts to remedy this by time-variant balancing leads to a trace that can, at best, be tied to a well in a local time zone but which has misties above and below that zone. Nonstationary deconvolution or inverse Q filtering can potentially address these effects but the former relies on a statistical reflectivity model while the latter requires knowledge of Q. Well tying can be improved by using deconvolution algorithms and well-tying methodologies that are consistent with constant-Q theory.



Understanding the Nonstationary catastrophe



Parallel VSP Experiment

Paul E. McGee and Robert J. Ferguson

ABSTRACT

Shot record modelling of VSP surveys can be computationally time intensive. To address this issue, we parallelize the running of forward modeling code, and we discuss the performance gains that result. The performance of this parallel implementation is measured on a cluster, and we find that performance gains are achieved with only small changes to the original code.

To discuss hardware effects on performance, hardware factors are tabulated with the most expensive factors being number of processors, the processors themselves, cluster memory and the communications backbone. We derive an equation relating total computation time to size of the survey, they are related through hardware dependent coefficients.

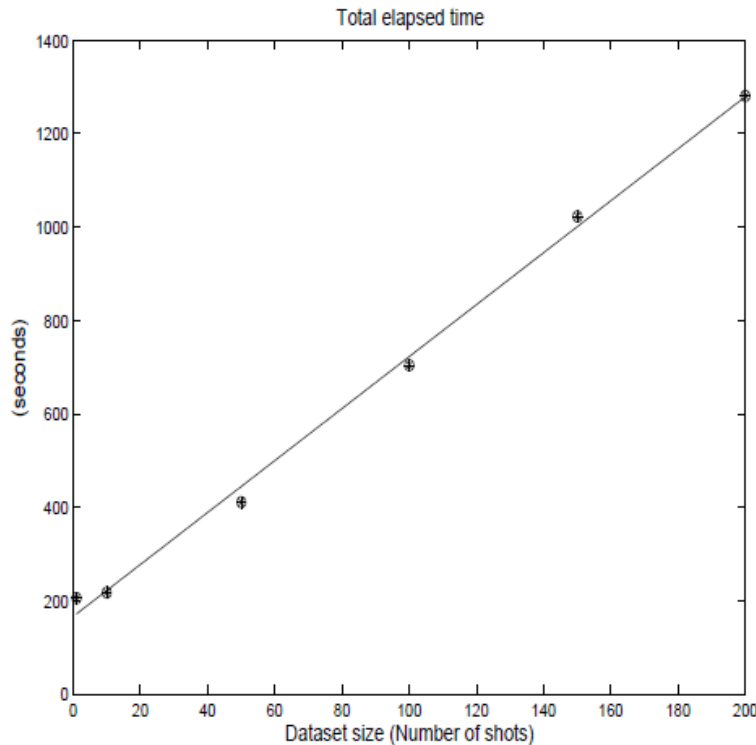


FIG. 1. Computation performance: X-axis is number of shots, Y-axis is the total elapsed time in seconds. The straight line is a linear fit to the performance data, circle and cross symbols are elapsed time measurements.

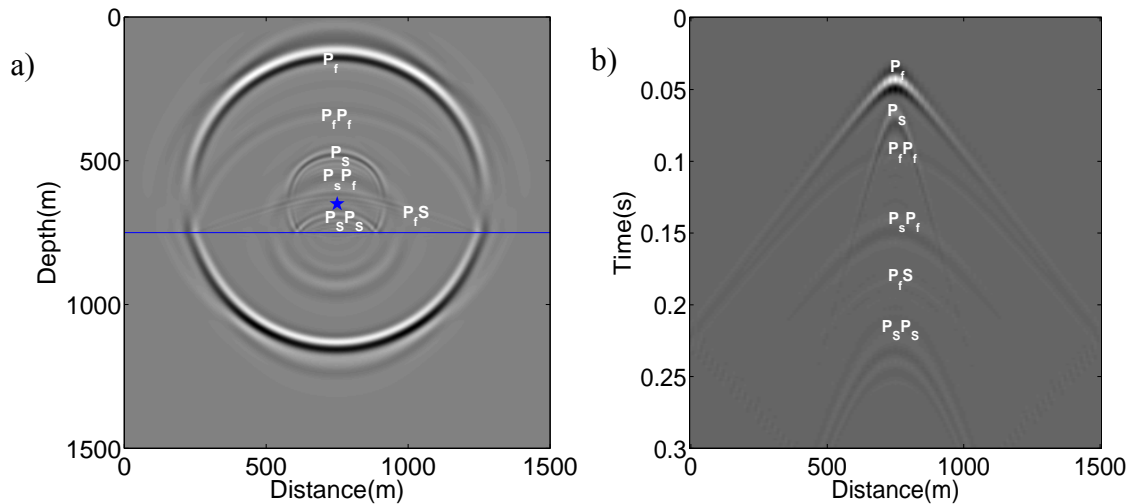
Software implementation was done most importantly using Matlab's Parallel Computing Toolbox (PCT) and inline methods. The VSP experiment was done with computation of different shots being distributed to Matlab workers.

Velocity-stress finite-difference modeling of poroelastic wave propagation

Shahin Moradi* and Don C. Lawton

ABSTRACT

A velocity-stress staggered-grid 2D finite difference algorithm was developed in Matlab to model the wave propagation in poroelastic media. The Biot's equations of motion were formulated using a finite difference algorithm with fourth order accuracy in space and second order accuracy in time. We examined two examples, where the first was a single layer sandstone saturated with brine and second, a two-layered sandstone model with same matrix properties in both layers, but with different fluid content. As predicted by Biot's theory a slow compressional wave was observed in the particle velocity snapshots. In the layered model, at the boundary, the slow P-wave converts to a P-wave that travels faster than the slow P-wave. The results showed that our algorithm handles the layered model perfectly and can be used for more complicated models as well. In the future, this finite difference algorithm could be used for inversion to obtain the properties of the porous media, including saturation.



The solid vertical particle velocity snapshot calculated for a two-layered model at the time 0.16 s (a), and the corresponding shot gather (b).

Viscoelastic scattering potentials and inversion sensitivities

Shahpoor Moradi* and Kris Inannen

ABSTRACT

The scattering formulation presented in 2012 by Stolt and Weglein for isotropic elastic waves, in addition to being a major contribution on its own, represents a jumping-off point for the description of the interaction of seismic waves with a wide range of heterogeneous media. In this paper we extend the scattering picture to include viscoelastic waves, focusing in particular on generalizing the layered medium results of Borchardt. The main theoretical challenge involves the choice of coordinate system over which to evaluate and analyze the waves, which in the viscoelastic case must be based on complex vector analysis. However, a good candidate system is determined, within which several of Borchardt's key results for layered media, concerning the reflection and conversion of homogeneous and inhomogeneous P- and S-wave modes, are shown to carry over to general multidimensional scattering. In addition to extending the domain of applicability of this type of viscoelastic wave theory in an intuitive way, the results when incorporated in a Born approximate wave data model are immediately applicable to both direct and full-waveform type inversion calculations.

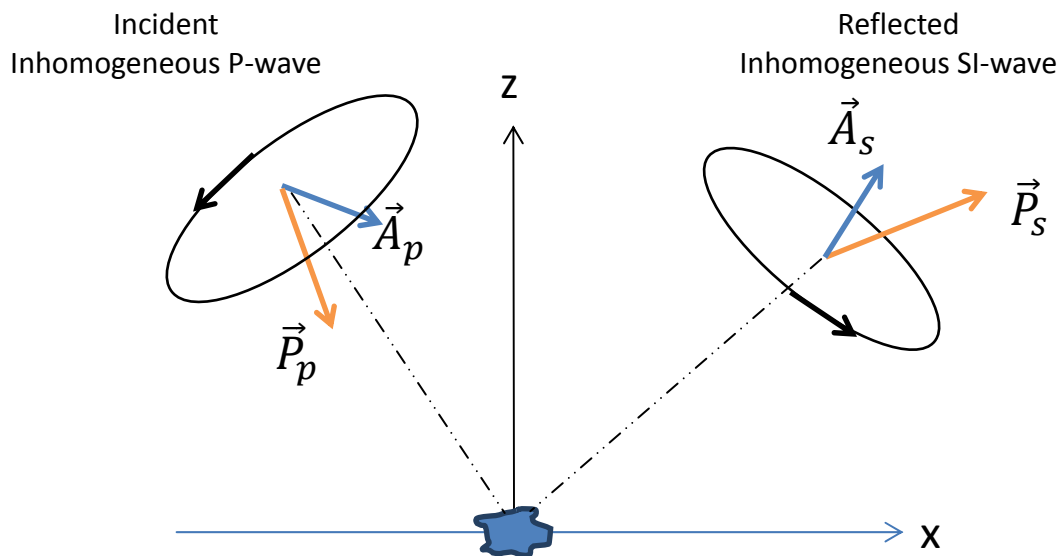


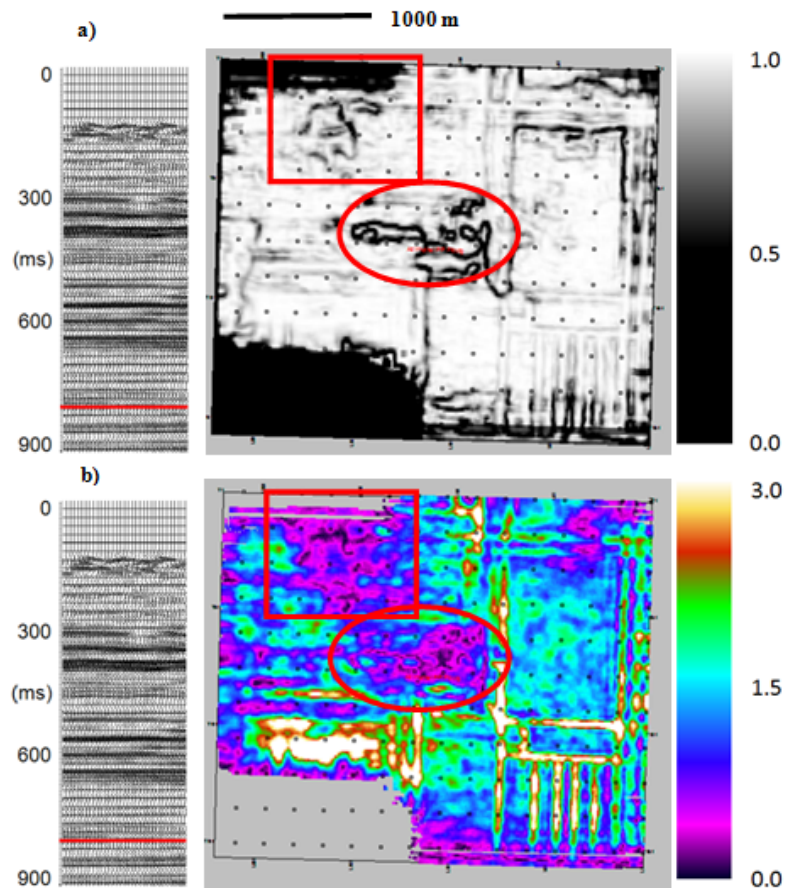
Diagram illustrating notation for directions and magnitude of propagation and attenuation vectors for the scattering of an inhomogeneous P-wave to an inhomogeneous SI-wave.

Fracture analysis using multicomponent seismic attributes: example from Saskatchewan

Andrew Nicol and Don Lawton

ABSTRACT

Multicomponent seismic attributes are used to analyse differences between seismic character from sample to sample and trace to trace in multi-component time-lapse seismic data. In this research, the semblance and amplitude envelope seismic attributes were used to better understand the nature of fracturing in the region. The results from this study confirm previous findings which indicate that fracturing extends from the Dawson Bay Formation vertically into the above Souris River Formation. Both attributes highlight mine workings within the Prairie Evaporite Formation and show anomalies which are interpreted to be the result of fractures within the stratigraphic section with no obvious alignment.



Baseline PP semblance (a) and amplitude envelope (b) time slices through the Prairie Evaporite Formation (792 ms) clearly show mine rooms. In the centre of the slice through the amplitude envelope volume, there is a low value anomaly which is significantly lower than that of the rest of the area. This anomaly has been interpreted to be the result of subsurface fracturing which does not have a preferential orientation.

Reservoir simulation for a CO₂ sequestration project

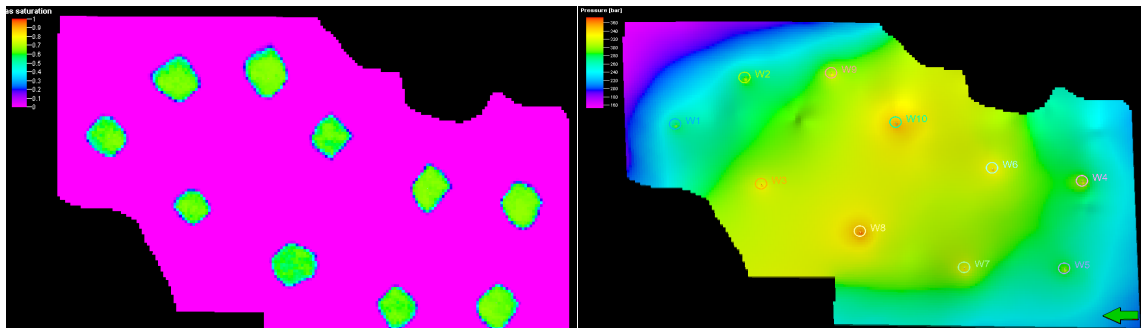
Davood Nowroozi and Donald C. Lawton

ABSTRACT

Time-lapse seismic surveys of a reservoir are an effective way to monitor alterations in the dynamic reservoir parameters and the fluid migration regimen during production or injection. The project is a study of a reservoir under a specified injection plan, using updated geological models in time and space. An existing reservoir model was utilized as the base case. This paper is the initial stage of a larger project; it's focus is reservoir simulation. The reservoir was chosen from the Wabamun Area Sequestration Project (WASP). The WASP project was a CO₂ sequestration that was led by the University of Calgary previously.

The target layer for injection is the Nisku aquifer. It is a Devonian carbonate formation with high capacity (porosity) and injectivity (permeability), capped by the Calmar shale. These properties make it a suitable medium for CO₂ injection and efficient storage. A geomodel of the project was available. For this research an injection plan was defined with ten wells and constant bottom-hole injection pressure. The behavior of the reservoir was simulated for 50 years of injection and a further 50 years for prediction of the CO₂ plume shape and pressure changes in the reservoir.

After 50 years injection with constant bottom-hole pressure, the CO₂ plume only covered approximately 10 % of the top layer of the Nisku aquifer of the geomodel area, but pressure changes occurred over the entire reservoir. For 50 years after injection termination, the mass of the plumes did not change meaningfully but pressure equalized across the entire reservoir. The defined plan can only store 25% of the expected total CO₂ locally available for sequestration (20 Mt/year).



CO₂ plumes for injection wells (left) and pressure distribution in the reservoir (right) at the end of injection (50 years).

1D internal multiple prediction in a multidimensional world: errors and recommendations

Pan Pan* and Kris Innanen

ABSTRACT

Internal multiples are more difficult to estimate and eliminate than free surface multiples. To eliminate these effects, internal multiple prediction becomes a necessity. In this paper, we employ the 1D internal multiple algorithm due to the work of Weglein and collaborators in the 1990s. We review the basic principles of the internal multiple prediction algorithm. The key characteristic of the inverse scattering series based method is that information from the subsurface is not a requirement, as they are fully data-driven. Internal multiples from all possible generators are computed and shown in the output. Its performance is demonstrated using complex synthetic data sets with encouraging results. Then we systematically study how the presence of offset and the existence of dipping angle in the reflectors affect the 1D internal multiple prediction algorithm. Finally, we give some recommendations for the applications of this method. We do not recommend applying this method when the offset is greater than 300m. Although this theory is based on a flat layered structure, the result of small dipping angle layers is acceptable. All results up and until dipping angle equals 10 degrees show good results.

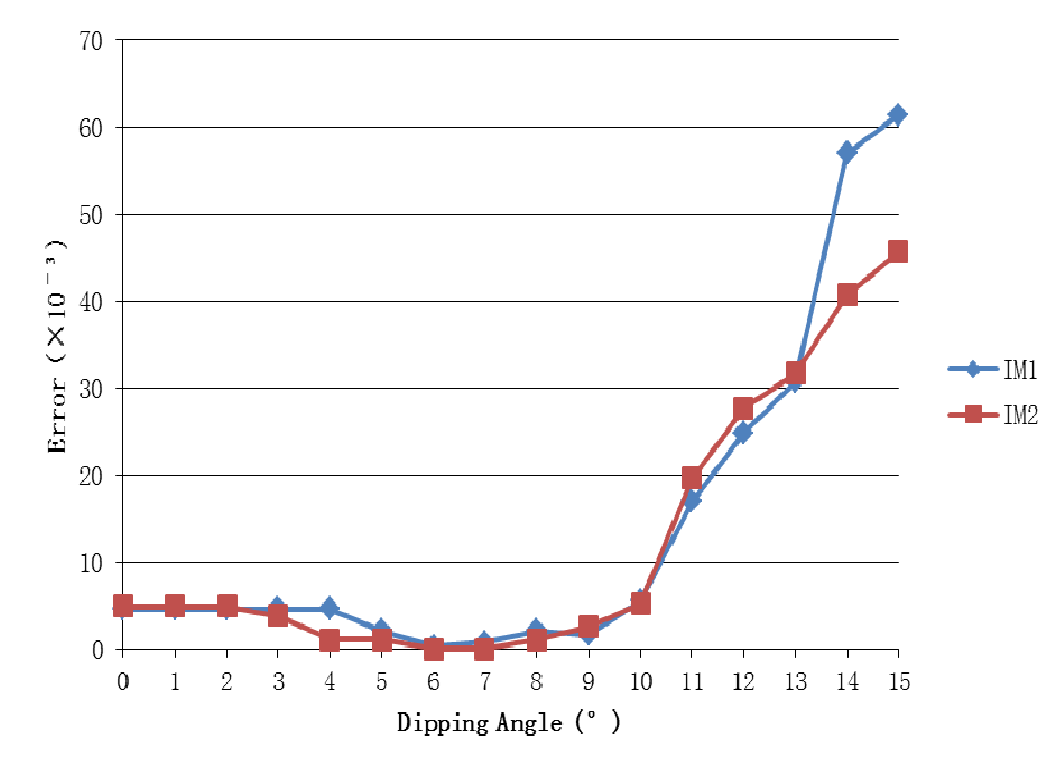


FIG. 1. Prediction errors in the zero offset trace plotted against an increasing series of dipping angles, the generator is the dipping interface. The blue line is the prediction error of the internal multiple 1 and the red line is the prediction error of the internal multiple 2.

Numerical analysis of 1.5D internal multiple prediction

Pan Pan and Kris Innanen

ABSTRACT

Multiples attenuation is a key process in seismic data processing, and the quality of multiples elimination will affect the final imaging directly. In this paper, we present a 1.5D MATLAB implementation of the inverse scattering series internal multiple prediction algorithm developed by Weglein and collaborators in the 1990s. Compared to 2D algorithm, the computation cost of 1.5D has been dramatically reduced. With fewer wavenumbers participating in the calculation, it is much cheaper and faster than 2D. This method does not require any subsurface information. However, near offset traces information will be needed for applying this method. We discuss the whole prediction operation, and illustrate the procedure with a synthetic example. Effects of various epsilon values chosen will reveal a more efficient method of choosing the epsilon value. Usefulness of our 1.5D internal multiple prediction algorithm in situations where primaries are mixed together with internal multiples, and dipping interface exists are also demonstrated.

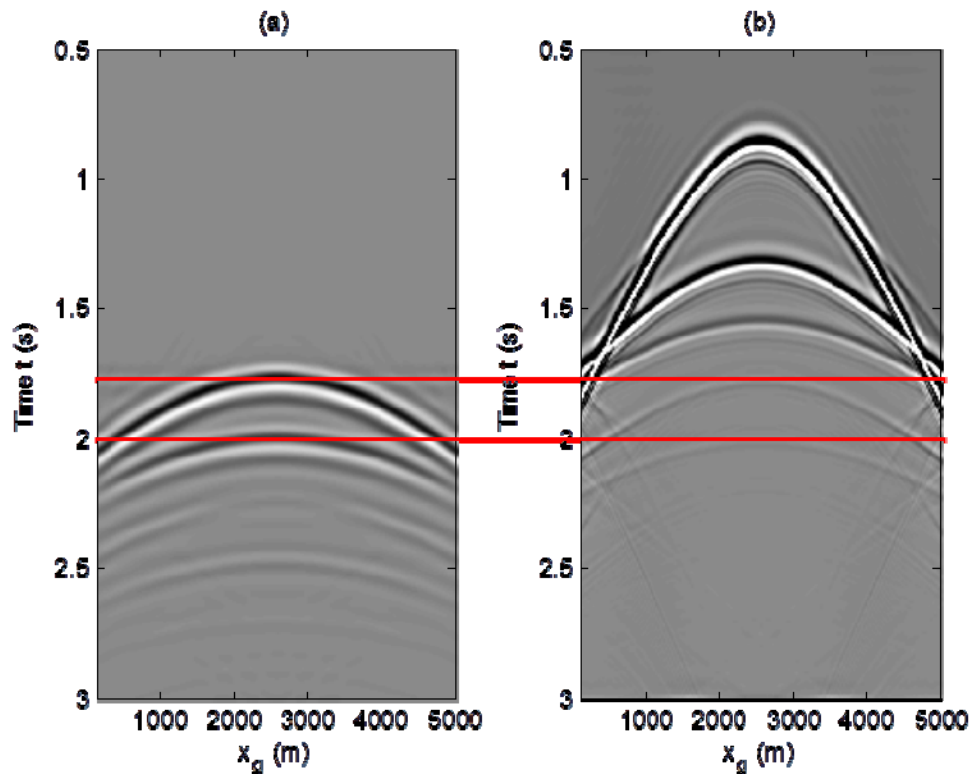


FIG. 1. The output of the 1.5D internal multiple prediction with epsilon value equals 200. (a) The prediction, in which two internal multiples are predicted. (b) The original data with both primaries and internal multiples shown in the data set. Red lines indicate the positions of the internal multiples, which mean the zero offset travel times are correctly predicted.

A review of internal multiple prediction

Pan Pan and Kris Innanen

ABSTRACT

Multiple events can be mistaken for primary reflections, and may distort primary events, and obscure the task of interpretation. So, to eliminate these effects, internal multiple prediction becomes a necessity in the industry. In this paper, we determine the definitions of primaries, multiples, and the most important concept in this research, internal multiples. Inverse scattering series will be introduced here. Then we review the basic principles of the 1D and 2D internal multiple prediction algorithm, which were introduced to geophysics literature in the 1990s, and demonstrate 1D algorithm's use to 1D synthetic data using a MATLAB implementation. Also the basic idea of a lower-higher-lower relationship will be discussed. Then the role and importance of the parameter ϵ are emphasized and the effects of badly chosen epsilon values are shown. For smaller epsilon values, artifacts will be seen at the arrival times of primaries in the output data, while larger epsilon values could damage important information present in the output data. If the overestimation of the value is large enough, the output data will not show any events at all. The 1D internal multiple algorithm has been tested with good results on band-limited synthetic data. Analytical and numerical examples will be used to exemplify the usefulness of 1D internal multiple prediction algorithm.

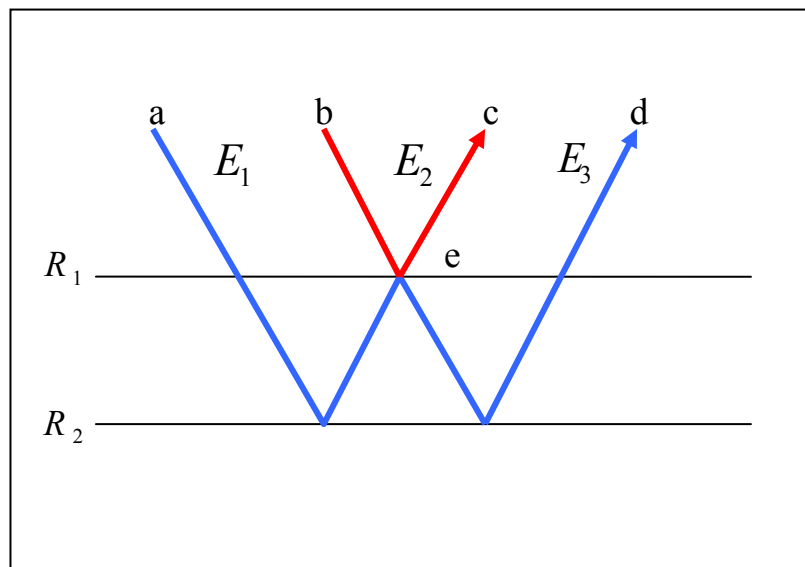


FIG. 1. Construction of an internal multiple using subevent interpretation. The first subevent is a primary reflection that travels from point 'a', reflected from the second reflector, and is received at point 'c'. The second subevent is a primary that propagates from point 'b', reflected from the first interface 'e', and received at point 'c'. The third one is a primary from point 'b' to point 'd', reflected from the second interface.

1D scalar full waveform inversion inferring convergence properties with analytic and numerical examples

Wenyong Pan, Kris Innanen

ABSTRACT

Formulated as a least-squares form, Full waveform inversion (FWI) seeks to minimize the difference between the modeling data and the observed data and estimate the subsurface parameters. It has been widely studied in recent years, but some problems still remain to be addressed. In this research, we performed the analytic analysis of 1D scalar FWI. The analysis to this simplest condition can help us achieve some new ideas and discoveries in FWI. A simple two-interface model and a homogeneous background model are used as the true velocity model and initial velocity model respectively. And two iterations are performed for analysis based on some optimal assumptions. We found that: (1) after the first iteration, the placement error at the second interface is influenced by the velocity contrast and interfaces distance; (2) after the second iteration, the placement error at the second interface become smaller for small velocity contrast, but may become larger for large velocity contrast; (3) and the noises produced in the cross-correlation have a negative influence to the amplitude recovery of the second interface, which will decrease the convergence rate of FWI; (4) but the noises have no significant influence to the placement error of the second interface.

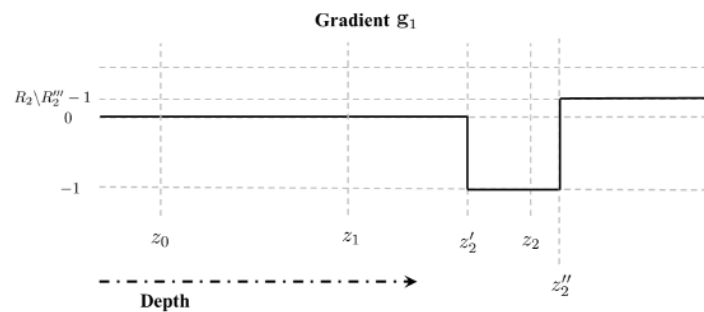


FIG. 1. Gradient g_1 in the second iteration.

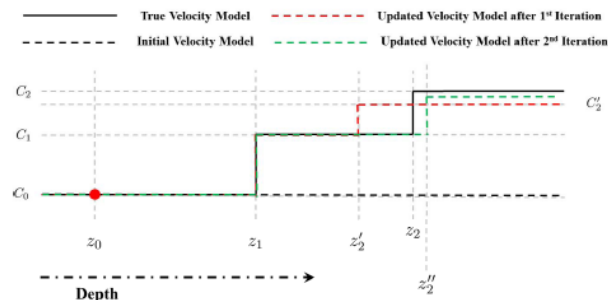


FIG. 2. The inverted velocity model after the second iteration. The black dash line and black solid line are the initial velocity model and true velocity model respectively. The red dash line indicates the velocity model after the 1st iteration. And the green dash line indicates the inverted velocity model after the 2nd iteration.

A comparison of different scaling methods for least-squares inversion/migration

Wenyong Pan, Kris Innanen, Gary Margrave

ABSTRACT

The least-squares inverse problem, such as full waveform inversion and least-squares migration, can be performed iteratively using a gradient based method. While the convergence rate of this method is very slow for that it assumes the Hessian matrix as an identity matrix. The poorly scaled gradient can be enhanced considerably by multiplying the inverse Hessian matrix. Hessian matrix works as a nonstationary deconvolution operator to compensate the geometrical spreading effects and recover the deep reflectors amplitudes. It can also sharp or focus the gradient by suppressing the multiple scattering effects and improve the resolution of the gradient. While direct calculation of the Hessian matrix is considered to be unfeasible in practical application for its expensively computational burden. Many Hessian approximations have been proposed to scale the gradient and improve the convergence rate of the gradient method. In this research, we compared different scaling methods in the least-squares inverse problem based on different Hessian approximations. The pseudo-Hessian, constructed by two virtual sources, can compensate the geometrical spreading effects obviously. While it is still not enough to balance the amplitude for that it ignores the receiver-side Green's functions. The Hessian approximation based on double illumination method, the linear and chirp phase encoded Hessian can balance the amplitude better for taking the receiver-side Green's functions into consideration. The chirp phase encoding method introduced in this research can approach the exact approximate Hessian better with the same number of simulations compared to the linear phase encoding method.

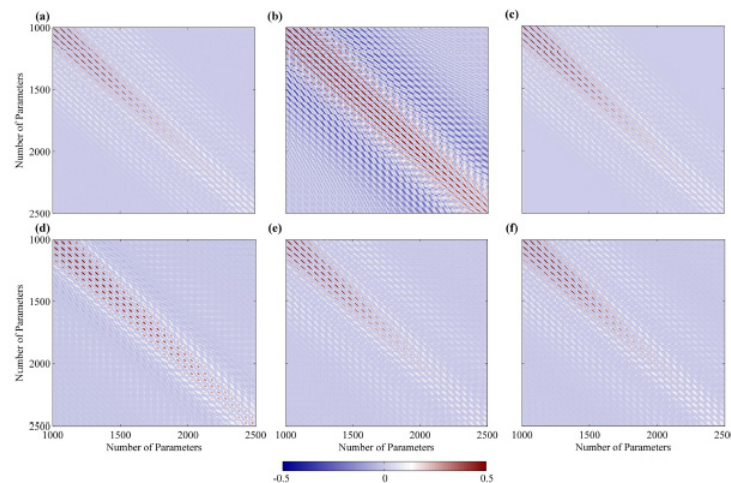


FIG. 1. The approximate Hessian and its approximations constructed with 9 sources and 50 receivers. (a) is the exact approximate Hessian; (b) is the pseudo Hessian; (c) is the Hessian approximation based on double illumination method; (d) is the phase encoded Hessian contaminated by crosstalk artifacts when ray parameter $\rho = 0$. (e) and (f) are the linear phase encoded Hessian and chirp phase encoded Hessian and the ray parameters range from -0.3s/km to 0.3s/km with a step of 0.1s/km .

Efficient full waveform inversion with phase encoded pseudo-Hessian

Wenyong Pan, Kris Innanen, Gary Margrave

ABSTRACT

Full waveform inversion (FWI) is a very important method for estimating the subsurface parameters. While it suffers from extensively computational cost, large memory requirements, slow convergence rate, cycle skipping, etc, which impede its practical application. In our implementation, a linear source encoding strategy is used for the gradient calculation in time-ray parameter domain. The plane wave encoding approach forms super-gathers by summing densely distributed individual shots, and can reduce the computational burden considerably. We also construct the diagonal part of the pseudo-Hessian using a hybrid source encoding method. The diagonal part of the encoded pseudo-Hessian is a good approximation to the full Hessian matrix, which preconditions the gradient. The preconditioning is equivalent applying a deconvolution imaging condition in prestack reverse time migration. To avoid the local minimum problem, a multi-scale approach in the time domain is employed, by (1) applying a low-pass filtering to the data residuals and (2) increasing the frequency bands step by step. This has been proved to be effective against cycle skipping. We assemble this suite of tools and carry out a numerical experiment with a modified Marmousi model, analyzing the effectiveness of this combination of the strategies.

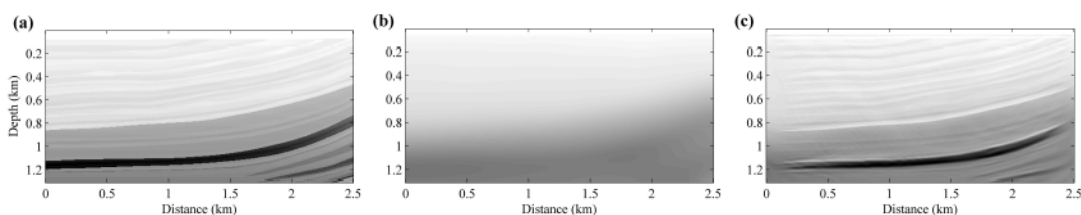


FIG. 1. (a) is the true velocity model; (b) is the initial velocity model; (c) is the inverted velocity preconditioned by phase encoded pseudo-Hessian after 200 iterations using one ray parameter $p = -0.2s/km$.

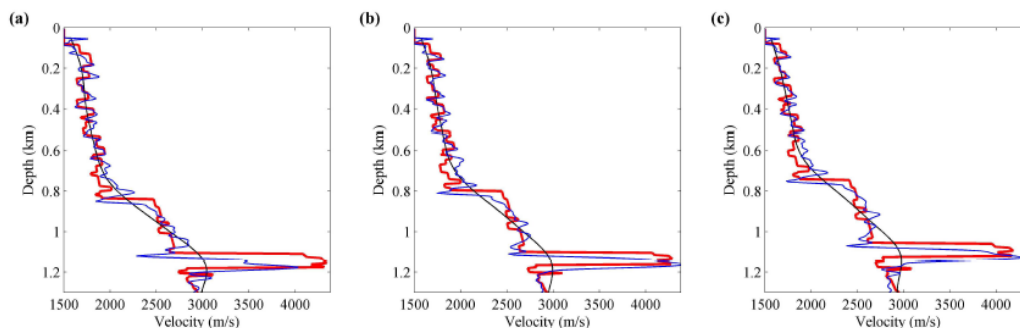


FIG. 2. Inverted results using fixed ray parameter at $0.5km$ (a), $1km$ (b) and $1.5km$ (c) respectively. The black and red lines indicate the initial velocity model and the true velocity model respectively. And the blue lines denote the inverted velocity model.

Efficient pseudo Gauss-Newton full waveform inversion in the time-ray parameter domain

Wenyong Pan*, Kris Innanen, Gary Margrave

ABSTRACT

Full Waveform Inversion (FWI) has been widely studied in recent years but still cannot be practiced in industry effectively. Generally, its failure can be attributed to expensively computational cost, slow convergence rate, cycle skipping problem and so on. For traditional FWI, the gradient is calculated shot by shot based on the adjoint state method. The computational burden rises significantly when considering large 2D velocity model or 3D experiments. A linear phase encoding strategy is employed to construct the gradient in the time-ray parameter domain. The phase encoding approach forms supergathers by summing densely distributed individual shots and can reduce the computational burden considerably. Furthermore, we propose the gradient be calculated using one single ray parameter per FWI iteration, with the ray parameter value varied for different iterations. The computational cost is reduced further within this strategy. The gradient is a poorly scaled image which can be considerably enhanced by multiplying the inverse Hessian. The Hessian matrix serves as a nonstationary deconvolution operator to compensate the geometrical spreading effects and suppress the multiple scattering effects. While explicit calculation of the gradient is also considered to be unfeasible. Under the assumption of high frequency limitation, the diagonal Hessian can work as a good approximation and it can also be constructed by the phase encoding method. In this research, preconditioning the gradient using the diagonal part of the phase encoded Hessian forms one pseudo Gauss-Newton step. Several numerical examples are presented to analyze the gradient contributions and compare different Hessian approximations. Finally, a modified Marmousi model is illustrated for full waveform inversion. we compared the effects for fixed ray parameter and varied ray parameter and analyzed the sensitivity to the ray parameter range, sensitivity to the Gaussian noise and sensitivity to the number of encoded sources. And the inversion results with different scaling methods are also provided for comparison.

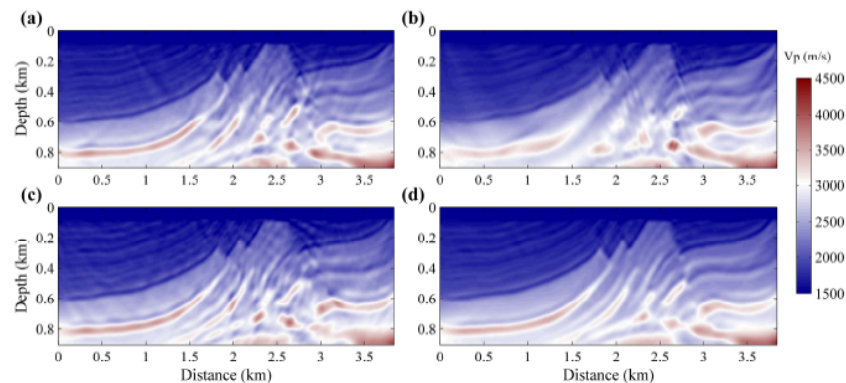


FIG. 1. FWI results after 50 iterations with single ray parameter in each FWI iteration. (a) ray parameter is fixed at $p = 0s/km$; (b) ray parameter is fixed at $p = -0.2s/km$; (c) ray parameter is fixed at $p = 0.2s/km$; (d) ray parameter varies from $-0.3s/km$ to $0.3s/km$ with a step of $0.1s/km$.

Multisource reverse time migration in anisotropic media

Wenyong Pan, Kris Innanen, Gary Margrave

ABSTRACT

Reverse Time Migration (RTM), a two-way wave equation method for accurate imaging, has attracted geophysicists' attention for many years for its great power in imaging the complex structures with dip angles. While seismic anisotropy in dipping shales can result in imaging and positioning problems for underlying structures. Isotropic RTM also suffers from seismic anisotropy. In this research, the pseudo-spectral method is used to solve the P-wave equation in Titled Transversely Isotropic (TTI) media for anisotropic RTM. Furthermore, RTM suffers from extensively computational cost for traditional shot by shot method, which limits its practical application considerably. The plane-wave source migration with densely distributed sources has been introduced in seismic imaging to reduce the computational cost. This strategy forms supergathers by summing densely distributed individual shots and can improve the efficiency of RTM considerably. While in practical application, the sources are always sparsely arranged. In this condition, the crosstalk artifacts which arise from the undesired interactions between unrelated shot and receiver wavefields will become very obvious. The phase encoding technique is introduced to shift or disperse these crossterms by slant stacking over sufficient number of ray parameters. In this research, we applied the phase encoded anisotropic RTM on Hess VTI (Vertical Transversely Isotropic) model. We also analyzed the influence of the number of encoded sources to the phase encoded images. And the imaging results for different phase encoding methods are also compared and discussed.

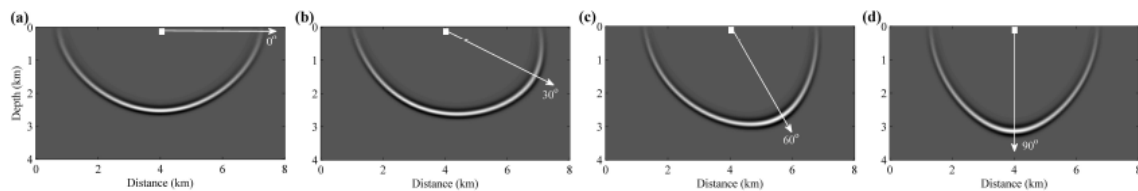


FIG. 1. Snapshots in anisotropic media. ($\epsilon = 0.18$ and $\delta = 0.15$). (a) Snapshot in VTI media ($\phi = 0^\circ$); (b) Snapshot in TTI media ($\phi = 30^\circ$); (c) Snapshot in TTI media ($\phi = 60^\circ$); (d) Snapshot in TTI media ($\phi = 90^\circ$).

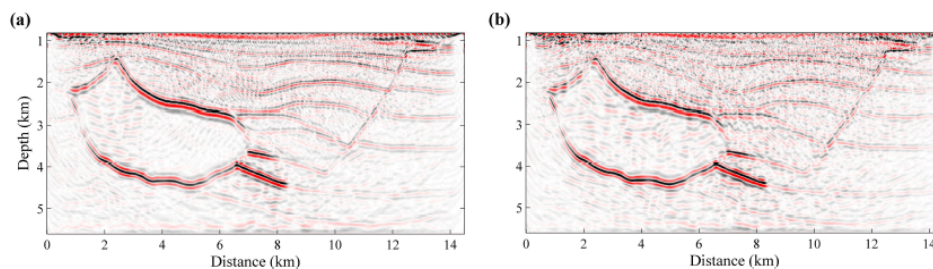


FIG. 2. (a) and (b) are the imaging results by linear phase encoding method and chirp phase encoding method with 7 simulations ranging the ray parameter from $-0.06s/km$ to $0.06s/km$ with a step of $0.02s/km$. 71 sources are arranged from $0.2km$ to $14 km$ with a spacing of $0.2 km$.

On the role of the deconvolution imaging condition in full waveform inversion

Wenyong Pan*, Gary Margrave, Kris Innanen

ABSTRACT

Full Waveform Inversion (FWI) employs full waveform information to inverse the subsurface properties through a iterative process. It has been widely studied in recent years but still cannot be practiced effectively in industry. FWI with a steepest descent method assumes the Hessian matrix as an identity matrix and suffers from slow convergence rate. The Hessian matrix can compensate the energy loss during wave-propagation and then improve the convergence rate of FWI. While calculating the inverse Hessian matrix directly is thought to be unfeasible because of its extensively computational cost. Even though the researchers have developed various methods to approximate the full Hessian matrix, this problem remains to be addressed. So, how to improve the computational efficiency and the convergence rate of FWI is a hot research topic present. It is known that FWI and Reverse Time Migration (RTM) share the same algorithmic structure and the calculation of the gradient in FWI is formally identical to a RTM image with a cross-correlation imaging condition. In this research, we found that auto-correlation of the forward modeling wavefields, namely, the source illumination is actually equivalent to the diagonal part of the pseudo-Hessian. And the gradient scaled by the auto-correlation of the forward modeling wavefields is equivalent to a RTM image based on the deconvolution imaging condition. Furthermore, deconvolution imaging condition based gradient is much more close to the reflectivity. Hence, it is possible for us to estimate the model perturbation through the traditional impedance inversion method. Combing FWI and traditional impedance inversion forms the Iterative Modelling Migration and Inversion (IMMI) method by Margrave et al.(2012). Finally, we practiced this strategy on a portion of Marmousi model and the phase encoding method was introduced to construct the gradient and diagonal pseudo-Hessian. And the iteration-dependent ray parameter setting strategy in the iterative process has also been involved to reduce the computational burden and balance the update.

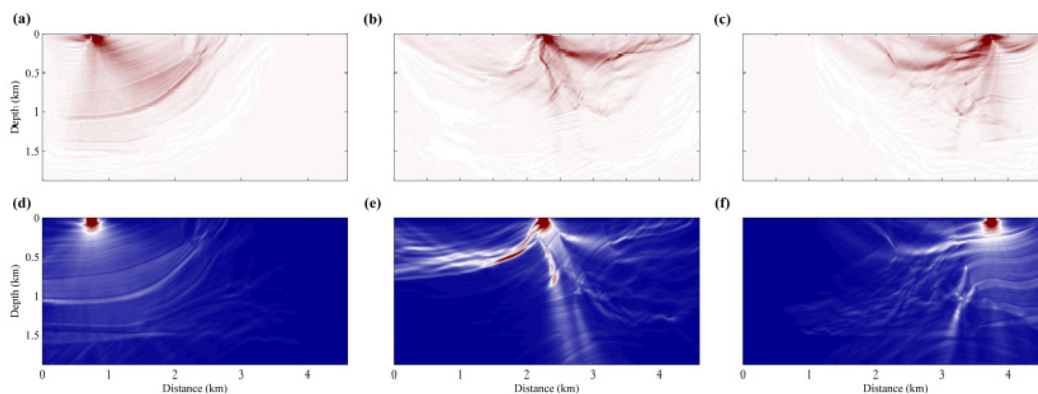


FIG. 1. Imaging results based on cross-correlation imaging condition. (a), (b) and (c) are the Imaging results based on cross-correlation imaging condition when the source is located at 0.75km, 2.25km and 3.75km respectively. And (d), (e) and (f) are the source illuminations corresponding to different source locations.

Poroelastic scattering potentials and inversion sensitivities

Wenyong Pan, Kris Innanen

ABSTRACT

Estimating the seismic wavefields response corresponding to the small model parameters' perturbations is a classical problem in inverse scattering problem of exploration geophysics. The Fréchet derivatives or sensitive matrices play a crucial role in perturbation analysis and are considered as sensitivity kernels in least-squares inverse problems. The forward modeling problem in poroelastic media has been studied by many researchers, while the inverse problem for poroelastic media has rarely been investigated. The scattering potentials indicating the perturbations of model parameters can be considered as engines for seismic wave scattering. And they are closely related to the Fréchet derivatives. In this research, we reviewed the Biot's theory for poroelastic wave equations and derived the poroelastic scattering potentials represented by different field variables firstly. And then we derived the coupled poroelastic Fréchet derivatives with respect to 9 poroelastic parameters, namely, the Lamé coefficients of the dry frame λ_{dry} and μ , porosity/fluid term f , density of saturated medium ρ_{sat} , fluid density ρ_f , C , M , $\sim\rho$, and mobility of the fluid m using perturbation method and non-perturbation method. The porosity/fluid term f involved by Russell et al. (2011) for linearized AVO analysis is considered as a poroelastic parameter for sensitivity analysis. The explicit expressions for these Fréchet derivatives with respect to different poroelastic parameters are provided. When wave propagating in poroelastic media, there are two kinds of compressional waves: the fast compressional wave and the slow compressional wave. In this research, we also derived the P-SV Fréchet derivatives in which the fast compressional wave and slow compressional wave are coupled together.

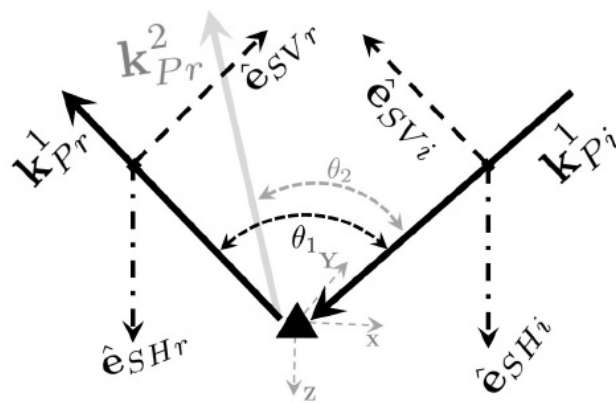


FIG. 1. Scattering scheme in poroelastic medium. k_{Pr}^1 is the incident fast P -wave wavenumber. k_{Pr}^1 and k_{Pr}^2 are the reflected fast P -wave and slow P -wave wavenumbers respectively. \hat{e}_{SVi} and \hat{e}_{SHi} are the unit direction vectors for incident SV wave and SH wave. \hat{e}_{SVr} and \hat{e}_{SHr} are the unit direction vectors for reflected SV wave and SH wave. θ_1 is the open angle between the incident fast P -wave and reflected fast P -wave. θ_2 is the open angle between the incident fast P -wave and reflected slow P -wave.

Thin-bed AVO and AVF continued

Wenyong Pan, Kris Innanen

ABSTRACT

Zoeppritz equations are the basis for traditional AVO analysis, which plays a significant role in oil and gas exploration. While they are not suitable for quantitative analysis of the amplitude response of thin-bed. In this paper, we continued our research on thin-bed AVO analysis. Firstly, we review our method for thin-bed AVO analysis. And then we extend our analysis of thin-bed AVO with attenuation from a dispersion-free system to the dispersion system, which means that the amplitude response is frequency dependent. And we found that if the thin-bed thickness and Q are both fixed, with increasing frequency, the Real part of R_{PP} AVO curve departs that with no attenuation, while the Real part of R_{PS} AVO curve approaches that without attenuation. What's more, the influence of Q on Real parts of the reflections increases with thin-bed thinning. Then we tested a linear approximation analysis following Liu and Schmitt's (2003) method. We concluded that with thin-bed thinning, the approximations approach the exact values better. Finally, we compared our method for thin-bed AVO analysis with the numerical modeling results. And the amplitudes calculated by our method match the numerical results very well, which also prove the correctness of our method.

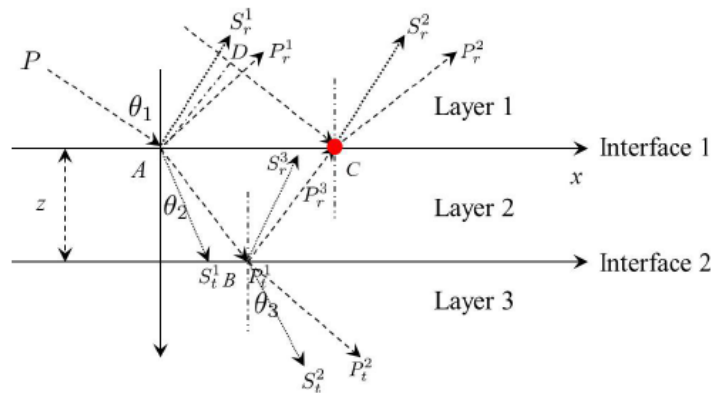


FIG. 1. Three layer model for thin-bed AVO analysis.

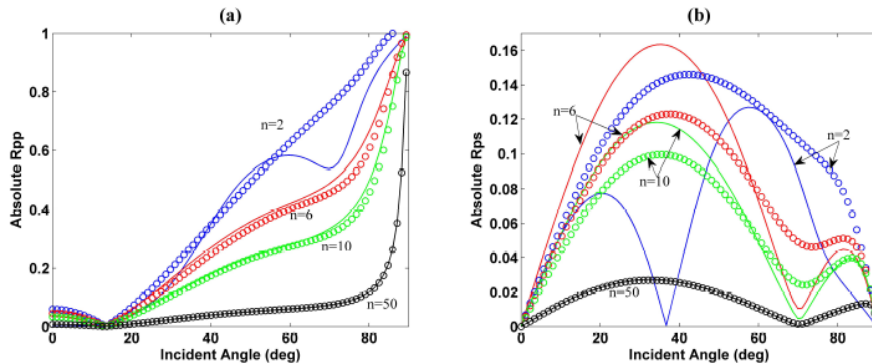


FIG. 2. Linear approximation analysis for P - P reflection (a) and P - S reflection (b) when $n = 2, 6, 10, 50$. The solid lines and cycle lines are the exact AVO curves and approximations respectively.

Exploring potential applications of Gaussian Ball Filters in Sharpe's Hollow Cavity Model

Christopher C. Petten, Gary F. Margrave

ABSTRACT

We investigate potential applications of Gaussian Ball Filters in Sharpe's Hollow Cavity Model. The dominant frequency was observed to decrease with increased Gaussian Ball width, which is very similar to the observations noted in Sharpe's model.

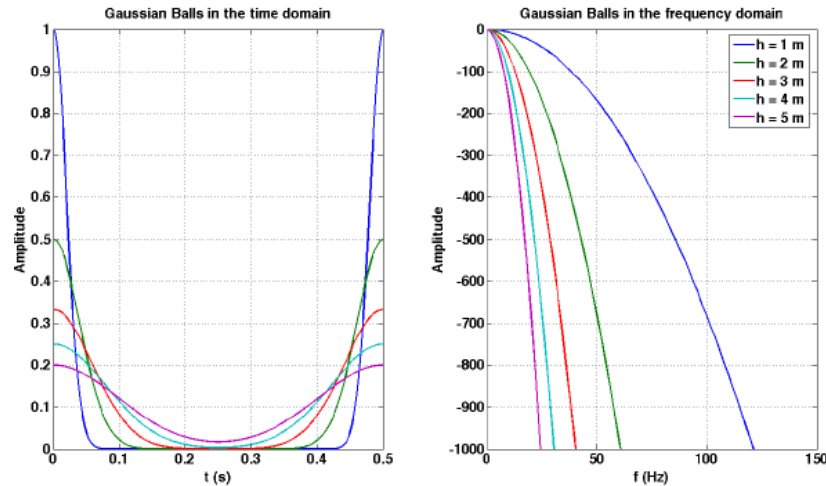


FIG. 1. A series of Gaussian Ball filters to be applied to an arbitrary pressure pulse in the Gaussian Ball model. Note that the width of the Gaussian Ball influences width of the frequency spectra, which may provide a crucial component in linking charge size to cavity radius in Sharpe's model.

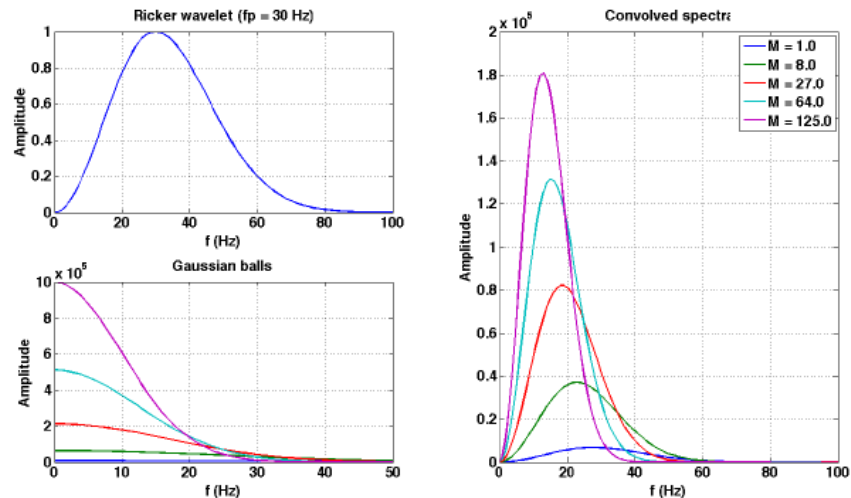


FIG. 2. A series of Gaussian Ball filters that have been convolved with a Ricker wavelet. Note that the dominant frequency decreases with charge size while the amplitude response increases. This result matches Sharpe's observations, which could prove to be a crucial link between the two models.

The S function and its applications

Brian Russell*¹

ABSTRACT

The sigmoidal, or *S*, function is one of the most useful functions in mathematics and physics, and has many applications in modelling and inversion. In its simplest form, the *S* function can be written

$$x(t) = \frac{1}{1 + e^{-t}}. \quad (1)$$

Equation 1 is called the logistic function and a graph of its shape, shown in Figure 1, illustrates why it is called the *S* function. The logistic function was initially derived by solving the differential equation for the predator-prey problem. In this article I will first describe the function itself and its origin and derivation.

I will then look at the other main form of the *S* function, the hyperbolic tangent (tanh) function, which is found in both the paramagnetic and ferrimagnetic equations used in modelling sandstone minerals and also in the Cole-Cole equation for heavy oil viscosity modelling. Both of these applications will be discussed. I will finish with an example which shows how the *S* function (and its limit, the step function) is used as the underlying function in neural networks. Specifically, I will apply the multi-layer perceptron (MLP) neural network to the solution of a straightforward AVO classification problem. I will do that in two ways. First, I will show intuitively how a MLP can be trained to recognize the top and base of a gas sand using a step function. Then, I will show the full implementation of the MLP using the tanh function.

This talk will cover a range of applications of a very simple, but ubiquitous, modelling equation that is often overlooked.

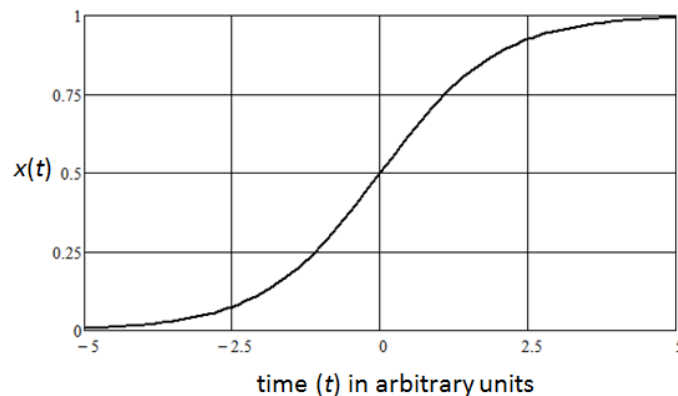


FIG. 1. The logistic function, which is the simplest form of the *S* function, goes from 0 to 1 with a graceful “S” shape.

¹ Hampson-Russell, A CGG Company, Calgary, Alberta, brian.russell@cgg.com

Madagascar - a powerful software package for multidimensional data analysis and reproducible computational experiments

Adrian D. Smith, Sergey Fomel¹, Robert J. Ferguson

ABSTRACT

Reproducibility of published scientific findings is critical toward exposure of ideas and results to independent testing and replication by other scientists. Computational experiments are made readily reproducible in theory due to systematic characteristics of computer programs, but this proves more difficult in practice. Madagascar is a Unix-based open source software package that provides an environment for computational data analysis in geophysical and related fields. It incorporates functionality from pre-existing geophysical analysis libraries, and it allows the end user to completely package publications in a reproducible format using SCons and LaTeX. We present two simple computational examples illustrating the functionality of Madagascar. A local reconstruction of several figures from a published paper is given to highlight the power of Madagascar as a vehicle for generating reproducible research. Existing programs developed within CREWES can be incorporated into Madagascar's library. The installation of Madagascar on CREWES servers is highly recommended.

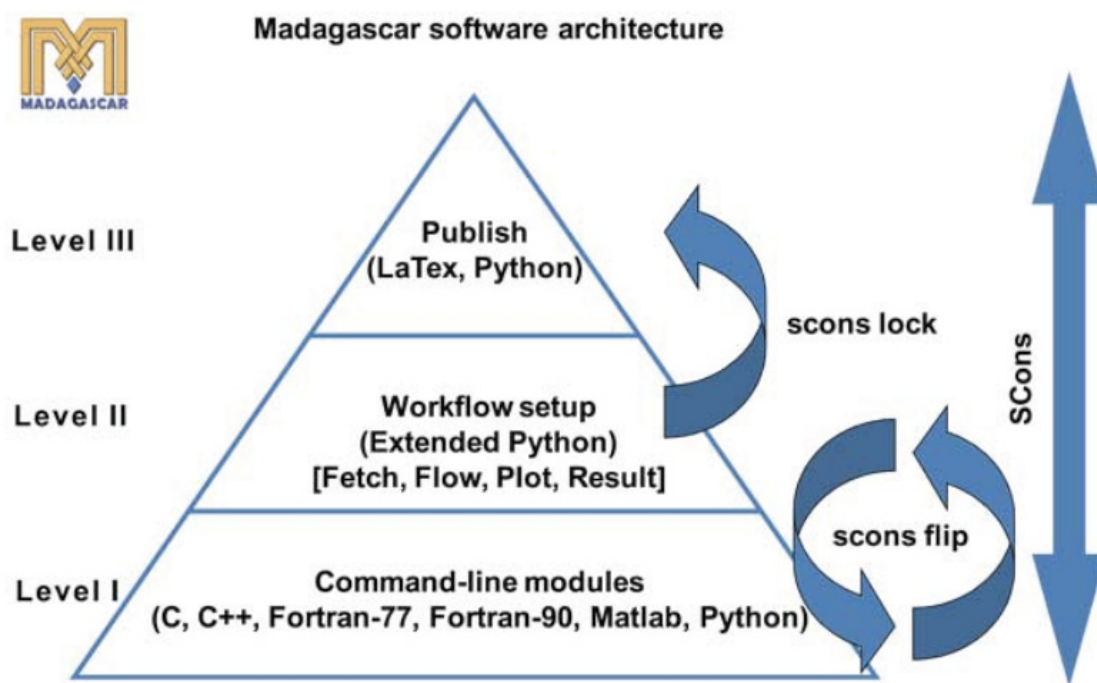


FIG. 1. Illustration of architecture of the Madagascar software package. The three levels can be described as follows: (I) - Implementation of new computational algorithms for data analysis, involving writing low-level programs (II) - Testing of new algorithms or workflows on data. This involves assembling workflows from existing command-line modules and tuning their parameters through repeated computational experiments (III) - Documentation level. Results (figures) get referenced in the output publication.

¹ Bureau of Economic Geology, University of Texas at Austin

Processing of tissue sensing adaptive radar data - an analogue for georadar

Adrian D. Smith, Jérémie Bourqui¹, Yuhong (Kay) Liu¹, Elise C. Fear¹, Robert J. Ferguson

ABSTRACT

Frequency domain georadar data have several advantages over time domain data but are much more cumbersome to acquire. A medical imaging technique developed in the Department of Electrical Engineering at the University of Calgary known as "tissue sensing adaptive radar" (TSAR) makes use of monostatic radar data acquired in the frequency domain. Simulated data were generated and processed using a workflow that has been previously developed and implemented successfully on georadar data. We discover that the simulated TSAR data are mixed phase, violating the minimum-phase assumptions of deconvolution. We show through synthetic examples that deconvolution of these data does not recover reflectivity accurately. Although nonstationary Gabor deconvolution has been shown to be effective when applied to georadar data, our work with the TSAR data shows that we must take care to ensure that radar data be minimum phase during deconvolution, especially with data acquired in the frequency domain.

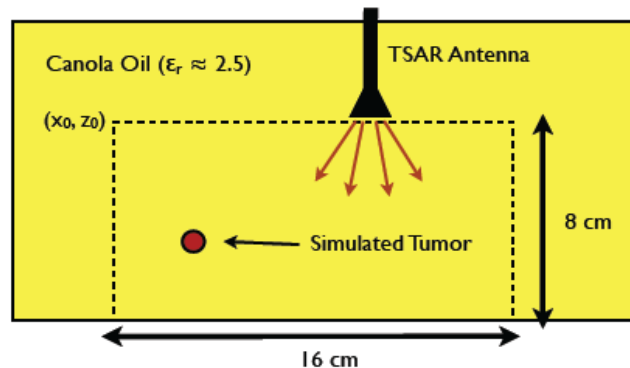


FIG. 1. Schematic of the TSAR simulation space.

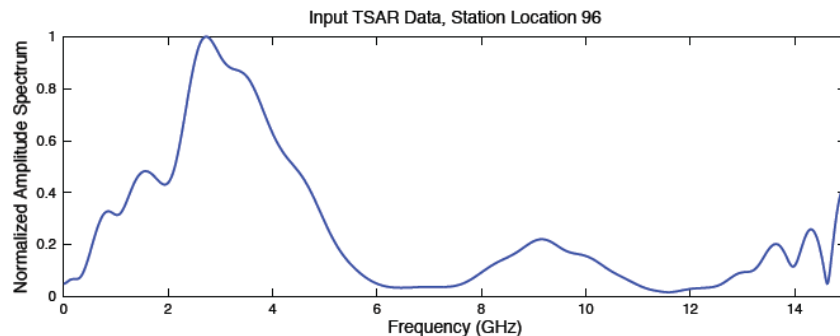


FIG. 2. Normalized amplitude spectrum of a simulated TSAR data trace.

¹ Department of Electrical Engineering, University of Calgary

Imaging lateral discontinuities with reflected surface waves

Robert R. Stewart, Craig Hyslop, and Minyu Zhang

University of Houston
 Department of Earth and Atmospheric Sciences
 312 Science and Research
 Houston, Texas 77204-5007

ABSTRACT

Determining lateral change in the subsurface is important for many scales of geophysical investigation: It is helpful in constraining models for tectonic behavior, structural mapping on a regional scale, characterizing reservoirs, and identifying faults for engineering applications. Surface-seismic survey geometries and reflection processing methods are well suited for imaging horizontal layers in the subsurface; however, illuminating and analyzing near-vertical features and lateral discontinuities may be more difficult. Processing surface waves directly can provide additional information about lateral change in the subsurface. We have developed a processing flow for imaging faults using reflected surface waves. The method relies on VSP-type procedures as well as the undoing of dispersive effects. It provides a way to locate lateral change and the discontinuity depth using extracted surface-wave reflectivity. We apply the method to synthetic datasets generated from a buried fault model and find interpretable images of the fault. Next, we use surface-wave reflectivity for interpreting a near-surface fault in field data from the Hockley Fault system near Houston Texas (Figure 1). We note that a major fault breaks the surface (pavement) at 400m.

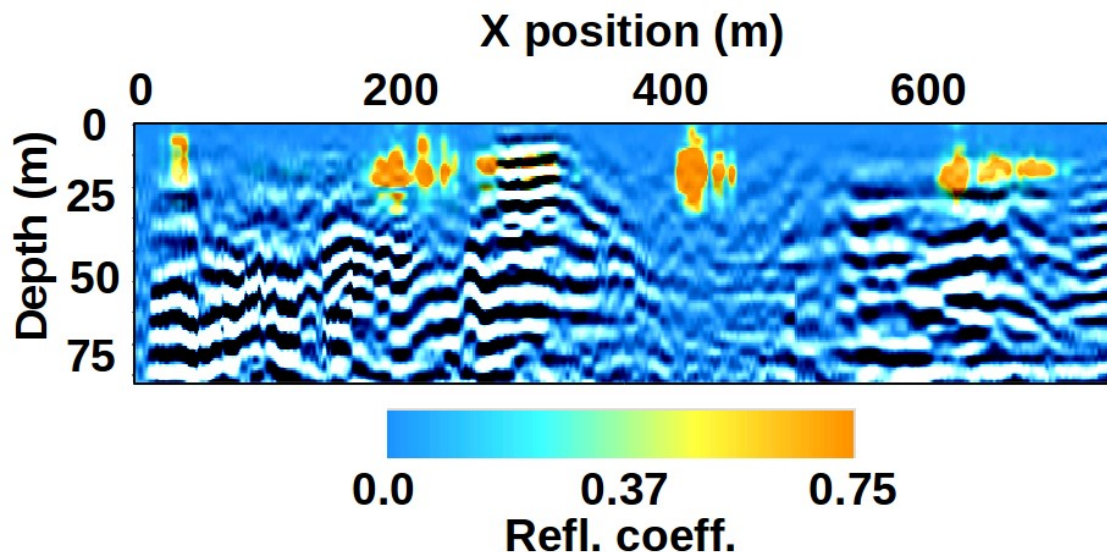


FIG. 1. Near-surface seismic reflection section with overlain ground-roll reflectivity from the Hockley Fault System near Houston, Texas.

Searching for the 2010 Haiti earthquake fault

Robert R. Stewart, Eray Kocel, Paul Mann, and Li Chang

University of Houston
Department of Earth and Atmospheric Sciences
Houston, Texas 77004

ABSTRACT

On January 12, 2010 Haiti suffered a major earthquake with subsequent tragic human and infrastructural loss (Figure 1a). Surface expression of the earthquake fault has not yet been unambiguously identified. Thus, key geologic components of the devastating event are not well resolved. The Haiti Subsurface Imaging (HASI) Project, supported by the SEG Foundation, aspires to find expression of this “blind” fault. We have made two geophysical reconnaissance surveys to Haiti: Undertaking GPS and gravity surveys near Port-au-Prince, and ten days of seismic, GPS, and gravity surveys in the Léogâne Delta region (close to the earthquake’s epicenter). These surveys have provided near-surface rock properties as well as some evidence of faulting (Figure 1b). Further east along the main Enriquillo-Plantain Garden Fault zone, lies Lake Enriquillo. We have conducted sonar surveys on the Lake which have produced some exciting details of the main faults. We anticipate that the top of the proposed 2010 blind fault could be some several kilometers deep. While our shallow, short seismic lines show some evidence of disruption, the image is not clear and the discontinuities are not necessarily part of a larger fault system required to create the 2010 earthquake. Thus, we must return and image deeper in the section with a larger source (in March, 2014).



FIG. 1a. The Haiti Presidential Palace (left) on January 14, 2012. The grounds have been cleaned, but the building is largely destroyed. Clean-up continues in Port-au-Prince (right).

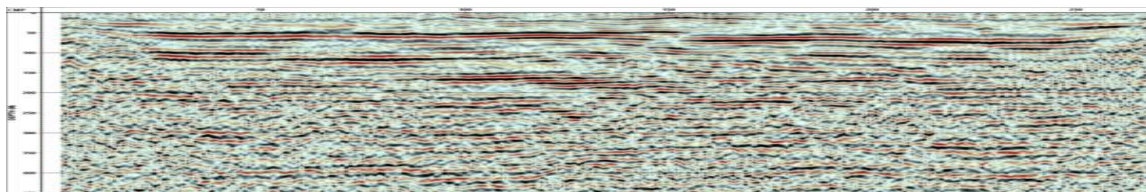


FIG. 1b. Hammer-seismic stacked section converted to depth (400m) from the Léogâne Delta, Haiti.

Controlling a land vibrator with m-sequences: a field test

Joe Wong, Malcolm Bertram, Kevin Bertram, Eric Gallant, and Kevin Hall

ABSTRACT

We conducted initial field measurements to test the idea of driving a land vibrator with maximal-length sequences (m-sequences). Seismograms were recorded with the CREWES IVI EnviroVibe vibrator controlled by m-sequence pilots, and compared to seismograms acquired with the vibrator controlled with a conventional frequency sweep. The m-sequence data were also compared to seismograms acquired with an accelerated weight-drop source. The experiment indicated significant issues regarding how hydraulically-powered vibrators respond to pilot signals that try to force very sharp accelerations on the reaction mass. Despite these issues, the results from this initial field test are encouraging, and point to possible modifications to the m-sequence pilots to make them more compatible with the mechanical characteristics of a land vibrator.

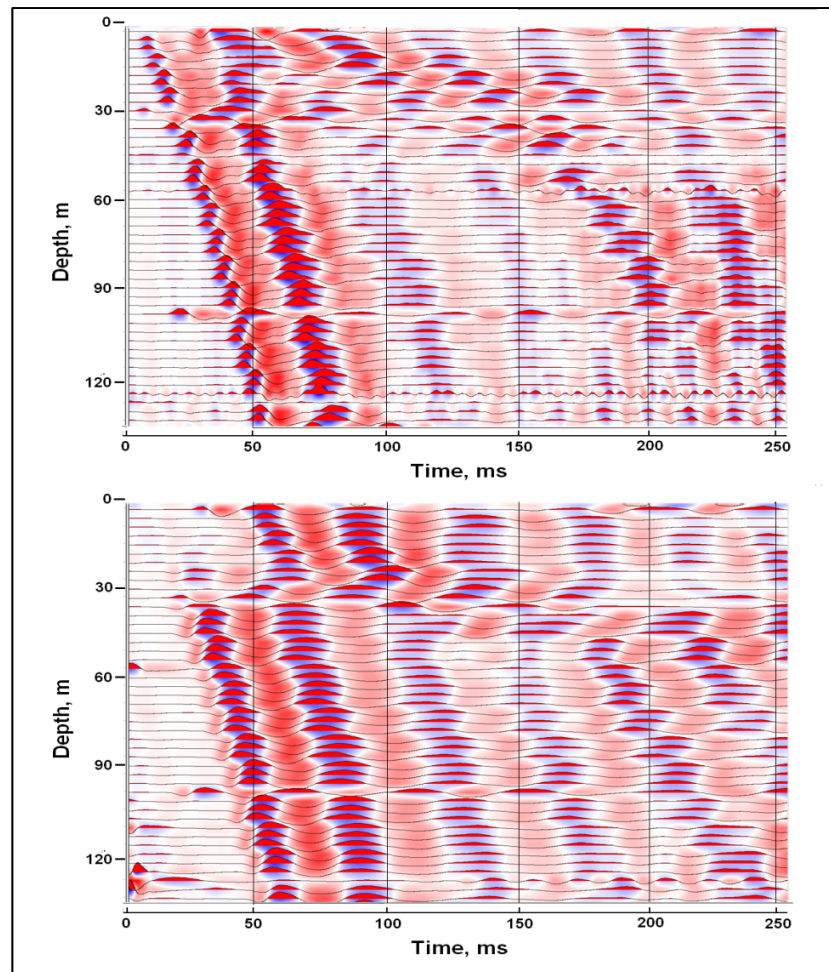


FIG. 1. Vertical component seismograms from 45 geophones cemented in a well, recorded with two different sources located near the well. Top: acquired with accelerated weight drop source. Bottom: acquired with EnviroVibe vibrator driven by an m-sequence pilot.

Exact formulas for qP , qS_V , and SH group velocities in VTI media

Joe Wong

ABSTRACT

For analyzing traveltimes of qP and qS arrivals propagating through media with transversely isotropic or VTI symmetry, geophysicists often use the Thomsen linearized formulas for phase velocities to approximate group velocities. However, the Thomsen approximations are suitable only for weak anisotropy and for small angles relative to the VTI symmetry axis. When the anisotropy is strong and for larger angles, exact expressions for group velocity may be more appropriate. The exact group velocity formulas are not widely familiar to most applied geophysicists. This report summarizes the derivation of these exact formulas using the method of characteristics, and presents them in forms that facilitate calculation of traveltimes relevant to all the common acquisition geometries (surface reflection, VSP, and crosswell).

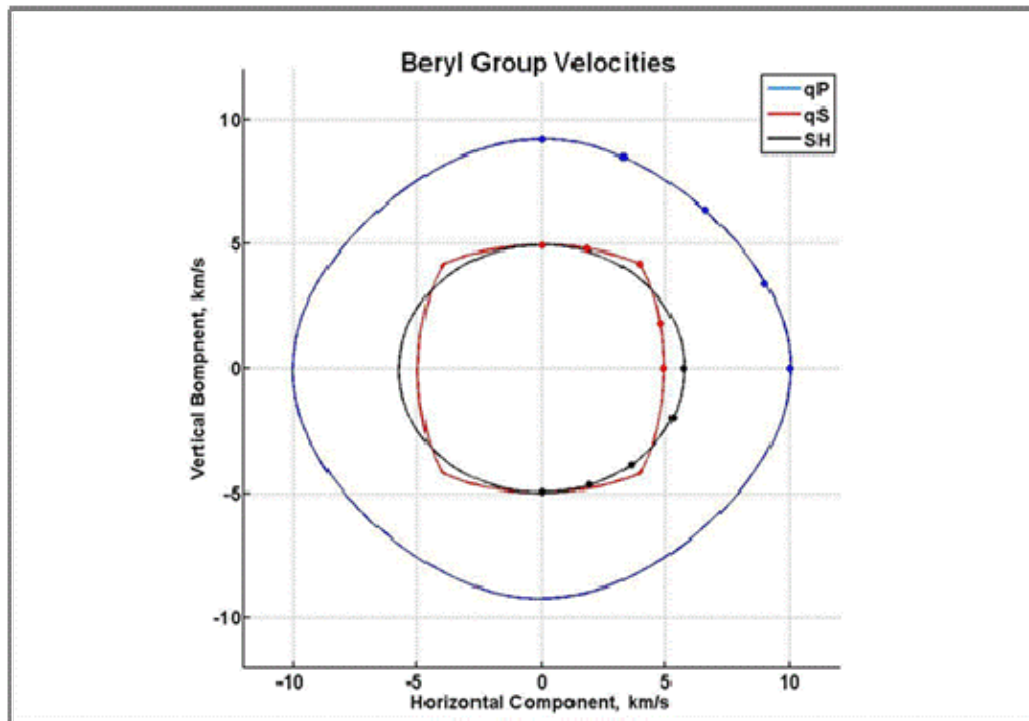


FIG. 1: Group velocities for beryl: $\rho = 2850\text{kg/m}^3$, $C_{11} = 287.3$, $C_{33} = 241.8$, $C_{55} = 70.2$, $C_{66} = 94.2$, and $C_{13} = 72.8$ (C_{mn} units = GPa). Lines are values calculated using the exact formulas in the full report; solid dots are values taken from the diagram for beryl in Musgrave's 1970 book, "Crystal Acoustics".

Operating instructions for mFD2D, MATLAB code for generating seismograms in 2D elastic media

Joe Wong

ABSTRACT

The MATLAB software package mFD2D.m uses a finite-difference, time-stepping method to simulate elastic wave propagation in 2D media and generate common source gathers of seismograms for a variety of acquisition geometries. The resulting gathers of seismograms are written to SEGY files that can be used directly in processing packages. The production code executes on desktop or laptop computers using the Windows (XP, 7, or 8) operating system. This report provides detailed instructions and information on how to set up input files to control and execute the modeling by mFD2D.

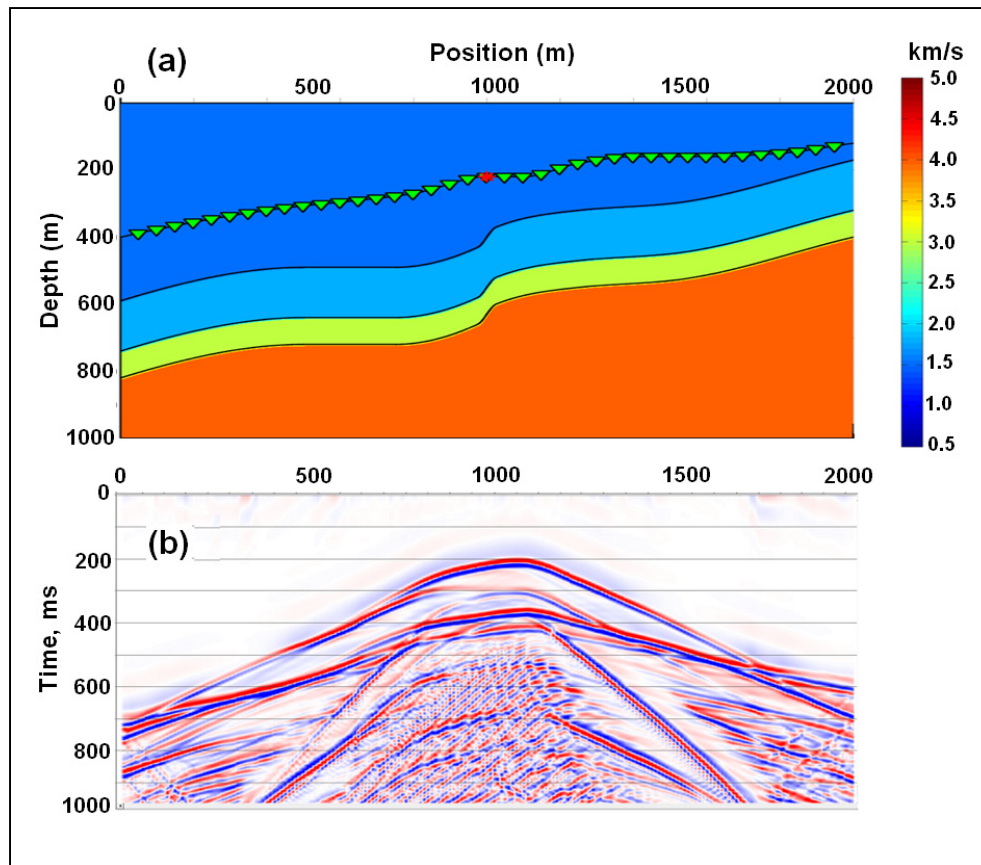


FIG. A2. An example of an acquisition line on a topographic surface; green triangles represent nominal geophone positions; red star indicate position of source; (b) common source gather of x-component reflection seismograms; Rayleigh waves and direct arrivals have been excluded. Details for generating these seismograms are found in the full report.

Seismic physical modeling I: acquisition of 2D and 3D surveys involving HTI targets

Joe Wong*

ABSTRACT

Physical modeling of 2D land and 3D marine seismic surveys has been carried out over several models. The land surveys were done using different combinations of P-type and S-type piezoelectric transducers, in an effort to simulate real-world three-component acquisition. The 3D marine surveys recorded data using an array of eight sources firing simultaneously into a single receiver. This procedure significantly increased acquisition speed, but produces super gathers equivalent to the sum of eight separate common-source gathers. Depending on the area covered and the spatial sampling, 3D marine surveys using multiple simultaneous sources were completed within 6 to 22 days.

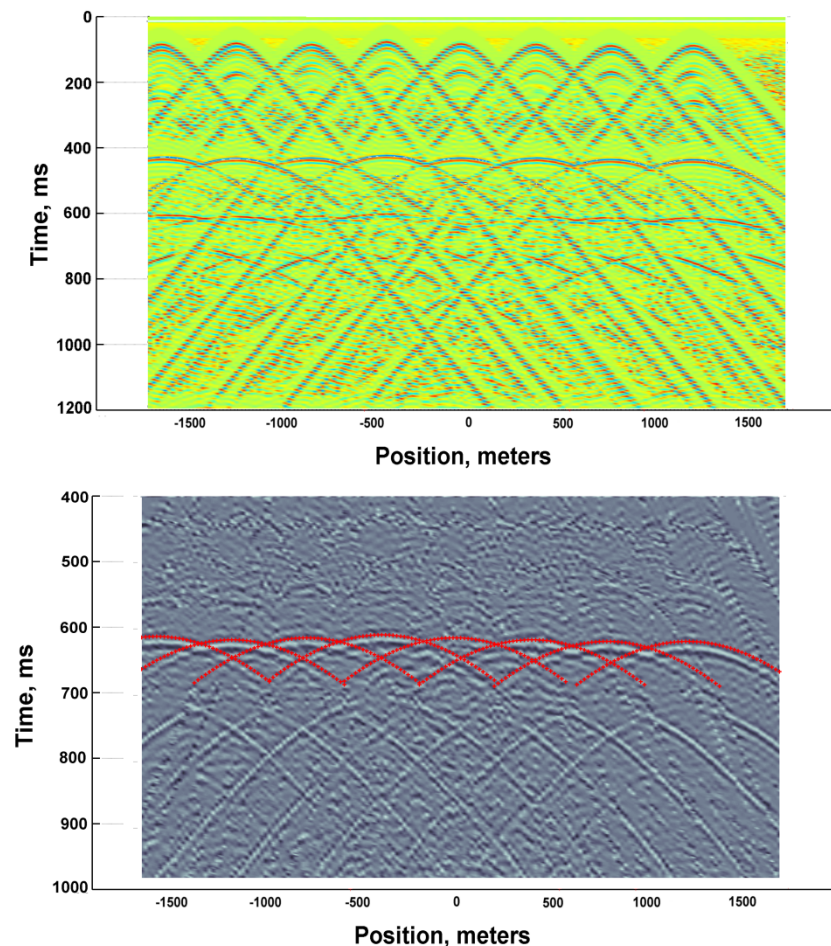


FIG. 1. A super gather of seismograms recorded with eight simultaneous sources. Top: AGC plot of unprocessed seismograms. Bottom: AGC plot after elimination of the direct water arrival, emphasizing the reflections just below 600ms. Note the PP amplitude anomaly at positions near 0m. Also note the likely PS hyperbolas below the PP reflections.

Seismic physical modeling II: VVAZ and AVAZ effects observed on reflections from isolated HTI targets

Joe Wong

ABSTRACT

Physically-modeled land surveys, carried out for a two-layer model consisting of an isotropic Plexiglas layer overlying an HTI Phenolic layer, produced transmission and reflection seismograms that exhibit VVAZ effects (Figure 1). Physically-modeled 3D marine surveys were conducted over isolated HTI Phenolic targets embedded in an isotropic Plexiglas slab. By using acquisition methods designed to emphasize AVAZ effects of reflections from the HTI targets, we obtained reflection amplitudes that clearly map the positions and sizes of the HTI targets (Figure 2). Slight differences in the target amplitudes may be indicative of differences in the HTI symmetry axis directions.

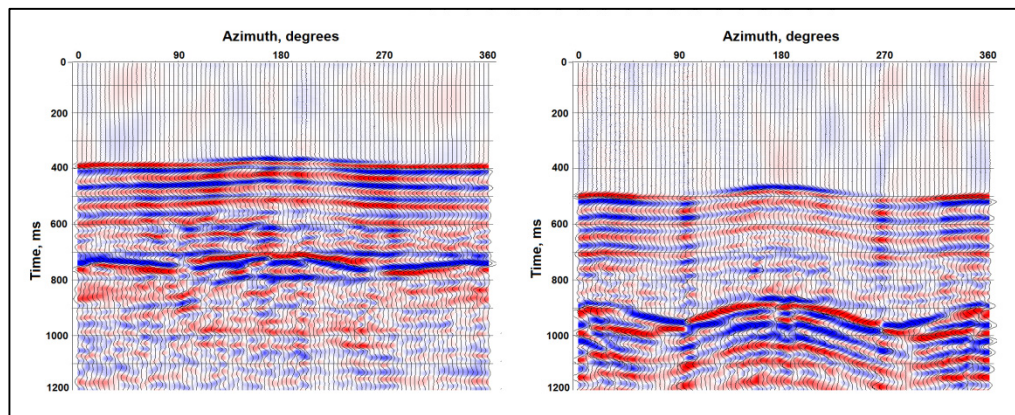


FIG. 1. Seismograms through the two-layer model, simulating data from land multi-azimuth VSP surveys. Source-receiver radial offsets are 500m and 1000m for the left and right gathers.

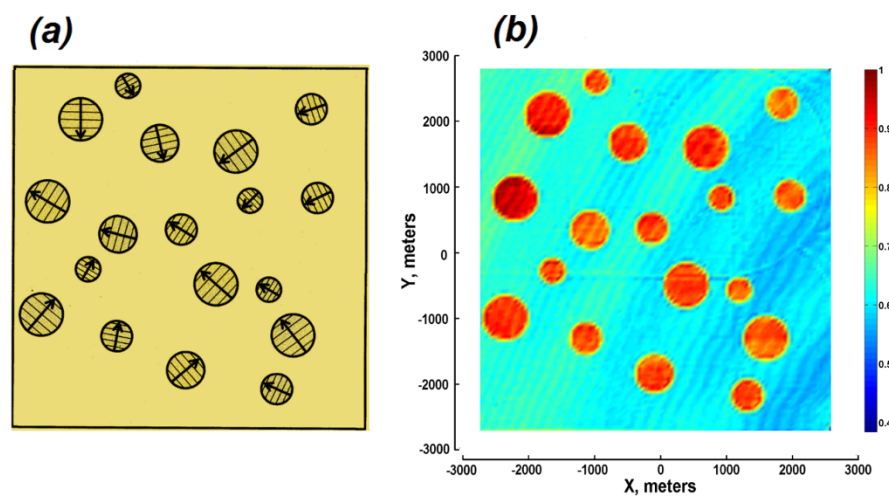


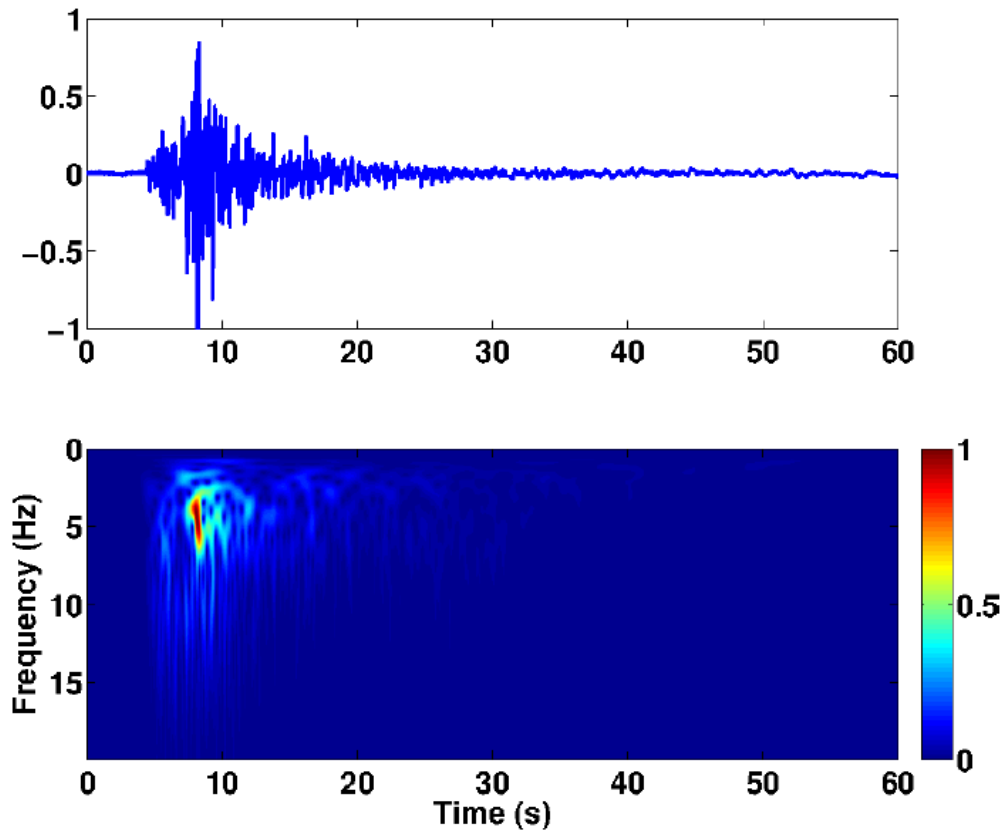
FIG. 2. (a) Plan view of HTI pucks embedded in a Plexiglas slab. (b) Map of normalized vertical-incidence reflection amplitudes observed in the 3D marine survey over the model in (a).

Instantaneous frequency computation: theory and practice

Matthew J. Yedlin^{*1}, Gary F. Margrave², and Yochai Ben Horin³

ABSTRACT

We present a review of the classical concept of instantaneous frequency, obtained by differentiating the instantaneous phase and also show how the instantaneous frequency can be computed as the first frequency moment of the Gabor or Stockwell transform power spectrum. Sample calculations are presented for a chirp, two sine waves, a nonstationary reflectivity trace and a very large quarry blast. The results obtained clearly demonstrate the failure of the classical instantaneous frequency computation via differentiation of the instantaneous phase, the necessity to use smoothing and the advantage of the first moment computation which always results in a positive instantaneous frequency as a function of time. This research points to the necessity of devising an objective means to obtain optimal smoothing parameters. Future work will focus on using linear and nonlinear inverse theory to achieve this goal.



Record of a 10^3 kg TNT quarry blast (normalized amplitude) and its Stockwell transform magnitude.

¹ Department of Electrical and Computer Engineering, University of British Columbia

² Geoscience, University of Calgary

³ SOREQ, Yavneh, Israel

Elastodynamic FWI in 2D with partial stacking

Vladimir Zubov*, Gary F. Margrave and Michael P. Lamoureux

ABSTRACT

The partial stacking approach is the focus of the present study. It is applied to the elastodynamic iterative full waveform inversion (FWI) method as source splitting on groups and switching from group to group in iterations of the FWI. Both density and bulk modulus inversion is implemented and studied on the synthetic data. The applicability of the partial stack FWI is estimated by studying both the iterative FWI convergence behavior and the algorithm resistance to non-uniform noise in observations.

The elastodynamic 2D model is implemented with the Marmousi density field as FWI exact solution. The vertical resolution of the original Marmousi model is preserved. By choosing the horizontal scales in about 9 times greater than vertical, we succeed in full stack reduction by up to 6 shots, which keeps FWI stable and convergence successful even with partial stacking with each fourth source used. Special attention is paid to low frequencies estimation by the partial stack algorithm, where the FWI starts with an initial estimate of the reflection coefficient field, absent the low frequency trend of the solution.

The comparison of the density field partial stack FWI with corresponding bulk modulus partial stack FWI is made with the same horizontally simplified Marmousi model (Figure 1) with vertical resolution preserved. Based on it and other experiments, a further strategy of partial stacking development using a misfit data frequency filtering approach is proposed.

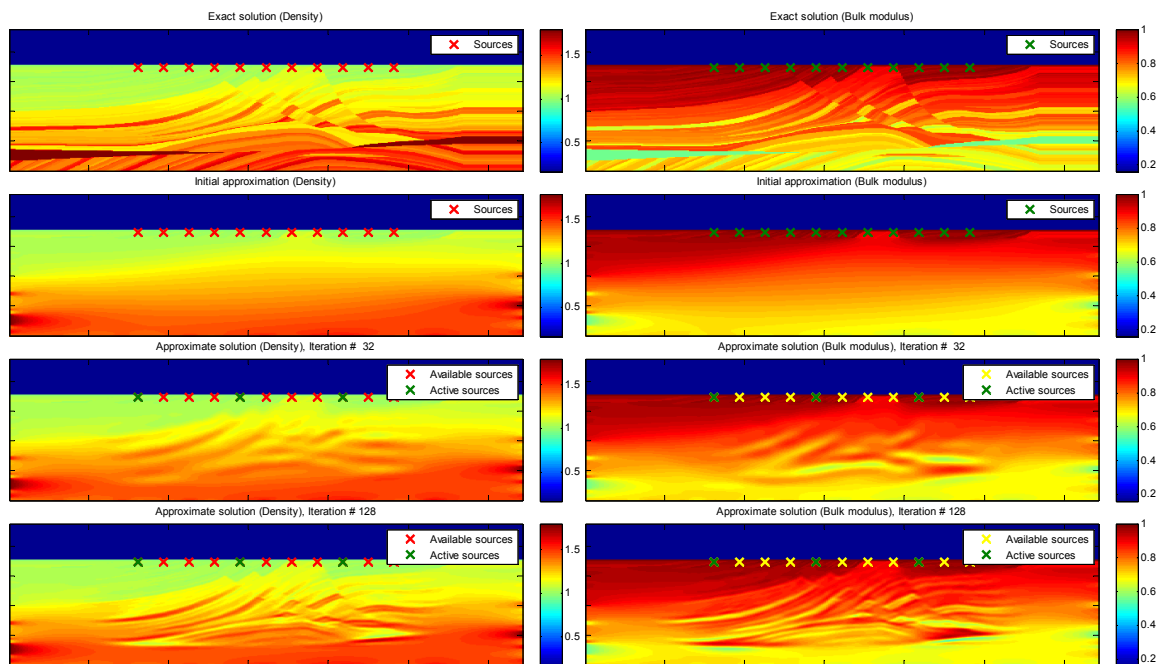


FIG 1. Partial stack FWI convergence behavior: density field inversion on the left; bulk modulus field inversion on the right.